AN ABSTRACT OF THE DISSERTATION OF

Esha Chatterjee for the degree of Doctor of Philosophy in Chemistry presented on November 7, 2011.

Title: Detection Techniques for Biomolecules using Semi-Conductor Nanocrystals and Magnetic Beads as Labels

Abstract approved:

Vincent T. Remcho

Continued interest in the development of miniaturized and portable analytical platforms necessitates the exploration of sensitive methods for the detection of trace analytes. Nanomaterials, on account of their unique physical and chemical properties, are not only able to overcome many limitations of traditional detection reagents but also enable the exploration of many new signal transduction technologies. This dissertation presents a series of investigations of alternative detection techniques for biomolecules, involving the use of semi-conductor nanocrystals and magnetic beads as labels.

Initial research focused on the development of quantum dot-encapsulating liposomes as a novel fluorescent label for immunoassays. This hybrid nanomaterial was anticipated to overcome the drawbacks presented by traditional fluorophores as well as provide significant signal amplification. Quantum dot-encapsulating liposomes

were synthesized by the method of thin film hydration and characterized. The utility of these composite nanostructures for bioanalysis was demonstrated. However, the long-term instability of the liposomes hampered quantitative development.

A second approach for assay development exploited the ability of gold nanoparticles to quench the optical signals obtained from quantum dots. The goal of this study was to demonstrate the feasibility of using aptamer-linked nanostructures in FRET-based quenching for the detection of proteins. Thrombin was used as the model analyte in this study. Experimental parameters for the assay were optimized. The assay simply required the mixing of the sample with the reagents and could be completed in less than an hour. The limit of detection for thrombin by this method was 5 nM. This homogeneous assay can be easily adapted for the detection of a wide variety of biochemicals.

The novel technique of ferromagnetic resonance generated in magnetic bead labels was explored for signal transduction. This inductive detection technique lends itself to miniaturization, is capable of mass production and is inexpensive to fabricate. The device consisted of a microwave circuit in which a slotline and a coplanar waveguide were integrated with a biochemically activated sensor area. The magnetic beads were immobilized at the sensor area by bio-specific reactions. Experiments conducted on this prototype show promising results for using ferromagnetic resonance -based detection of magnetic labels for fabrication of portable and inexpensive sensor devices.

The next stage of work addresses the issue of patterning of sensing surfaces with biomolecules. The ability to selectively immobilize biomolecules on surfaces has far-reaching applications, including sensor development. A simple and widely applicable method for the photopatterning of chitosan films with biotin was presented. Chitosan is a biocompatible and biodegradable polymer. The proposed method was capable of forming spatially defined biotin features on the order of tens of microns, together with a significant reduction of non-specific protein binding and increase in hydrophilicity of the sensor surface. The entire patterning process, inclusive of the blocking step, could be completed in under an hour. This straightforward method for the selective patterning of the biocompatible polymer chitosan is expected to be widely useful in the field of bioanalysis.

Detection Techniques for Biomolecules using Semi-Conductor Nanocrystals and Magnetic Beads as Labels

by
Esha Chatterjee

A DISSERTATION

submitted to

Oregon State University

in partial fulfillment of
the requirements for the
degree of

Doctor of Philosophy

Presented November 7, 2011
Commencement June 2012

Doctor of Philosophy dissertation of Esha Chatterjee presented on November 7, 2011

APPROVED:

Major Professor, representing Chemistry

Chair of the Department of Chemistry

Dean of the Graduate School

I understand that my dissertation will become part of the permanent collection of Oregon State University libraries. My signature below authorizes release of my dissertation to any reader upon request.

Esha Chatterjee, Author

ACKNOWLEDGMENTS

I would like to take this opportunity to express my heartfelt gratitude to my advisor, Prof Vincent Remcho for his encouragement and support at all stages of my graduate study. His keen insight, able mentorship and enthusiasm have made this an enriching experience for me. I would like to sincerely thank Dr. Michael Lerner, Dr. Chih-hung (Alex) Chang, Dr. Neal Sleszynski and Dr. Michael Qian, members of my thesis committee, for their commitment and advice on the dissertation content throughout the committee meetings and examinations.

Over the course of time, I have been fortunate to work with some exceptional people in the Remcho research group. I would like to warmly thank Myra Koesdjojo, Jintana (Dao) Nammoonnoy, Yolanda Tennico, Tae-Hyeong Kim, Daniela Hutanu, Natalia Pylypiuk, David Mandrell, Saki Kondo, Adeniyi Adenuga, Yuanyuan Wu, Chris Heist, Beth Dunfield, Ryan Frederick, Brian Fuchs, Jack Rundel, Corey Koch, and Carlos Gonzales. Your friendship, advice and good cheer kept me going through the ups and downs of graduate school.

I would like to thank Simon Ghionea and Tim Marr, our collaborators on the FMR project, for introducing me to the concept of FMR and their expert help with sensor fabrication. I am grateful to Dr. Pallavi Dhagat for her advice and help with writing of Chapter 4 of this dissertation. I would like to acknowledge Joe Bartel and Chad Teters for their excellent mentorship that made my internship at Life Technologies a very rewarding experience. I would also like to extend my

appreciation to the faculty and staff from the Department of Chemistry at OSU for their help during my stay at OSU. I would also like to acknowledge the Department of Chemistry and College of Science at OSU for travel grants.

I wish to thank all of my friends, especially Hasini Perera and Sharmistha Nag, for their moral support. I would like to thank all my family members for their good wishes. I wish to thank my parents, Ashish and Chandana Chatterjee, for their love, sacrifices and encouragement. None of this could have been possible without your inspiration and blessings. I would also like to thank my parents-in-law, for their encouragement and blessings. Special thanks to my brother, Anirban, for his moral support. Last, but not the least, I would like to thank my husband, Sundeep, for his understanding and constant encouragement, through thick and thin.

CONTRIBUTION OF AUTHORS

Dr. Vincent T. Remcho edited and assisted in the writing of all chapters in this dissertation. His name appears on all published and submitted work contained herein. Dr. Pallavi Dhagat edited and assisted in the writing of Chapter 4 in this dissertation. Tim Marr assisted with the sensor design, data collection and writing of Chapter 4.

TABLE OF CONTENTS

TABLE OF CONTENTS (Continued)

Page

TABLE OF CONTENTS (Continued)

Page

TABLE OF CONTENTS (Continued)

Page

TABLE OF CONTENTS (Continued)

Page

LIST OF FIGURES

LIST OF FIGURES (Continued)

LIST OF FIGURES (Continued)

Figure Page

LIST OF TABLES

DETECTION TECHNIQUES FOR BIOMOLECULES USING SEMI-CONDUCTOR NANOCRYSTALS AND MAGNETIC BEADS AS LABELS

CHAPTER 1

INTRODUCTION

This chapter serves as a general introduction to the concept of biosensors. The necessary components of a biosensor are described, with an emphasis on the most commonly used methods of signal transduction. Subsequently, the discussion is focused on the use of various nanomaterials and their applications for bioanalysis. The four nanomaterials covered are: (a) quantum dots (b) liposomes (c) gold nanoparticles and (d) magnetic nanoparticles or beads. The final part of the introduction discusses the use of the naturally-derived polymer, chitosan, for bioanalytical applications. This chapter is meant to provide an overview of the properties and uses of nanomaterials and chitosan for bioanalysis, the particular applications of which are subsequently described in chapters 2, 3, 4 and 5.

1.1. Biosensors

Biosensors are analytical devices composed of a biological recognition element (such as enzyme, antibody, receptor or microorganisms) coupled to a chemical or physical transducer (electrochemical, mass, optical and thermal)[1]. Biosensors are often integrated with electronic circuits such that they yield a digital signal proportional to the concentration of the analyte (or analytes) of interest. These devices may be

configured such that they are disposable after a single measurement or are capable of continuous monitoring. The most popular examples of biosensors are the ubiquitous blood glucose monitoring systems and the at-home pregnancy test kits. Biosensors, however, are a very diverse group and range from systems that are nanoparticle-based[2] to those that are whole cell-based[3]. Over the last three decades, there has been a tremendous interest in the area of biosensor research fuelled by their advantages such as portability, specificity, speed and low cost[4]. They have been applied to wide variety of analytical applications in biomedical research, medicine, biotechnology, environmental analysis, agriculture, food industries and defense, to name a few.

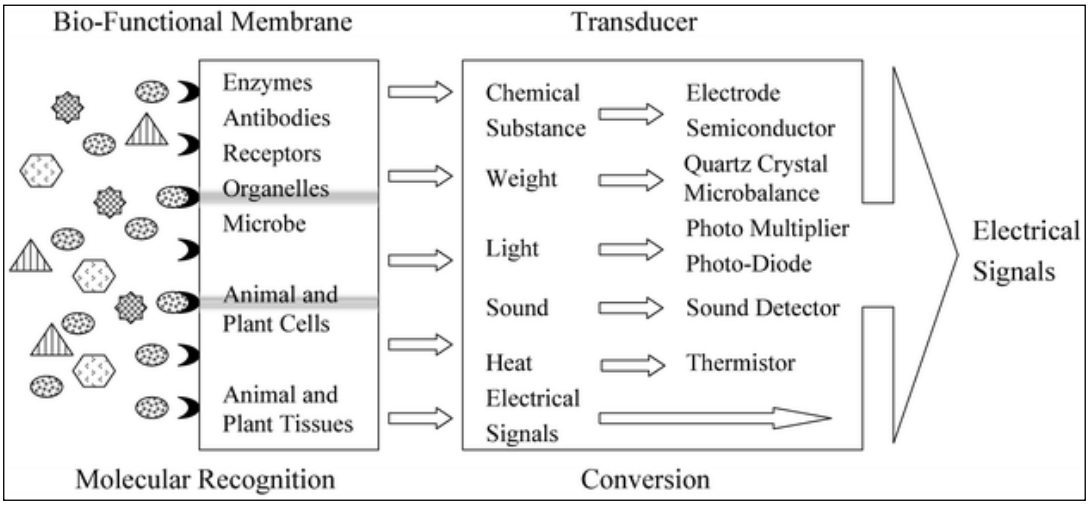

Figure 1.1 The principles of the biosensor. Reprinted with kind permission from Springer Science + Business Media from Analytical and Bioanalytical Chemistry, 'Current research activity in biosensors,' 377, 2003, p.447, H.Nakamura, Figure 1[5].

As shown in figure 1.1, a biosensor consists of two key components (a) a bio-functional membrane with various bio-specific ligands that serve the purpose of molecular recognition and (b) a transducer where the molecular recognition event

causes the generation of signals by different mechanisms which are eventually converted to electrical signals that can be easily read. The choice of the molecular recognition elements and method of transduction used in biosensors depends on the analyte of interest and the physical property to be measured. Molecular recognition elements impart selectivity to the biosensors and can range from antibodies, aptamers, nucleic acids, chemoreceptors, enzymes to larger entities such as whole cells, cell organelles and plant or animal tissue sections. These elements of biological recognition are usually immobilized directly onto or placed in close spatial contact with the transduction layer.

1.1.1. Methods of transduction in biosensors

The methods of transduction commonly used in biosensors can be classified into the following categories:

1. Electrochemical- This is the most popular method of transduction in the field of biosensor development[4]. Such devices are accurate and sensitive but simple and inexpensive to integrate. Depending on the method, electrochemical biosensors can be further classified as:
    1.1. Potentiometric sensors – These devices incorporate ion-selective electrodes, which sense the presence of active species and generates a potential which is proportional to the logarithm of the concentration of the

active species. These devices can measure changes in ion concentration and pH.

1.2. Amperometric sensors – These sensors apply a constant potential and monitor the current associated with the oxidation and reduction of the electroactive species involved in biorecognition. These sensors are fast, have high sensitivity and a wide linear range[4]. The response is directly proportional to the concentration of the analyte. However, the selectivity of these devices is determined by the redox potential of the electroactive species present and hence, susceptible to interferences. Amperometric and potentiometric transducers are the most commonly used techniques for electrochemical biosensing.

1.3. Conductimetric sensors – These sensors are based on the principle of change in conductivity of the medium associated with the generation of ionizable intermediates from uncharged substrates. The change in conductivity of the medium between two electrodes is detected. Conductimetric biosensors have not been widely used as they are usually non-specific and have a poor signal-to-noise ratio[1].

1.4. Impedimetric sensors – These biosensors are based on the principle that microbial metabolism results in an increase in both conductance and capacitance, causing a decrease in the impedance. Impedance is usually measured by a bridge circuit, with a reference module often included to

account for non-specific changes in the test module. This method is most indicated for the detection of microbes[1].

2. Optical – The interaction of the target molecule with the sensing moiety causes a change in the optical properties of the complex. These changes can be quantified by monitoring properties such as UV-Vis absorption, fluorescence/ phosphorescence, bio/chemiluminescence, reflectance, scattering, evanescent waves and refractive index. With advances in fiber optics, laser technologies and miniaturization of other optical components, biosensing by optical detection is gaining popularity. The potential to utilize the wide electromagnetic spectrum is also advantageous as it enables multiplexed detection.

3. Piezoelectric – In these transducers, the surface of a crystal is modified by the immobilizing biomolecules. The specific interaction of these biomolecules with the analyte of interest causes a change in the mass of the crystal, which is manifested as a change in the frequency of oscillation. This method of detection is advantageous for gas phase sensing but suffers from low sensitivity and non-specific binding in fluids[6].

4. Thermal – The change in energy (heat) in chemical reactions catalyzed by enzymes or microbes is monitored by such devices. This method of

transduction is suitable for miniaturization but requires complex instrumentation and lacks selectivity[1].

The above-mentioned methods simply provide an overview of the most commonly used sensing methods and do not constitute a comprehensive listing of transduction mechanisms. The advantages and disadvantages of the commonly used methods have been summarized in table 1.1. Though the applications listed pertain to the food and drink industry, they provide an idea of the types of analyses that each method is suited for.

Table 1.1 Types of transducers, their characteristics and application in the food industry. Reprinted from *Food Chemistry, 77*, L. D. Mello and L. T. Kubota, 'Review of the use of biosensors as analytical tools in the food and drink industries,' p.244, **2002** with permission from Elsevier[1].

Transducer	*Advantages*	*Disadvantages*	*Application*
Ion-selective electrode (ISE)	Simple, reliable, easy to transport.	Sluggish response, requires a stable reference electrode, susceptible to electronic noise.	Amino acids, carbohydrates, alcohols and inorganic ions
Amperometric	Simple, extensive variety of redox reaction for construction of the biosensors, facility for miniaturize.	Low sensitivity, multiple membranes or enzyme can be necessary for selectivity and adequate sensitivity.	Glucose, galactose, lactate, sucrose, aspartame, acetic acid, glycerides, biological oxygen demand, cadaverine, histamine, etc.
FET	Low cost, mass production, stable output, requires very small amount of biological material, monitors several analytes simultaneously.	Temperature sensitive, fabrication of different layer on the gate has not been perfected.	Carbohydrates, carboxylic acids, alcohols and herbicide
Optical	Remote sensing, low cost, miniaturizable, multiple modes: absorbance, reflectance, fluorescence, extensive electromagnetic range can be used.	Interference from ambient light, requires high-energy sources, only applicable to a narrow concentration range, miniaturization can affect the magnitude of the signal.	Carbohydrates, alcohols, pesticide, monitoring process, bacteria and others…
Thermal	Versatility, free from optical interferences such as color and turbidity.	No selectivity with the exception of when used in arrangement	Carbohydrates, sucrose, alcohols, lipids, amines
Piezoelectric	Fast response, simple, stable output, low cost of readout device, no special sample handling, good for gas analysis, possible to arrays sensors.	Low sensitivity in liquid, interference due to non specific binding.	Carbohydrates, vitamins, pathogenic microorganisms (e.g. *E. coli*, Salmonella, Listeria, Enterobacter), contaminants (e.g. antibiotics, fungicides, pesticides), toxic recognition as bacterial toxins.

1.2. Nanomaterials for bioanalysis

The trend towards miniaturization of analytical platforms presents the need for investigation and development of sensitive methods for the detection of trace analytes. In this context, there has been a resurgence of interest in the use of nanomaterials for biosensing applications. Nanoparticles are generally defined as structures between 1 and 100 nm in diameter[7]. These dimensions impart large surface-areas and many unique properties which can be exploited for the sensitive detection of analytes. The scope of this section, however, also includes some applications of particles that are in the sub-micron or micron size range. This section provides information, with an emphasis on bioanalytical applications, for four classes of nanomaterials: (a) quantum dots (b) liposomes (c) gold nanoparticles and (d) magnetic nanoparticles or beads.

1.2.1. Quantum dots

1.2.1.1. Properties of Quantum dots

Semi-conductors with all three dimensions in the ~1-10 nm size range are referred to as "quantum dots"[8]. Quantum dots (QDs) are an emerging class of fluorophores which find ever increasing applications in the fields of biological imaging and diagnostics. They are nanometer-sized crystals comprised of atoms of elements from groups II to VI (e.g., Cd, Zn, Se, Te) or III-V (e.g., In, P, As) in the periodic table[9]. The unique optical properties of QDs arise due to strong quantum confinement effects and present many advantages over conventional fluorophores.

Many of the organic dyes and protein-based fluorophores in current use suffer from drawbacks such as pH dependence, self-quenching at high concentrations, susceptibility to photo-bleaching, short-term aqueous stability, narrow absorption windows coupled to broad red-tailed emission spectra via small Stokes shifts, and short excited state fluorescent lifetimes[10]. On the other hand, QDs have high molar absorptivities and broad absorption spectra which allow efficient excitation of multiple QD-based fluorophores with a single excitation line. They have narrow and symmetric emission peaks and high quantum yields which make them ideally suited for multiplexed detection without crosstalk between different detection channels[11]. QDs are highly photostable which makes them ideal for ultrasensitive detection of biomolecules, possibly at the single molecule level. Semiconductor nanocrystals can be visualized by electron microscopy, which in conjunction with fluorescence detection, can provide information about the localization of these dots in a biological environment[12]. Compared specifically to an organic dye like rhodamine, QDs have been reported to be 20 times brighter, 100 times more stable against photobleaching and one-third as wide in spectral linewidth[13]. A comparison of the properties of organic fluorophores and quantum dots is presented in table 1.2.

Table 1.2 Comparison of the properties of organic/protein fluorophores and quantum dots[10]

Property	Fluorophores	Quantum Dots
Photophysical		
Absorption spectra	Variable/narrow generally a mirror of the emission spectra	Broad spectra, steadily increases towards the UV from the first absorption band edge
Molar extinction coefficients	Variable, Generally < 200,000$M^{-1}cm^{-1}$	High, 10-100 that of fluorophores
Emission Spectra	Broad, asymmetric red-tailed emission	Narrow-full width at half-maximum 25-40 nm for CdSe core materials
Maturation time	Needed for fluorescent proteins	NA
Effective Stokes shifts	Generally < 100 nm	>200 nm possible
Tunable emission	NA	Unique to QDs/ can be size-tuned from the UV to IR
Quantum Yield	Variable, low to high	Generally high, 0.2 to 0.7 in buffer depending upon surface coating
Fluorescent lifetime	Short < 5 ns	Long ~10-20 ns or greater
Spectral Range	Necessitates a different dye every 40-60 nm	UV-IR depending upon binary/ternary material Vis-CdSe
Photostability	Variable to poor	Excellent, strong resistance to photobleaching several orders of magnitude that of dyes
Multiphoton cross section	Variable to poor	Excellent >2-3 orders of magnitude that of dyes
Single-molecule capabilities	Variable	Excellent
FRET capabilities	Variable, mostly single donor-single acceptor configurations	Excellent donors, size tune emission to improve the overlap with an acceptor dye, single donor-multiple acceptor configurations possible
Multiplexing capabilities	Rare	Excellent, largely unexplored
Intermittency (blinking)	Negligible	Maybe problematic in isolated circumstances (single molecule tracking)
Chemical		
Chemical resistance	Variable	Excellent
Reactivity	Multiple reactivities commercially available	Limited conjugation chemistries availble
Mono-valent attachment	Easy	Difficult
Multi-valent attachment	Rare-mostly *bis*-functional	Good possibilities, can attach several molecules to QDs depending upon size
Other		
Physical size	< 0.5 nm	4-7 nm diameter for CdSe core material
Electrochromicity	Rare	Largely untapped
Cost effectiveness	Very good/multiple suppliers	Poor/2 commercial suppliers

1.2.1.2. QDs for biosensing

The first use of QDs for biological labeling was reported in 1998 by the groups of Alivisatos[14] and Nie[13]. Since then, QDs have been employed in different modalities for a wide range of biosensing applications including immunoassays[15], DNA detection[16], as ion-selective probes[17] and for in-vivo imaging[18]. Photoluminescence is the most commonly used mode for detection by QDs. The ability of QDs to function as highly efficient resonant-energy transfer-donors has also been widely exploited in assays involving binding events that turn the QD fluorescence "on" or "off [19-21]. A rather off-beat use of QDs involves the dissolution of QD label and subsequent detection of released ions by electrochemical means[16,22]. An excellent review of the biosensing applications of QDs was compiled by Sapsford and Pons[10].

Some of the most promising applications of QDs revolve around their potential for multiplexed detection and optical barcoding. Multiplexed detection with organic dyes is challenging on account of their broad emission bands and the overlap of absorption and emission spectra of different dyes. The narrow, symmetric emission bands of QDs coupled with their broad absorption, enables multiple types of QDs to be excited by a single light source. This feature is particularly advantageous for miniaturized detection platforms as it simplifies the construct. However, very few reports exist about the detection of multiple analytes with different QDs. The potential for multiplexed detection was demonstrated in a recent report where five differently colored QDs were used for simultaneous probing of a tissue section[23].

1.2.1.3. Disadvantages of QDs

Inspite of the great interest in QDs for biosensing, very few quantitative applications have been actually realized till date[24]. This is because most QDs suffer from several different kinds of instabilities, such as[24] :

1. Aggregation of QDs due to non-optimal surface chemistry, resulting in loss of colloidal stability during biolabelling applications.
2. Blue shift and bleaching of the QD spectra due to photooxidation in air, which leads to an effective shrinkage of the QD core (can be diminished by suitable shells).
3. Photoblinking of single QDs due to photoionization by an Auger process.
4. "Photobrightening" of QDs on continuous excitation due to traps within the nanocrystals.

1.2.2. Liposomes

Liposomes were first described by Bangham in 1965 while studying the nature of cell membranes[25.] Liposomes are essentially spherical vesicles, comprised of one or more phospholipid bilayers surrounding an aqueous cavity. The phospholipid molecules undergo self-assembly in an aqueous environment such that the hydrophobic tails of the lipids form the bilayer while the polar head groups are oriented towards the external medium and inner cavity. Phospholipids with different polar headgroups can be used to reduce aggregation of the liposomes or to introduce

functional groups for further bioconjugation. Cholesterol is often included with the membrane phospholipids to reduce the permeability of the membrane towards the encapsulated materials. Hydrophobic substances may be incorporated into the lipid bilayer while the aqueous cavity may encapsulate different hydrophilic substances such as drugs[26], fluorophores[27], enzymes[28], electrochemical markers[29] etc. This makes liposomes versatile enough to be used in a variety of applications, such as a model for cell membrane[30], for drug delivery[31], in cosmetic formulations[32,33] and as analytical tools[34].

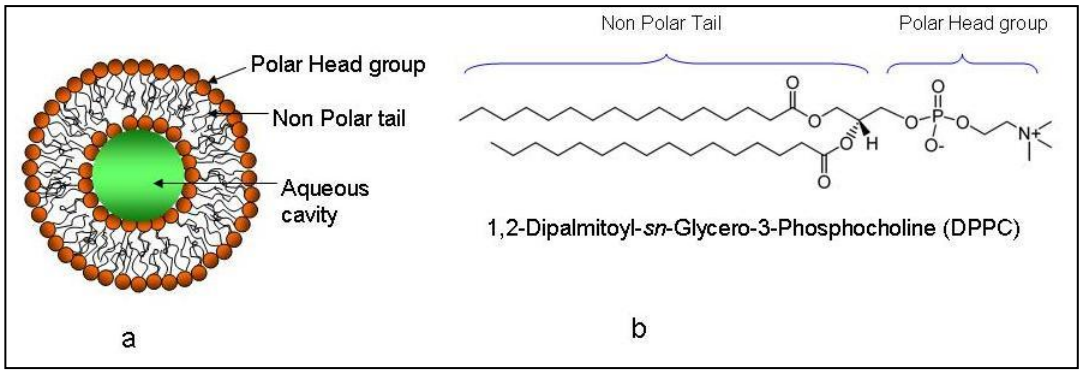

Figure 1.2 a) Structure of a unilamellar liposome showing the orientation of the polar head groups and the non-polar tails constituting the lipid bilayer **b)** Chemical structure of a lipid commonly used to prepare liposomes (DPPC), depicting the polar and non-polar regions

1.2.2.1. Classification of liposomes

Liposomes can be classified depending on the number of lipid bilayers contained in the vesicles[35]. Small unilamellar vesicles (SUVs) contain one bilayer shell and range in size from 25-50 nm. Large unilamellar vesicles (LUVs) and giant unilamellar vesicles (GUVs) also contain a single bilayer but range in sizes from 100

nm-1µm and 1µm-200µm, respectively. Multi-lamellar vesicles (MLVs) contain multiple, concentric bilayers and usually, range in size from 0.1-15µm. Multi-vesicular vesicles (MVVs) range in size from 1.6 -10.5µm and contain several smaller liposomes encapsulated within them. Figure 1.3 shows a schematic of the different types of liposomes.

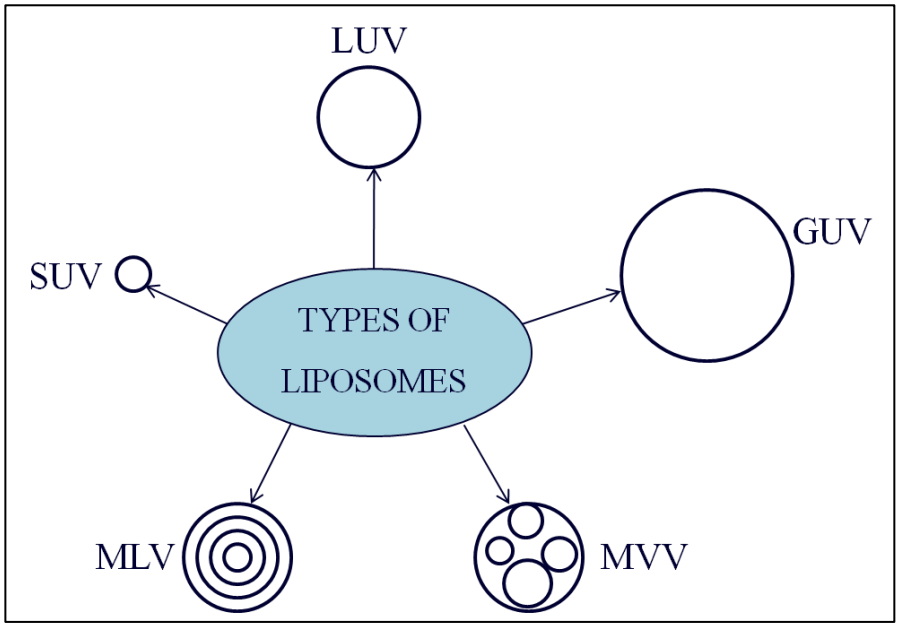

Figure 1.3 Types of liposomes based on the number of bilayer shells. SUV: Small unilamellar vesicle; LUV: Large unilamellar vesicle; GUV: Giant unilamellar vesicle; MVV: Multi-vesicular vesicle; MLV: Multi-lamellar vesicle.

1.2.2.2. Methods of liposome preparation

The methods of liposome preparation can be divided into the following four basic groups depending on the mechanism of vesicle formation[25] :

1. Mechanical methods – This includes the thin film hydration method where a mixture of phospholipids, sterols and other amphiphilic molecules are

dissolved in an organic solvent, followed by the removal of the solvent at low pressure in a rotary evaporator. A dry film of lipids is deposited on the walls of the flask, which is then hydrated by adding a buffer and agitating the flask. The aqueous suspension must be heated above the phase transition of the lipids in order for the liposomes to form. This results in the formation of MLVs which can be homogenized to by extrusion through polycarbonate membranes. SUVs can be formed by ultrasonication of the aqueous dispersion of the phospholipids with a probe or bath sonicator.

2. Methods based on replacement of organic solvents – This category includes the commonly used method of reverse-phase evaporation in which an aqueous solution of markers is added to a mixture lipids dissolved in organic solvents. The mixture is vortexed to form an emulsion, followed by the removal of the organic phase at a controlled reduced pressure (by means of a rotary evaporator) to yield a gel-like suspension of liposomes.

    The techniques of ether-vaporization or solvent-injection involve the injection of a mixture of lipids in an organic solvent (diethyl ether, ethanol etc.) into an aqueous solution. This results in the formation of unilamellar vesicles with well-defined size distributions and high volume trapping efficiencies. The organic solvent is subsequently removed by elevation of the temperature above its boiling point.

3. Methods based on detergent removal – This category includes the detergent-dialysis method. An aqueous solution of markers is added to a mixture of lipids

dissolved in an organic solvent. The removal of the organic solvent at low pressures results in the formation of a lipid film. The lipids are solubilized using detergents at their critical micelle concentration and results in the formation of lipid/detergent micelles. Upon the removal of the detergent by dialysis, the micelles become progressively richer in phospholipids and combine to form SUVs or LUVs (depending on experimental conditions).

4. Methods relying on size transformation or fusion of preformed vesicles – In the freeze-thaw method, previously formed MLV dispersions are subjected to repeated cycles of quickly freezing (in liquid nitrogen) and thawing (in warm water). This causes the rupture and reformation of MLV bilayers, resulting in liposomes with fewer bilayers and greater encapsulation volumes.

   The dehydration-rehydration method involves the mixing of buffer-loaded SUVs with a marker or drug-containing solution. This mixture is dried using vacuum or freeze-drying, causing the small vesicles to fuse to form large aggregates that encapsulate the marker or drugs within. Upon controlled hydration, LUVs with very high encapsulation efficiencies can be formed. The majority of the liposomes used for analytical purposes are prepared by the methods of thin film hydration or reverse-phase evaporation. Sizing or homogenization is often performed after synthesis by the extrusion through membranes with defined pore-sizes. Gel chromatography may be used to obtain monodisperse fractions of liposomes as well as remove unencapsulated

materials. Ultracentrifugation, dialysis and ultrafiltration are some of the commonly used methods for removal of unencapsulated molecules.

1.2.2.3. Characterization of liposomes

Prior to their application in analysis, liposomal preparations need to be characterized for:

1. Average size and its size distribution – Dynamic light scattering techniques (DLS) have been widely used for characterizing the average size and polydispersity of liposomes. These techniques are also known as photon-correlation spectroscopy (PCS). In this technique, the Brownian motion of the liposomes is observed using a laser and the intensity fluctuations of the scattered light are correlated by mathematical functions to extract the diffusion co-efficient. The diffusion co-efficient is used to calculate the size of the liposomes. Morphological features, such as the lamellarity of the liposomes, may also be determined by freeze-fracture electron microscopy (cryo-TEM)[36].
2. Encapsulation efficiency – The amount of encapsulated marker relative to the total amount of marker or lipids used in preparation has been defined in various ways[25]. These encapsulation parameters are elucidated by measurement of the marker released after complete lysis of the liposomes and relation of this quantity to the total amount of marker or lipid used.

1.2.2.4. Liposomes and bioanalysis

Although liposomes have been widely studied for their applications in the field of drug delivery, they have found limited use as labels in immunoassays. By virtue of their ability to encapsulate numerous labeling molecules per vesicle, liposomes can instantaneously amplify signals generated by an immunocomplex formation by several orders of magnitude[37-39]. Liposomes can be adapted for application in a variety of immunoassays since the phospholipid bilayers can be easily modified, pre or post synthesis, with various functional groups or molecules for biorecognition such as antibodies or DNA. Liposomes, encapsulating various markers, have been used for the detection of a variety of analytes in immunoassays- polychlorinated biphenyls[27], herbicides[40], toxins[41,42], nucleic acid sequences[29] and proteins[43], to name a few. A detailed review of liposome based immunoassays has been compiled by Edwards et al.[34]. All of these assays have employed fluorescent dyes, enzymes or electrochemical markers. The main drawback of using an organic dye for encapsulation is that they tend to photobleach easily, while enzymatic labels introduce an extra incubation step, thereby lengthening the analysis time. Electrochemical markers offer limited potential for multiplexed detection. In this scenario, the use of encapsulated QDs as a marker holds promise for highly sensitive, multi-analyte detection. The investigation of QD-encapsulating liposomes as fluorescent labels has been described in chapter 2 of this dissertation.

1.2.3. Gold nanoparticles

1.2.3.1. Properties of gold nanoparticles

Historically, gold nanoparticles (AuNPs), also known as colloidal gold, have been used for purposes as diverse as a colorant of glass ("Purple of Cassius"), ceramics and silk and in medieval medicine as tonics and elixirs. However, the scientific beginning of the chemistry of gold colloids can be traced back to the year 1857 when Michael Faraday performed his famous experiments to generate gold colloids[44]. In recent times, AuNPs have been investigated for their role in a range of fields such as chemical catalysis, non-linear optics, supramolecular chemistry, charge storage systems, molecular recognition and bio-sensing[24]. The widespread use of AuNPs is enabled by their unique size-dependant physical, chemical and electronic properties. For the purposes of bioanalysis, the optical properties of AuNPs are most widely exploited.

The most striking optical property of AuNPs is the phenomenon of surface plasmon resonance (SPR) which is manifested as a deep-red color in AuNP colloids. According to the Mie theory[45], when the wavelength of light is much larger than the AuNP size, SPR arises due to the induction of collective oscillations of the free electrons on the AuNP surface by the electromagnetic field of incoming light[46]. As shown in figure 1.4, incoming light waves interact with AuNPs, causing polarization of the electron density to one surface and then to the other surface, in resonance with the frequency of the light beam[47]. Since the oscillation of electrons is localized on the AuNP surface, it is referred to as SPR. The oscillation frequency is in the visible range

for AuNPs, giving rise to a surface plasmon band (SPB) – a broad absorption band centered at about 520nm. The SPB is absent for AuNPs smaller than 2 nm in diameter and as well as for bulk gold while AuNPs ranging in size from 9 to 99 nm exhibit distinct SPB[48]. The SPB is found to depend on the shape and size of the particles, the inter-particle distance and the dielectric constant of the surrounding medium[47,49].

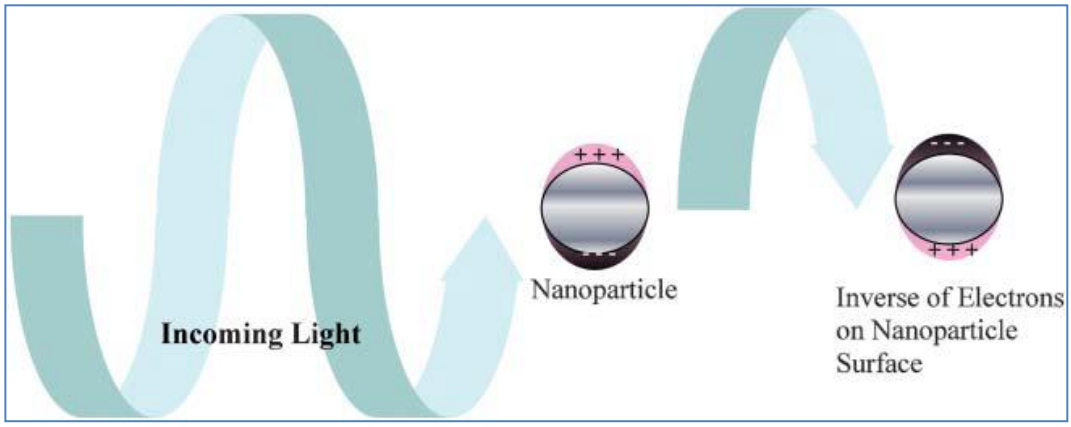

Figure 1.4 Origin of surface plasmon resonance due to coherent interaction of the electrons in the conduction band with light. Reproduced with permission from Eustis, S.; EI-Sayed, M. A. *Chemical Society Reviews* 2006, 35,209-21. Copyright 2006, RSC Publishing[47].

AuNPs exhibit both absorption and scattering characteristics which can be revealed by spectroscopic techniques. The SPB of AuNPs show very high extinction co-efficients (ranging from 10^6 -10^9 M^{-1} cm^{-1})[50], making them strong absorbers and scatterers. The proportion of light absorbed or scattered by AuNPs largely depends on their size. Absorption is predominant in AuNPs smaller than 20 nm in diameter, while the ratio of scattering to absorption increases with an increase in size of the particles[46]. The strong SPB of AuNPs in the visible range and its sensitivity to factors such as the dielectric constant of surrounding medium lend them to many applications in

biological labeling and sensing. The high scattering cross-section of large AuNPs is useful for imaging techniques based on light scattering.

Gold nanorods (AuNRs) are another form of gold nanostructures that are gaining popularity. AuNRs have two plasmon resonance bands, the transverse band and the longitudinal band, corresponding to electron oscillations in the short and the long axes of the nanorod, respectively[47,51]. The absorption of the longitudinal band can be tuned from visible to the near infrared region (NIR) as a function of the aspect ratio of the nanorods[52]. AuNRs have certain distinct advantages over AuNPs such as NIR light compatibility for in-vivo applications and the possibility of double detection using independent interrogation of the two SPR bands of a single nanorod[52].

1.2.3.2. Synthesis and functionalization of AuNPs

The most popular method for the synthesis of spherical AuNPs for biological applications is the citrate reduction method of Turkevitch et al.[53]. The advantage of this method is that it is straightforward, involves no organic solvents, has a high-yield and yields a stable aqueous colloid. The Turkevitch method involves the reduction of an aqueous solution of chloroauric acid ($HAuCl_4$) with sodium citrate. The negatively citrate ions are adsorbed onto the surface of the AuNPs and serve to stabilize the colloid from aggregation by electrostatic repulsion of the charged particles. The use of citrate ions as a capping agent enables easy subsequent replacement by other capping agents, e.g. thiolated DNA, which can impart additional functionalities such as binding

to the biological molecule of interest[49]. Typically, this method yields AuNPs about 20 nm in diameter[48]. However, variation of the trisodium citrate-to-gold ratio has been reported to yield AuNPs of predetermined sizes between 16 and 147 nm[54]. Recent modifications of the Turkevitch method enable control of AuNP sizes within the 9-120 nm range as well as yield improved size distribution of the AuNPs[55]. A number of other methods have also been investigated for the synthesis of water-soluble AuNPs with different surface functionalities that can be used for biological diagnostics[56-59].

For diagnostic applications, AuNPs need to be functionalized with various molecules capable of biospecific interactions. This involves the conjugation of various ligands capable of biomolecular recognition via bifunctional linkers. Most protocols favor the use of linkers with a thiol group at one end due to the ease with which gold-sulfur bonds are formed. Some of the most popular biomolecules (and associated chemistries) that have been used for the functionalization of AuNPs are:

1. Oligonucleotides –The most common method for immobilization onto the AuNP surface is by the use of a thiol-modified oligonucleotide which can be readily synthesized or procured commercially[60-62].
2. Antibodies – Antibodies are usually conjugated to AuNPs by means of physical adsorption[63-65] while methods of covalent attachment are used less frequently[66, 67].
3. Carbohydrates – Schemes for the conjugation of carbohydrates to AuNPs usually involve covalent bonding using various thiolated linkers[68-70].

4. Biological pairs and miscellaneous bioligands – Biological pairs such as the streptavidin-biotin have been used for the conjugation of biomolecules to AuNPs[71]. A variety of other molecules, such as biotin[72], peptides[73] and enzymes[74] have also been used for the modification of AuNPs.

1.2.3.3. Bioanalytical applications of AuNPs

The use of the enhanced optical properties of AuNPs for bioanalysis can be broadly classified into four categories[47] :

1. Color changes of AuNP on aggregation – AuNPs functionalized with ssDNA (or other biomolecules) undergo aggregation in the presence of target analyte and exhibit a change in color[61, 75, 76].
2. Fluorescence-based methods with AuNPs as a quencher – AuNPs can quench the fluorescence of organic dyes or QDs when in close proximity to the surface. The presence of an analyte affects the separation between the AuNPs and fluorophores, thereby modulating the fluorescence signal[62, 77].
3. Enhanced Rayleigh (Mie) scattering – The SPR scattering of AuNPs increases with an increase in the size of the nanoparticle, such as when they aggregate upon binding to a target. This enhanced scattering can be observed by dark field microscopy and used to detect abnormalities in tissues and cells[78,79].
4. Surface enhanced raman scattering (SERS) of adsorbed molecules – In SERS, the Raman vibrational modes of a molecule located in close proximity to a nanosized metal surface are strongly enhanced, providing structural and orientational

information about the adsorbate[80]. Due to the signal enhancement (by several orders of magnitude), SERS has found widespread use in biological systems[46,80].

1.2.4. Magnetic particles

1.2.4.1. Properties of magnetic particles

Magnetic particles , in the micrometer and nanometer size ranges, are being increasingly used in a multitude of different applications such as magnetic fluids, catalysis, data storage, environmental remediation, magnetic separation, magnetic resonance imaging (MRI), hyperthermic treatments for malignant cells, site-specific drug delivery and recently, as labels in biosensors[81-83]. Most applications ideally call for particles that are in the 10-20 nm size range (depending on the material) and hence, superparamagnetic in nature[82]. Each particle in this size range behaves as a single magnet and shows a fast response to applied magnetic fields, with negligible remanence (residual magnetism) and coercivity (magnetic field required to bring magnetization to zero)[82]. Thus, superparamagnetic particles can be easily manipulated with external magnetic fields and show minimal aggregation due the absence of magnetic forces between the particles. These properties make superparamagnetic nanoparticles attractive for a broad range of biomedical applications.

Magnetic nanoparticles have a very high surface area to volume ratio which leads to instability over longer periods of time. Such particles tend to aggregate readily in order to reduce the surface energy. The large surface area also renders these nanoparticles highly chemically active and prone to oxidation or hydrolysis, resulting

in loss of magnetism and colloidal stability. Hence, it is essential to stabilize these particles by additional coating with organic layers of surfactants or polymers, or shelling with inorganic layers such as carbon or silica[82]. The additional coating can often be further modified by ligands of choice to tailor the particles for specific applications.

Magnetic nanoparticles have been synthesized with different compositions and phases such as iron oxides (Fe_3O_4 and γ-Fe_2O_3), pure metals (such as Fe, Co and Ni), spinel-type ferromagnets (such as $MgFe_2O4$, $MnFe_2O4$, and $CoFe_2O4$) and alloys (such as $CoPt_3$ and FePt)[82]. The most commonly used magnetic materials for biomedical applications are particles comprised of iron oxides such as magnetite (Fe_3O_4) or its oxidized form maghemite (γ-Fe_2O_3)[84]. Their biocompatibility makes them suitable for *in-vivo* application. Stable preparations of magnetic particles in the micron and submicron sizes are readily available from a number of commercial suppliers. However, since they are often comprised of a mixture of metal oxides, their magnetic properties may not be well-defined and reproducible[85]. Pure metals, on the other hand, are advantageous in applications that benefit from a homogeneous composition of the magnetic core (e.g. use of magnetic particles as labels as described in a subsequent chapter). However, toxicity concerns associated with Co and Ni precludes their application *in-vivo*. These particles are highly susceptible to oxidation, necessitating the introduction of additional coating layers to improve the chemical stability[84, 85].

For the detection of magnetic bead labels by ferromagnetic resonance (FMR) as described in chapter 4 of this dissertation, magnetic nanoparticles with a Co core were chosen as labels since Co has a higher magnetization of 1400 emu/cm than that of Fe_3O_4 at 480 emu/cm,(measured in bulk materials)[83]. As shown in figure 1.5 (b) and (c), the Co cores were shelled with a silica layer to improve their stability and enable biomolecule conjugation. However, the instability of the nanoparticles in aqueous media hampered further experiments. Hence, commercially available magnetic particles (MagSense and Nanomag-D), comprised mainly of magnetic oxides, were used to obtain preliminary data.

1.2.4.2.Synthesis and functionalization of magnetic particles

Co-precipitation is the most commonly employed method for the synthesis of iron oxide (either Fe_3O_4 or γ-Fe_2O_3) nanoparticles. Aqueous solutions of Fe^{2+}/Fe^{3+} salts are co-precipitated by the addition of a base under inert atmosphere at room temperature or elevated temperatures[82]. A black precipitate of magnetite (Fe_3O_4) is formed. The overall chemical reaction may be written as[86]:

$$Fe^{2+} + 2Fe^{3+} + 8OH^- \rightarrow Fe_3O_4 + 4H_2O \qquad [1]$$

The size, shape and composition of nanoparticles depends on the type of salts used, the Fe^{2+} and Fe^{3+} ratio, pH and ionic strength of the media[86]. The magnetite thus formed is susceptible to oxidation and reacts in the presence of oxygen, as follows:

$$Fe_3O_4 + 0.25O_2 + 4.5H_2O \rightarrow 3Fe(OH)_3 \qquad [2]$$

Oxidation of magnetite adversely affects the physical and chemical properties of the nanoparticles. Hence, the nanoparticles produced by reaction [1] are coated with a protective organic or inorganic layer during the precipitation process. Organic coatings include non-polymeric materials like long chain fatty acids and polymers (both synthetic and natural) such as polystyrene and gelatin[86]. Inorganic coatings include gold and silica, which also enable the subsequent conjugation of biomolecules.

Cobalt nanoparticles can be synthesized by the commonly used method of borohydride reduction[85, 87, 88]. This synthesis involves the reduction of cobalt chloride by sodium borohydride in an aqueous solution containing citric acid. The reduction of cobalt ions to metallic cobalt proceeds according to the following reactions[88]:

$$2CoCl_2 + 4NaBH_4 + 9H_2O \rightarrow Co_2B + 4NaCl + 12.5H_2 + 3B(OH)_2 \qquad [3]$$

$$4Co_2B + 3O_2 \rightarrow 8Co + 2B_2O_3 \qquad [4]$$

The reduction of $CoCl_2$ with $NaBH_4$ yields ultrafine particles of Co_2B. When exposed to oxygen, a sacrificial reaction occurs in which boron is oxidized while cobalt is reduced, leading to the formation of metallic cobalt. In the first step, a nucleation burst occurs followed by growth of the nuclei by capture of additional atoms. In the second step, depending on the reaction conditions, the nuclei undergo aggregation to form larger particles together with a narrowing of the size distribution[88]. The size of the nanoparticles is determined by the amount of oxygen present in the solution together with the citrate/Co^{2+} molar ratio. The citrate ions prevent further growth through double-layer repulsion between negatively charged

cobalt nanoparticles[85]. A silica shell is deposited immediately following the precipitation of the cobalt cores by means of an ethanolic solution of tetraethyl orthosilicate (TEOS). TEOS is hydrolyzed to deposit a silica shell on the cobalt cores. The silica shell protects the core from oxidation and offers potential for facile conjugation of biomolecules. Figure 1.5(a) depicts a schematic of the synthesis of cobalt nanoparticles by the method of borohydride reduction while figure 1.5(b) and (c) show images of such nanoparticles obtained by electron microscopy.

A wide variety of functionalization strategies have been employed to stabilize nanoparticles and render them biocompatible. Functionalization, often, serves an additional purpose by introducing end groups that can be used for grafting additional moieties onto the nanoparticle surface. Surface modification of nanoparticles by means of surfactant addition or surfactant exchange is very common[89]. Various types of coatings have been investigated for this purpose. Polymeric coating materials such as lipids, dendrimers, proteins, gelatin, dextrans, polyethylene glycol (PEG), poly (lactic-co-glycolic acid) (PLGA) or poly (vinyl alcohol) (PVA) have been commonly employed. Silica and silanes are popular inorganic coating materials for nanoparticles[86, 87]. In a few instances, bifunctional molecules, such as 2, 3-dimercaptosuccinic acids (DMSA) and dopamine were also investigated for use in nanoparticle functionalization[89].

Magnetic nanoparticles can be tailored for specific targets by grafting of various biological molecules such as antibodies, proteins, targeting ligands, etc by covalent coupling via amide or ester bonds. Some commonly used linker molecules

used to attach hydrophilic nanoparticles to bio-specific molecules are 1-ethyl-3-(3-dimethylaminopropyl) carbodi-imide hydrochloride (EDC), N-succinimidyl 3-(2-pyridyldithio) propionate (SPDP), N-hydroxysuccinimide (NHS) and N, N´ methylene *bis* acrylamide (MBA)[86].

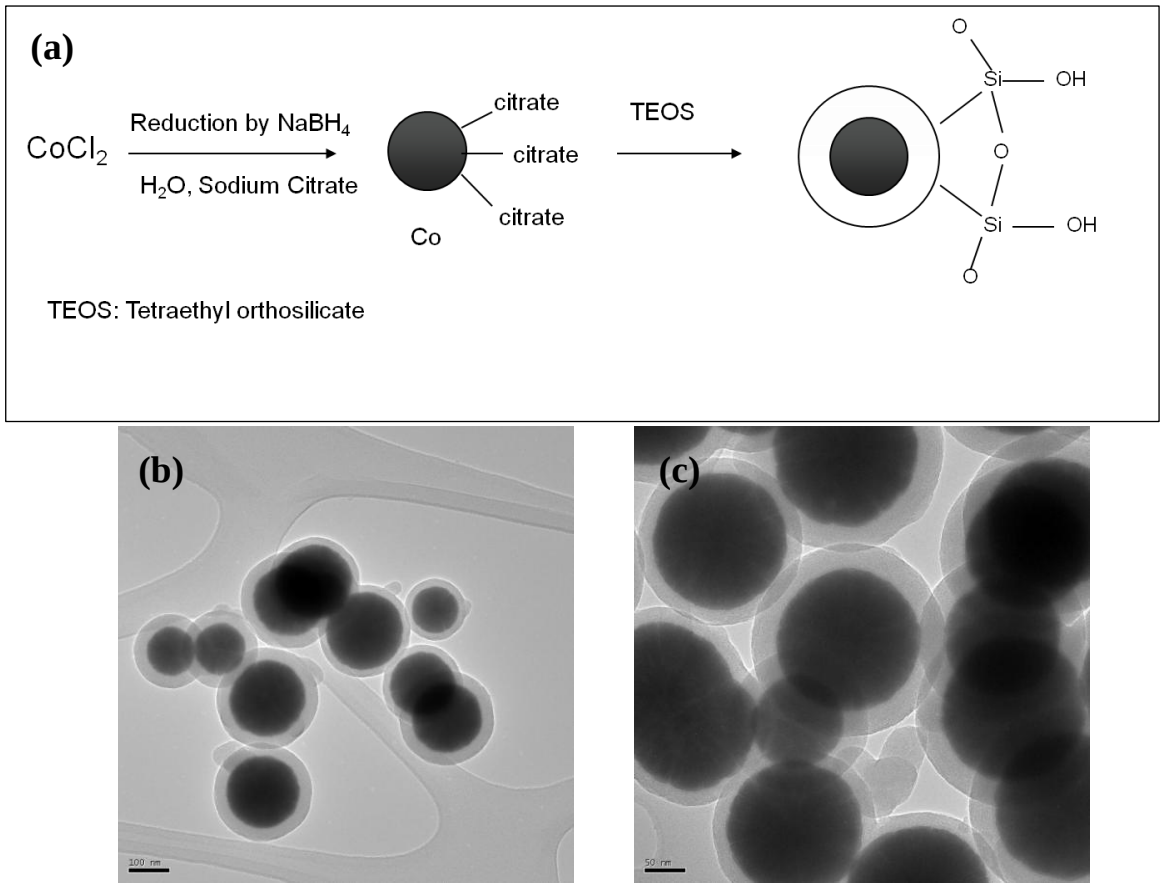

Figure 1.5 (a) Schematic of the synthesis of cobalt-silica core-shell nanoparticles by the borohydride reduction method. **(b)** and **(c)** TEM images of cobalt-silica core-shell nanoparticles at different magnifications.

1.2.4.3. Magnetic particles as labels in biosensors

Magnetic particles of micro and nano dimensions have found a host of applications in the biomedical arena, ranging from tissue repair, drug delivery,

hyperthermic therapies and magnetofection[86]. In the late 1990s, magnetoelectronics emerged as one of the several new technologies for biosensor development[90]. This involves the use of bio-functionalized micrometer or nanometer-sized magnetic labels which can be detected by various methods using high-sensitivity microfabricated magnetic-field sensors. Superconducting quantum interference devices (SQUID), magnetoresistive sensors and Hall sensors use magnetometers and can be used to directly detect magnetic particles[91]. Magnetic resonance-based techniques, on the other hand, use magnetic nanoparticles as proximity sensors to accelerate the relaxation rate of neighboring water molecules. This technique is analogous to magnetic resonance imaging (MRI), which is used to look inside the human body, and has been dubbed diagnostic magnetic resonance (DMR) [91]. There are some instances of SQUID and Hall sensors in literature[92-95].However, magnetoresistive sensors and DMR have been used to detect a wide variety of target molecules and have been extensively reviewed[83, 90, 91].

1.3. Chitosan for bioanalytical applications

The integration of biological components into sensing systems for the development of integrated biosensors continues to present significant challenges. The fragile nature of biological molecules together with their tendency to bind non-specifically to surfaces makes this a complex step. The harsh processing conditions and reagents used in traditional microfabrication are often incompatible with the biological components. Further, patterning biomolecules in defined areas of a sensor

device can be time-consuming and tedious. Hence, many alternative materials as well processes have been explored which could allow the facile integration of biomolecules into sensor devices. Some approaches that have been used to accomplish this are the use of surface immobilized polymers, self-assembled monolayers and polyelectrolyte bilayers[96-99]. The naturally abundant polymer, chitosan, is a very promising material in this context.

Chitosan is derived from chitin. Chitin, poly (β-(1→4)-N-acetyl-D-glucosamine), is a natural polysaccharide and is the structural component of the shells of crustaceans and insects. It is the second most widespread natural polymer on earth after cellulose[98]. Chitosan is a linear β-1, 4-linked amino polysaccharide and is obtained by the partial deacetylation of chitin. When the degree of deacetylation of chitin reaches about 50% (depending on the origin of the polymer), it becomes soluble in aqueous acidic media and is called chitosan[100]. Due to incomplete deacetylation of chitin, chitosan is actually a copolymer composed of glucosamine and *N*-acetylglucosamine[101]. The molecular weight of chitosan ranges from 300 kD to over 1000 kD, depending on the source and preparation procedure. The degree of deacetylation of commercially available chitosan ranges from 50 to 90%[102]. The structural formulae of chitin and chitosan are depicted in figure 1.6.

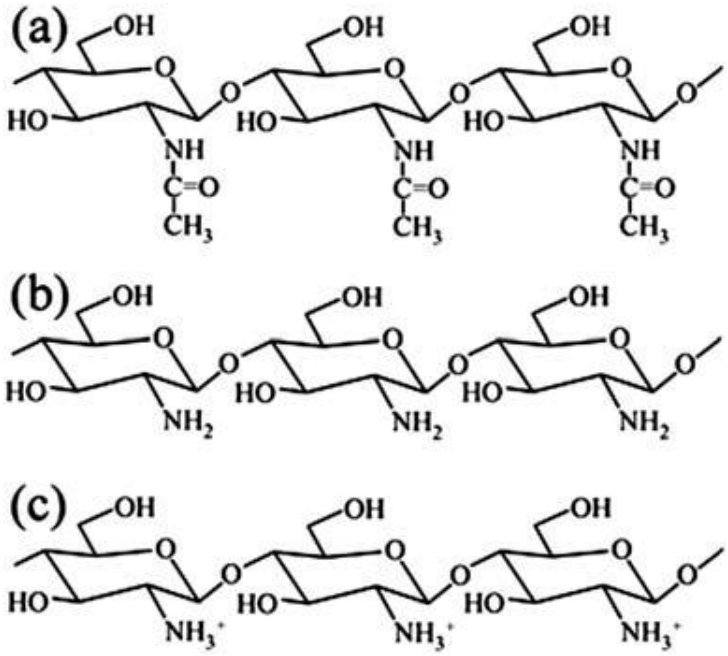

Figure 1.6 Structural formulae of chitin and chitosan showing the three possible states of the amine group: (a) chitin, amine group acetylated; (b) chitosan, amine group free; (c) chitosan, amine group protonated[98]. (Reproduced *by permission of The Royal Society of Chemistry*.)

Chitosan is a biocompatible and biodegradable polymer, which displays a number of interesting properties relevant for bioanalysis. Most of these properties result from the presence of a primary amine group on almost every subunit of the polymer. These amine groups have a pKa of about 6.5[98], which is manifested in the pH dependant solubility of chitosan. Under highly acidic conditions (pH < 6.5), the amine groups are protonated (figure 1.6 (c)) and the positive charge renders chitosan soluble. At neutral or basic pH, the amines are increasingly deprotonated and chitosan becomes insoluble. Hence, chitosan can form stable films under neutral or basic conditions. The pH dependent solubility allows stable chitosan films to be deposited on various surfaces via methods such as solution casting, precipitation,

electrodeposition and spinning. (Chitosan films have also been formed via imprinting). Chitosan films thus formed can be dissolved and removed by a mildly acidic wash and the sensing surface can be regenerated, in theory, multiple times. The structure of the film formed is dictated by the molecular weight of chitosan and its degree of deacetylation and the deposition conditions [98].

Another important attribute of chitosan from a bioanalytical perspective is its ability to be modified with various biomolecules. The presence of the primary amine groups enables molecules such as enzymes, DNA and antibodies to be covalently attached to the surface. Chitosan films can also be modified (especially by negatively charged molecules) by physical means such as surface absorption or entrapment within the polymeric network. Chitosan chains can also be covalently crosslinked with each other, improving the strength and chemical resistance of the resulting film[98]. Table 1.3 provides a comprehensive listing of the different molecules and nanostructures that have been used to modify chitosan surfaces, indicating the versatility of this natural polymer.

Table 1.3 Survey of chitosan modifications reported in literature[98]. (*Reproduced by permission of The Royal Society of Chemistry*.)

Modifying substance	Purpose of modification
Proteins	
Collagen	Scaffolds for cell assembly
Gelatin	Used as a model protein
Gelatin	pH responsive hydrogels
Green fluorescent protein (GFP)	Used as a model protein
Hemoglobin	Direct electrochemistry of proteins
Myoglobin	Direct electrochemistry of proteins
Protein A	Attachment of antibodies
Protein G	Attachment of antibodies
Enzymes	
Acetylcholinesterase	Pesticides detection
Alcohol oxidase	Ethanol detection
Catalase	Hydrogen peroxide detection
Creatinine iminohydrolase	Creatinine detection
Glucose dehydrogenase	Glucose detection
Glucose oxidase	Glucose detection
Glutamate oxidase	Glutamate detection
Horseradish peroxidase	Hydrogen peroxide detection
Laccase	Catechol detection
Lactate oxidase	Lactate detection
Lipase	Processing of lipids
Polyphenol oxidase	Phenol detection
S-adenosylhomocysteine nucleosidase (Pfs)	Studies of bacterial signaling
Sulfite oxidase	Sulfite detection
Tyrosinase	Phenol detection
Urease	Urea detection
Uricase	Uric acid detection
Antibodies	
Alginate-factor B	Detection of factor B in blood plasma
Anti-CEA	Detection of carcinoembryonic antigen
Carbohydrate antigen 19-9	Detection of carbohydrate antigen
Immunoglobulin G	Used as model antibody
DNA	
dsDNA	Effect of drugs on dsDNA
ssDNA	Sequence specific detection of DNA (hybridization)
Nanostructures	
Carbon nanotubes	pH responsive hydrogels
Carbon nanotubes	Glucose detection
Carbon nanotubes	Fabrication of composite films
Carbon nanotubes	Insulin detection
Fe3O4 nanoparticles	Phenol detection
Gold nanoparticles	Pesticides detection
Gold nanoparticles	Glucose detection
Gold nanoparticles	Hydrogen peroxide detection
Metallophthalocyanines	Dopamine detection
Tobacco mosaic virus	Assembly of nanoscale materials
Vesicles (liposomes)	Drug delivery, chemical signaling

Table 1.3 (*Contd.*)[98] (*Reproduced by permission of The Royal Society of Chemistry.*)

Modifying substance	Purpose of modification
Polymers	
Cellulose	Electroactive polymers for actuation
Poly(acryl amide)	pH responsive hydrogels, drug delivery
Poly(diallyldimethylammonium chloride)	Temperature and pH responsive hydrogels
Poly(o-ethoxyaniline) and poly(methacrylic acid)	Impedance spectroscopy for copper ion detection
Polyaniline	Electroactive polymers for actuation
Polyvinyl alcohol (PVA)	pH responsive hydrogels
Dyes	
Acetyl yellow 9	Permeability control
Azure C	NADH detection
Lucifer yellow VS	Permeability control
4-(2-Pyridylazo)resorcinol	Detection of Cobalt
Procion brown, procion green	Affinity ligand for lysozyme purification
Prussian blue	Detection of glucose, glutamate, galactose
Redox salts	Glucose detection
Thionine	Optical pH sensor
Toluidine blue O	NADH detection
Tungsten oxide (WO3)	Electrochromic films

The abundant primary amine groups of chitosan also impart the property of pH dependent swelling. The pH of the solution determines the extent of protonation of amine groups on chitosan and thereby, the charge on the polymer chains. This charge affects the electrostatic repulsion between the polymer chains and in turn, the volume occupied. This swelling property can be exploited for actuation or controlled drug release[98].

The properties of chitosan make it conducive for incorporation in both optical and electrochemical sensor systems. Unmodified chitosan films are transparent in nature. Crosslinking of chitosan slightly increases its absorbance in the UV region but

is still low enough in the visible region to be used in optical sensors[98]. On the other hand, wet films of chitosan are porous and easily permeable to ions, enabling the design of electrochemical sensors containing chitosan-coated electrodes [98]. The mechanical properties of chitosan vary depending on the method of preparation. However, since it is commonly employed as a sensor coating or layer, as opposed to a structural component, the mechanical properties of chitosan do not significantly affect the sensor design.

In the context of bioanalysis, chitosan has been employed both as a substrate for the immobilization of biological components as well as an integrated bio-recognition layer within sensors. Co et al. have demonstrated the ability to sequentially pattern two different kinds of cells on chitosan films by the method of microcontact printing[103]. In 2006, Karp et al. used a photolithographic method to pattern a photocrosslinkable derivative of chitosan to create micropatterns for cellular attachment and expression for cardiomyocytes, cardiac fibroblasts and osteoblasts[104]. For the development of integrated sensing systems where chitosan anchors the biorecognition molecules, methods for the spatially selective deposition of chitosan are required. Electrodeposition is a very commonly employed method for the deposition of chitosan films at specific locations within the sensors[105-107]. Chitosan may be modified with molecules that impart desired selectivity either before or after the electrodeposition step[106, 108]. A number of microscale sensors have been developed using chitosan as the anchoring layer. These range from sensors for small molecules like glucose and phenols, DNA hybridization, cellular respiratory activity to those that

detect gases such as trimethylamine vapors. Modes of detection include electrochemical, optical and resonance-based methods. A thorough review of these sensors has been compiled by Koev et al.[98].

1.4. References

1. Mello, L.D. & Kubota, L.T. Review of the use of biosensors as analytical tools in the food and drink industries. *Food Chem.* **77**, 237-256 (2002).
2. Pingarrón, J.M., Yáñez-Sedeño, P. & González-Cortés, A. Gold nanoparticle-based electrochemical biosensors. *Electrochim. Acta* **53**, 5848-5866 (2008).
3. Struss, A., Pasini, P., Ensor, C.M., Raut, N. & Daunert, S. Paper strip whole cell biosensors: A portable test for the semiquantitative detection of bacterial quorum signaling molecules. *Anal. Chem.* **82**, 4457-4463 (2010).
4. Wang, J. Electrochemical biosensors: Towards point-of-care cancer diagnostics. *Biosens. Bioelectron.* **21**, 1887-1892 (2006).
5. Nakamura, H. & Karube, I. Current research activity in biosensors. *Anal. Bioanal. Chem.* **377**, 446-468 (2003).
6. Vadgama, P. & Crump, P.W. Biosensors: recent trends. A review. *Analyst* **117**, 1657-1670 (1992).
7. Whitesides, G.M. The "right" size in nanobiotechnology. *Nat. Biotech.* **21**, 1161-1165 (2003).
8. Seydack, M. Nanoparticle labels in immunosensing using optical detection methods. *Biosens. Bioelectron.* **20**, 2454-2469 (2005).
9. Zhong, W. Nanomaterials in fluorescence-based biosensing. *Anal. Bioanal. Chem.* **394**, 47-59 (2009).
10. Sapsford, K.E., Pons, T., Medintz, I.L. & Mattoussi, H. Biosensing with luminescent semiconductor quantum dots. *Sensors* **6**, 925-953 (2006).
11. Bailey, R.E., Smith, A.M. & Nie, S. Quantum dots in biology and medicine. *Physica E* **25**, 1-12 (2004).

12. Luccardini, C., Tribet, C., Vial, F., Marchi-Artzner, V. & Dahan, M. Size, charge, and interactions with giant lipid vesicles of quantum dots coated with an amphiphilic macromolecule. *Langmuir* **22**, 2304-2310 (2006).

13. Chan, W.C.W. & Nie, S. Quantum dot bioconjugates for ultrasensitive nonisotopic detection. *Science* **281**, 2016 -2018 (1998).

14. Bruchez, M., Moronne, M., Gin, P., Weiss, S. & Alivisatos, A.P. Semiconductor nanocrystals as fluorescent biological labels. *Science* **281**, 2013 -2016 (1998).

15. Sun, B. et al. Microminiaturized immunoassays using quantum dots as fluorescent label by laser confocal scanning fluorescence detection. *J. Immunol. Methods* **249**, 85-89 (2001).

16. Wang, J., Liu, G. & Merkoçi, A. Electrochemical coding technology for simultaneous detection of multiple DNA targets. *J. Am. Chem. Soc.* **125**, 3214-3215 (2003).

17. Xie, H.-Y. et al. Luminescent CdSe-ZnS quantum dots as selective Cu^{2+} probe. *Spectrochim. Acta A* **60**, 2527-2530 (2004).

18. Dubertret, B. et al. In vivo imaging of quantum dots encapsulated in phospholipid micelles. *Science* **298**, 1759 -1762 (2002).

19. Tang, B. et al. A new nanobiosensor for glucose with high sensitivity and selectivity in serum based on fluorescence resonance energy transfer (FRET) between CdTe quantum qots and Au nanoparticles. *Chem.-Eur. J.* **14**, 3637-3644 (2008).

20. Oh, E. et al. Inhibition assay of biomolecules based on fluorescence resonance energy transfer (FRET) between quantum dots and gold nanoparticles. *J. Am. Chem. Soc.* **127**, 3270-3271 (2005).

21. Shi, L., De Paoli, V., Rosenzweig, N. & Rosenzweig, Z. Synthesis and application of quantum dots FRET-based protease sensors. *J. Am. Chem. Soc.* **128**, 10378-10379 (2006).

22. Thürer, R. et al. Potentiometric immunoassay with quantum dot labels. *Anal. Chem.* **79**, 5107-5110 (2007).

23. Fountaine, T.J., Wincovitch, S.M., Geho, D.H., Garfield, S.H. & Pittaluga, S. Multispectral imaging of clinically relevant cellular targets in tonsil and lymphoid tissue using semiconductor quantum dots. *Mod. Pathol.* **19**, 1181-1191 (2006).

24. Seydack, M. Nanoparticle labels in immunosensing using optical detection methods. *Biosens. Bioelectron.* **20**, 2454-2469 (2005).

25. Rongen, H.A.H., Bult, A. & van Bennekom, W.P. Liposomes and immunoassays. *J. Immunol. Methods* **204**, 105-133 (1997).

26. Chonn, A. & Cullis, P.R. Recent advances in liposomal drug-delivery systems. *Curr. Opin. Biotech.* **6**, 698-708 (1995).

27. Roberts, M.A. & Durst, R.A. Investigation of liposome-based immunomigration sensors for the detection of polychlorinated biphenyls. *Anal. Chem.* **67**, 482-491 (1995).

28. Hwang, S.Y. et al. Characteristics of a liposome immunoassay on a poly(methyl methacrylate) surface. *Anal. Bioanal. Chem.* **389**, 2251-2257 (2007).

29. Goral, V.N., Zaytseva, N.V. & Baeumner, A.J. Electrochemical microfluidic biosensor for the detection of nucleic acid sequences. *Lab. Chip* **6**, 414 (2006).

30. Wittung, P. et al. Phospholipid membrane permeability of peptide nucleic acid. *FEBS Lett.* **365**, 27-29 (1995).

31. Egbaria, K. & Weiner, N. Liposomes as a topical drug delivery system. *Adv. Drug Deliver. Rev.* **5**, 287-300 (1990).

32. Moussaoui, N., Cansell, M. & Denizot, A. Marinosomes®, marine lipid-based liposomes: physical characterization and potential application in cosmetics. *Int. J. Pharm.* **242**, 361-365 (2002).

33. Lasic, D.D. & Barenholz, Y. *Handbook of Nonmedical Applications of Liposomes: From gene delivery and diagnostics to ecology*. (CRC Press: 1996).

34. Edwards, K.A. & Baeumner, A.J. Liposomes in analyses. *Talanta* **68**, 1421-1431 (2006).

35. Gómez-Hens, A. & Manuel Fernández-Romero, J. The role of liposomes in analytical processes. *TrAC-Trend. Anal. Chem.* **24**, 9-19 (2005).

36. Dams, R., Lambert, W.E., Comhaire, F. & De Leenheer, A.P. Production and characterization of sulforhodamine B containing large unilamellar vesicles labeled with atrazine. *Anal. Chim. Acta* **399**, 185-191 (1999).

37. Lee, M., Durst, R.A. & Wong, R.B. Comparison of liposome amplification and fluorophor detection in flow-injection immunoanalyses. *Anal. Chim. Acta* **354**, 23-28 (1997).

38. Ho, J.-an A. & Durst, R.A. Detection of fumonisin B1: comparison of flow-injection liposome immunoanalysis with high-performance liquid chromatography. *Anal. Biochem.* **312**, 7-13 (2003).

39. Edwards, K.A. & Baeumner, A.J. Optimization of DNA-tagged liposomes for use in microtiter plate analyses. *Anal. Bioanal. Chem.* **386**, 1613-1623 (2006).

40. Siebert, S.T.A., Reeves, S.G. & Durst, R.A. Liposome immunomigration field assay device for Alachlor determination. *Anal. Chim. Acta* **282**, 297-305 (1993).

41. Ho, J.-A.A. et al. Application of ganglioside-sensitized liposomes in a flow injection immunoanalytical system for the determination of cholera toxin. *Anal. Chem.* **79**, 246-250 (2007).

42. Singh, A.K., Harrison, S.H. & Schoeniger, J.S. Gangliosides as receptors for biological toxins: development of sensitive fluoroimmunoassays using ganglioside-bearing liposomes. *Anal. Chem.* **72**, 6019-6024 (2000).

43. Ou, L.-J., Liu, S.-J., Chu, X., Shen, G.-L. & Yu, R.-Q. DNA encapsulating liposome based rolling circle amplification immunoassay as a versatile platform for ultrasensitive detection of protein. *Anal. Chem.* **81**, 9664-9673 (2009).

44. Schmid, G. & Corain, B. Nanoparticulated gold: syntheses, structures, electronics, and reactivities. *Eur. J. Inorg. Chem.* **2003**, 3081-3098 (2003).

45. Mie, G. Beiträge zur optik trüber medien, speziell kolloidaler metallösungen. *Annalen der Physik* **330**, 377-445 (1908).

46. Boisselier, E. & Astruc, D. Gold nanoparticles in nanomedicine: preparations, imaging, diagnostics, therapies and toxicity. *Chem. Soc. Rev.* **38**, 1759 (2009).

47. Eustis, S. & El-Sayed, M.A. Why gold nanoparticles are more precious than pretty gold: Noble metal surface plasmon resonance and its enhancement of the radiative and nonradiative properties of nanocrystals of different shapes. *Chem. Soc. Rev.* **35**, 209 (2006).

48. Daniel, M.-C. & Astruc, D. Gold nanoparticles: assembly, supramolecular chemistry, quantum-size-related properties, and applications toward biology, catalysis, and nanotechnology. *Chem. Rev.* **104**, 293-346 (2004).

49. Baptista, P. et al. Gold nanoparticles for the development of clinical diagnosis methods. *Anal. Bioanal. Chem.* **391**, 943-950 (2007).

50. Liu, X., Atwater, M., Wang, J. & Huo, Q. Extinction coefficient of gold nanoparticles with different sizes and different capping ligands. *Colloid. Surface. B* **58**, 3-7 (2007).

51. Li, X., Qian, J., Jiang, L. & He, S. Fluorescence quenching of quantum dots by gold nanorods and its application to DNA detection. *Appl. Phys. Lett.* **94**, 063111 (2009).

52. Murphy, C.J. et al. Chemical sensing and imaging with metallic nanorods. *Chem. Commun.* 544-557 (2008).

53. Turkevich, J., Stevenson, P.C. & Hillier, J. A study of the nucleation and growth processes in the synthesis of colloidal gold. *Discuss. Faraday Soc.* **11**, 55-75 (1951).

54. Frens, G. Controlled nucleation for the regulation of the particle size in monodisperse gold suspensions. *Nature Phys. Sci.* **241**, 20-22 (1973).

55. Kimling, J. et al. Turkevich method for gold nanoparticle synthesis revisited. *J. Phys. Chem. B* **110**, 15700-15707 (2006).

56. Oh, E., Susumu, K., Goswami, R. & Mattoussi, H. One-phase synthesis of water-soluble gold nanoparticles with control over size and surface functionalities. *Langmuir* **26**, 7604-7613 (2010).

57. Lohse, S.E., Dahl, J.A. & Hutchison, J.E. Direct synthesis of large water-soluble functionalized gold nanoparticles using Bunte salts as ligand precursors. *Langmuir* **26**, 7504-7511 (2010).

58. Wangoo, N., Bhasin, K.K., Boro, R. & Suri, C.R. Facile synthesis and functionalization of water-soluble gold nanoparticles for a bioprobe. *Anal. Chim. Acta* **610**, 142-148 (2008).

59. Mangeney, C. et al. Synthesis and properties of water-soluble gold colloids covalently derivatized with neutral polymer monolayers. *J. Am. Chem. Soc.* **124**, 5811-5821 (2002).

60. Demers, L.M. et al. A fluorescence-based method for determining the surface coverage and hybridization efficiency of thiol-capped oligonucleotides bound to gold thin films and nanoparticles. *Anal. Chem.* **72**, 5535-5541 (2000).

61. Huang, C.-C., Huang, Y.-F., Cao, Z., Tan, W. & Chang, H.-T. Aptamer-modified gold nanoparticles for colorimetric determination of platelet-derived growth factors and their receptors. *Anal. Chem.* **77**, 5735-5741 (2005).

62. Wang, W., Chen, C., Qian, M. & Zhao, X.S. Aptamer biosensor for protein detection using gold nanoparticles. *Anal. Biochem.* **373**, 213-219 (2008).

63. Ao, L., Gao, F., Pan, B., He, R. & Cui, D. Fluoroimmunoassay for antigen based on fluorescence quenching signal of gold nanoparticles. *Anal. Chem.* **78**, 1104-1106 (2006).

64. Tanaka, R. et al. A novel enhancement assay for immunochromatographic test strips using gold nanoparticles. *Anal. Bioanal. Chem.* **385**, 1414-1420 (2006).

65. Elsayed, I., Huang, X. & Elsayed, M. Selective laser photo-thermal therapy of epithelial carcinoma using anti-EGFR antibody conjugated gold nanoparticles. *Cancer Lett.* **239**, 129-135 (2006).

66. Eck, W. et al. PEGylated gold nanoparticles conjugated to monoclonal F19 antibodies as targeted labeling agents for human pancreatic carcinoma tissue. *ACS Nano* **2**, 2263-2272 (2008).

67. Spindler, X., Hofstetter, O., McDonagh, A.M., Roux, C. & Lennard, C. Enhancement of latent fingermarks on non-porous surfaces using anti-L-amino acid antibodies conjugated to gold nanoparticles. *Chem. Commun.* **47**, 5602-5604 (2011).

68. Oh, E. et al. Nanoparticle based energy transfer for rapid and simple detection of protein glycosylation. *Angew. Chem.* **118**, 8127-8131 (2006).

69. Ojeda, R., de Paz, J.L., Barrientos, A.G., Martín-Lomas, M. & Penadés, S. Preparation of multifunctional glyconanoparticles as a platform for potential carbohydrate-based anticancer vaccines. *Carbohyd. Res.* **342**, 448-459 (2007).

70. Wang, X., Ramström, O. & Yan, M. A photochemically initiated chemistry for coupling underivatized carbohydrates to gold nanoparticles. *J. Mater. Chem.* **19**, 8944 (2009).

71. Copland, J.A. et al. Bioconjugated gold nanoparticles as a molecular based contrast agent: implications for imaging of deep tumors using optoacoustic tomography. *Mol. Imaging Biol.* **6**, 341-349 (2004).

72. Oh, E. et al. Inhibition assay of biomolecules based on fluorescence resonance energy transfer (FRET) between quantum dots and gold nanoparticles. *J. Am. Chem. Soc.* **127**, 3270-3271 (2005).

73. Kim, Y.-P. et al. Energy transfer-based multiplexed assay of proteases by using gold nanoparticle and quantum dot conjugates on a surface. *Anal. Chem.* **80**, 4634-4641 (2008).

74. Cui, R., Huang, H., Yin, Z., Gao, D. & Zhu, J.-J. Horseradish peroxidase-functionalized gold nanoparticle label for amplified immunoanalysis based on gold nanoparticles/carbon nanotubes hybrids modified biosensor. *Biosens. Bioelectron.* **23**, 1666-1673 (2008).

75. Elghanian, R., Storhoff, J.J., Mucic, R.C., Letsinger, R.L. & Mirkin, C.A. Selective colorimetric detection of polynucleotides based on the distance-dependent optical properties of gold nanoparticles. *Science* **277**, 1078 -1081 (1997).

76. Thanh, N.T.K. & Rosenzweig, Z. Development of an aggregation-based immunoassay for anti-protein A using gold nanoparticles. *Anal. Chem.* **74**, 1624-1628 (2002).

77. Lichlyter, D.J., Grant, S.A. & Soykan, O. Development of a novel FRET immunosensor technique. *Biosens. Bioelectron.* **19**, 219-226 (2003).

78. Sokolov, K. et al. Real-time vital optical imaging of precancer using anti-epidermal growth factor receptor antibodies conjugated to gold nanoparticles. *Cancer Res.* **63**, 1999 -2004 (2003).

79. El-Sayed, I.H., Huang, X. & El-Sayed, M.A. Surface plasmon resonance scattering and absorption of anti-EGFR antibody conjugated gold nanoparticles in cancer diagnostics: applications in oral cancer. *Nano Lett.* **5**, 829-834 (2005).

80. Gearheart, L.A., Ploehn, H.J. & Murphy, C.J. Oligonucleotide adsorption to gold nanoparticles: a surface-enhanced raman spectroscopy study of intrinsically bent DNA. *J. Phys. Chem. B* **105**, 12609-12615 (2001).

81. Ito, A., Shinkai, M., Honda, H. & Kobayashi, T. Medical application of functionalized magnetic nanoparticles. *J. Biosci. Bioeng.* **100**, 1-11 (2005).

82. Lu, A., Salabas, E.L. & Schüth, F. Magnetic nanoparticles: synthesis, protection, functionalization, and application. *Angew. Chem.Int. Edit.* **46**, 1222-1244 (2007).

83. Wang, S.X. & Guanxiong Li Advances in giant magnetoresistance biosensors with magnetic nanoparticle tags: review and outlook. *IEEE T. Magn.* **44**, 1687-1702 (2008).

84. Tartaj, P., Morales, M. P., Veintemillas-Verdaguer, S., Gonz lez-Carreno, T. & Serna, C.J. The preparation of magnetic nanoparticles for applications in biomedicine. *J. Phys. D: Appl. Phys.* **36**, R182-R197 (2003).

85. Kobayashi, Y., Horie, M., Konno, M., Rodríguez-González, B. & Liz-Marzán, L.M. Preparation and properties of silica-coated cobalt nanoparticles. *J. Phys. Chem. B* **107**, 7420-7425 (2003).

86. Gupta, A.K. & Gupta, M. Synthesis and surface engineering of iron oxide nanoparticles for biomedical applications. *Biomaterials* **26**, 3995-4021 (2005).

87. Salgueirino-Maceira, V. & Correa-Duarte, M.A. Cobalt and silica based core-shell structured nanospheres. *J. Mater. Chem.* **16**, 3593 (2006).

88. Salgueiriño-Maceira, V. et al. Synthesis and characterization of large colloidal cobalt particles. *Langmuir* **22**, 1455-1458 (2006).

89. Hao, R. et al. Synthesis, functionalization, and biomedical applications of multifunctional magnetic nanoparticles. *Adv. Mater.* **22**, 2729-2742 (2010).

90. Ferreira, H.A., Freitas, P.P. & Graham, D.L. Magnetoresistive-based biosensors and biochips. *Trends Biotechnol.* **22**, 455-462 (2004).

91. Haun, J.B., Yoon, T.-J., Lee, H. and Weissleder, R. Magnetic nanoparticle biosensors. *WIREs Nanomed. Nanobiotechnol.* **2**, 291-304 (2010).

92. Chemla, Y.R. et al. Ultrasensitive magnetic biosensor for homogeneous immunoassay. *P. Natl. Acad. Sci. USA* **97**, 14268 -14272 (2000).

93. Nawarathna, D. et al. SQUID-based biosensor for probing ion transporters in cell suspensions and tissue. *IEEE T. Appl. Supercon.* **17**, 812-815 (2007).

94. Hammond, J.W & Liu, C.C. Silicon-based microfabricated tin oxide gas sensor incorporating use of Hall effect measurement. *Sensor. Actuat. B-Chem.* **81**, 25-31 (2001).

95. Sandhu, A. et al. High efficiency Hall effect micro-biosensor platform for detection of magnetically labeled biomolecules. *Biosens. Bioelectron.* **22**, 2115-2120 (2007).

96. Holden, M.A., Jung, S.-Y. & Cremer, P.S. Patterning enzymes inside microfluidic channels via photoattachment chemistry. *Anal. Chem.* **76**, 1838-1843 (2004).

97. Doh, J. & Irvine, D.J. Photogenerated polyelectrolyte bilayers from an aqueous-processible photoresist for multicomponent protein patterning. *J. Am. Chem. Soc.* **126**, 9170-9171 (2004).

98. Koev, S.T. et al. Chitosan: an integrative biomaterial for lab-on-a-chip devices. *Lab. Chip* **10**, 3026-3042 (2010).

99. Ahn, J., Shin, Y.-B., Chang, W. S. & Kim, M. G. Sequential patterning of two fluorescent streptavidins assisted by photoactivatable biotin on an aminodextran-coated surface. *Colloid. Surface. B* **87**, 67-72 (2011).

100. Rinaudo, M. Chitin and chitosan: properties and applications. *Prog. Polym. Sci.* **31**, 603-632 (2006).

101. Yi, H. et al. Biofabrication with chitosan. *Biomacromolecules* **6**, 2881-2894 (2005).

102. Madihally, S.V. & Matthew, H.W.T. Porous chitosan scaffolds for tissue engineering. *Biomaterials* **20**, 1133-1142 (1999).

103. Co, C.C., Wang, Y. C. & Ho, C. C. Biocompatible micropatterning of two different cell types. *J. Am. Chem. Soc.* **127**, 1598-1599 (2011).

104. Karp, J.M. et al. A photolithographic method to create cellular micropatterns. *Biomaterials* **27**, 4755-4764 (2006).

105. Wu, L. Q, Ghodssi, R., Elabd, Y.A. & Payne, G.F. Biomimetic pattern transfer. *Adv. Funct. Mater.* **15**, 189-195 (2005).

106. Shi, X. et al. Chitosan biotinylation and electrodeposition for selective protein assembly. *Macromol. Biosci.* **8**, 451-457 (2008).

107. Liu, Y. et al. Chitosan to electroaddress biological components in lab-on-a-chip devices. *Carbohyd. Polym.* **84**, 704-708 (2011).

108. Koev, S.T. et al. Mechano-transduction of DNA hybridization and dopamine oxidation through electrodeposited chitosan network. *Lab. Chip* **7**, 103 (2007).

CHAPTER 2

APPLICATION OF QUANTUM-DOT ENCAPSULATING LIPOSOMES AS FLUORESCENT LABELS FOR MICROCHIP-BASED IMMUNOASSAYS

2.1. Abstract

Liposomes have been successfully used as reagents of signal amplification in numerous immunoassays. Most assays have employed fluorescent dyes as the encapsulated tracer molecule. In this study, quantum dots were used as the encapsulated fluorescent marker since, unlike organic dyes, they have higher quantum yields, are more stable to photobleaching and do not undergo self-quenching. Quantum dot (QD) encapsulating unilamellar liposomes were synthesized by the method of thin film hydration and characterized by the methods of fluorescence spectroscopy and dynamic light scattering. The number of QDs encapsulated within the liposomes was determined. The potential of the QD-encapsulating liposomes as a fluorescent label was explored by the binding of biotinylated liposomes to streptavidin-functionalized magnetic particles in a microfluidic chip. However, the long-term instability of the QD-liposomes was found to be a limiting factor for further quantitative analytical applications.

2.2. Introduction

This study investigates the feasibility of using quantum dot (QD)-encapsulating liposomes as fluorescent labels for bioanalytical applications.

Fluorescent labels are very commonly used for the purposes of bioanalysis and bioimaging. Organic fluorophores suffer from drawbacks such as self-quenching at high concentrations, susceptibility to photo-bleaching, short-term aqueous stability and narrow absorption windows coupled to broad red-tailed emission spectra. Many of these limitations can be overcome by the use of QDs which are semiconductor nanocrystals, ranging in size from 1-10 nm in diameter. QDs have generated a lot attention on account of their unique spectral properties. QDs have high molar absorptivities and broad absorption spectra which allow efficient excitation of multiple QD-based fluorophores with a single light source[1]. They have narrow and symmetric emission peaks and high quantum yields which make them ideal for multiplexed detection .Compared specifically to an organic dye like rhodamine, QDs have been reported to be 20 times brighter, 100 times more stable against photobleaching and one-third as wide in spectral linewidth[2].

Liposomes are essentially spherical vesicles, comprised of one or more phospholipid bilayers surrounding an aqueous cavity. The hydrophobic chains of the lipid comprise the bulk of the bilayer, with the hydrophilic head groups oriented towards the interior and exterior aqueous environment. The aqueous cavity may encapsulate different hydrophilic molecules such as fluorophores[3], enzymes[4], electrochemical[5] and chemiluminescent markers[6]. By virtue of their ability to encapsulate numerous hydrophilic tracer molecules in the aqueous cavity of each vesicle, liposomes can amplify the signal generated by formation of an immunocomplex by several orders of magnitude compared to a single tracer

molecule[7, 8]. The signal amplification with liposomes is instantaneous, unlike ELISA (Enzyme Linked Immunosorbent Assay), where the enzyme has to be incubated for a certain time with the corresponding substrate in order to produce a measurable signal. Liposomes can be adapted for application in a variety of immunoassays since the phospholipid bilayers can be easily modified, pre or post synthesis, with various functional groups or molecules for biorecognition such as antibodies.

Liposomes have been successfully used as agents of signal amplification in a wide variety of immunoassays[9, 10]. Most of these assays have employed fluorescent dyes as the encapsulated tracer molecule[3, 7, 11]. A few other reports have utilized fluorophore-labeled lipids[12], enzymes[4] or electrochemical markers[6] for liposome-based immunoassays. The main drawback of using organic dyes for encapsulation is that they tend to photobleach easily. Also, some organic dyes like sulforhodamine B undergo quenching when encapsulated at high concentrations, due to which the corresponding liposomes have to be lysed in order to perform detection. This adds an extra step in the performance of liposome-based immunoassays. Enzymatic labels introduce an extra incubation step, thereby lengthening the analysis time. Electrochemical markers offer limited potential for multiplexed detection. In this scenario, the use of quantum dots (QDs) as a marker in liposomes holds promise for highly sensitive, multi-analyte detection. The advantages of signal amplification derived from liposomes and the stronger fluorescent signal derived from QDs can be combined to provide a powerful analytical reagent for sensitive and multiplexed

detection of analytes. This is particularly useful when dealing with small sample volumes typical of microfluidic devices.

In the past, QDs have been encapsulated in vesicles primarily to facilitate their introduction into cells. The first instance of the encapsulation of QDs in phospholipid micelles and their application for in-vivo imaging was presented by Dubertret et al. in 2002[13]. A number of other studies using QD-liposomes for in-vivo labeling applications have since been published[14-17]. Kloepfer et al. synthesized liposomes with hydrophobic QDs embedded within the lipid bilayer to study fluorescent resonance energy transfer to lipid-soluble and water-soluble dyes[18]. Chen et al. reported the synthesis of QD-liposomes but no analytical applications were explored[19].

The aim of this study was to synthesize QD encapsulating liposomes and demonstrate their utility as labels for bioanalysis. QD-encapsulating liposomes were synthesized by the method of thin film hydration. The QD-liposome preparation was characterized by the methods of fluorescence spectroscopy and dynamic light scattering. The number of QDs encapsulated within the liposomes was determined. The potential of the QD-encapsulating liposomes as a fluorescent label was explored by the binding of biotinylated liposomes to streptavidin-functionalized magnetic particles in a microfluidic chip. However, the long-term instability of the QD-liposomes was found to be a limiting factor for further quantitative analytical applications.

2.3. Materials and Methods

2.3.1. Materials and reagents

All general reagents and solvents were procured from Sigma Aldrich or VWR (West Chester, PA, USA). All chemicals were used as received, without further purification. Dipalmitoylglycerophosphocholine (DPPC), dipalmitoyl-phosphatidylglycerol (DPPG), cholesterol, dipalmitoylphosphatidylethanolamine-N-(biotin)(DPPE−biotin) and the Avanti Mini-Extruder kit were purchased from Avanti polar Lipids (Alabaster, AL,USA). Quantum dots (Qdot® 525 and 655 ITK™ amino-(PEG), 8 μM) and magnetic beads (Dynabeads MyOne Streptavidin T1, 1μm in diameter) were purchased from Life Technologies (Eugene, OR, USA).The borate buffer solution consisted of a 0.1 %(w/v) solution of bovine serum albumin in 50 mM borate-buffer adjusted to pH 7.4 using dilute sulfuric acid. The Microfluor™ flat bottom, 96-well black plates (medium binding) were procured from Thermo Scientific (Pittsburgh, PA, USA). Ultrapure water, with specific resistance of 18 MΩ-cm, was obtained from a Barnstead™ E-Pure™ deionization system (Waltham, MA) and was used for rinses and the preparation of buffers throughout the experiments.

Fluorescence emission spectra and quantitative measurements were performed on a Spectramax Gemini XS microplate reader from Molecular Devices (Sunnyvale, CA, USA).

2.3.2. Synthesis of QD encapsulating liposomes

Liposomes were synthesized by minor modifications of the film hydration method described in earlier reports[20]. Biotin was incorporated into the lipid bi-layer for further conjugation by using DPPE-biotin. The lipid mixture used for the synthesis of liposomes consisted of a 50:40:10:0.5 molar ratio of DPPC, cholesterol, DPPG, and DPPE−biotin (20 μmol total) .The lipids were placed in a 10 ml pear-shaped flask and dissolved in 6mL of a solvent mixture comprised of 5:1 (v/v) volume ratios of chloroform and methanol. The lipid solution was sonicated for a minute to ensure homogeneous dispersion of the lipids. Subsequently, the organic solvent was removed by evaporation at 45 °C on a rotary evaporator. A thin film of lipid was left on the walls of the pear-shaped flask. 25 μL of QD 655, 8μM, was diluted to 500 μL with borate buffer to obtain a final concentration of 200nM and warmed to 45 °C before use. 500 μL of the warmed aqueous solution of QD was added to the lipid film and the flask was vigorously shaken at 45°C to form multilamellar vesicles. The suspension of liposomes thus obtained was sonicated for 15 minutes at 45°C. To obtain unilamellar liposomes, the resulting preparation were extruded 11 times, at 45°C, through two stacked polycarbonate membrane filters (pore size 0.2 μm) using the Avanti Mini-Extruder apparatus (Avanti Polar Lipids Inc., Alabaster, AL). The liposome suspension was stored at 4 °C until further use. The same method was followed for the synthesis of buffer loaded liposomes with the exception of using borate buffer instead of QD solution.

2.3.3. Characterization of QD encapsulating liposomes

2.3.3.1. Fluorescence spectroscopy

The emission spectra of the QDs, QD-liposomes and buffer loaded liposomes from 550nm to 750 nm were recorded on a Spectrmax Gemini XS microplate reader. A volume of 100µL was used for each sample. The concentration of the QD and QD - liposomes were adjusted to contain approximately 10 nM QD in the final sample. The samples were subjected to excitation at 405nm and a measurement step size of 2 nm was used.

2.3.3.2. Particle size and size distribution of liposomes

The hydrodynamic radii and size distribution of the liposomes were determined by photon correlation spectroscopy (PCS) using the N4 Plus from Coulter Electronics (Miami, FL, USA). Samples for PCS were prepared by diluting 5µL of the liposomes to 3.5 mL using borate buffer which had been filtered through a 0.22 µm hydrophilic filter. Measurements were performed at 90° scattering angle and the autocorrelation function (ACF) was acquired for 60 seconds. The intensity-weighted size distribution of the liposomal preparation (as obtained by SDP (Size Distribution Processor) analysis) was reported.

2.3.3.3. QD encapsulation efficiency of liposomes

Two methods were explored in order to determine the number of quantum dots encapsulated in each liposome. The first method involved quenching of the fluorescence of the QDs not encapsulated within liposomes by addition of copper chloride solution to a certain volume of the QD-liposome sample. In order to determine the concentration of copper required to completely quench a given amount of QDs, a titration curve for increasing amounts of Cu^{2+} added to a certain concentration of QDs was generated. The experiment was conducted in 96-well plates with a sample volume of 100 μL. Aliquots (50 μL) of 10 nM QD solutions were dispensed in wells of black, flat bottom Microfluor™ microtiter plates. Subsequently, 50 μL of copper (II) chloride solutions of different concentrations were added to the wells such that the total volume in each well was 100 μL and the final concentration of Cu^{2+} ranged from 0 to 50 μM while the final concentration of the QDs was 5 nM. The microplate reader was programmed to shake the microtiter plate for 60 seconds for sample mixing prior to fluorescence measurements. The fluorescence intensities corresponding to different concentrations of copper (II) chloride were plotted and the concentration of Cu^{2+} required to completely quench the QDs was determined.

In the next step, QD- liposomes prepared earlier were diluted 1:20 with borate buffer. Aliquots (50 μL) were dispensed in the wells of microtiter plates. To the wells acting as controls, 50 μL of borate buffer was added while to the other set 50 μL of 100 μM copper chloride solution was added. The fluorescence intensities were recorded after gentle mixing manually.

A second method was also followed to determine the number of quantum dots encapsulated in each liposome. In this method, the liposome preparation (~ 400 μL) was centrifuged gently (3000 rpm for 15 minutes) such that the unencapsulated QDs remain in the supernatant. After the centrifugation step, 300 μL of supernatant was obtained and the pellet was resuspended in 400 μL of borate buffer and the centrifugation step was repeated again to obtain 400 μL of supernatant. The supernatant from two such centrifuge/wash cycles were pooled and its concentration was determined by intrapolation from a standard curve of the fluorescence intensity of various concentrations of QDs.

2.3.4. Hybridization assay in microfluidic chip

A microfluidic chip with a single microchannel (500 μm wide × ~100 μm deep × 4.5 cm in length) was fabricated using previously reported methods[21] and was used for this assay. An externally placed neodyminum permanent magnet was used to immobilize the magnetic beads as a packed bed and enable visualization. Fluids were introduced into the microchannel by pipetting while washes were conducted by a syringe pump operated in the withdrawal mode. Fluorescence of liposomes was visualized by a Zeiss Axio Imager M1m microscope (Thornwood, NY, USA), equipped with Qdot® 525 and Qdot® 655 filter cube.

20 μL of the biotinylated QD-liposomes were mixed with 20 μL of streptavidin-functionalized Dynabeads (diluted to 1mg/mL) in a siliconized-

microcentrifuge tube and allowed to react for 30 minutes at room temperature. The magnetic beads were rinsed thrice with borate buffer followed by extraction with an external magnet. The liposome-labeled magnetic beads were resuspended in 80 μL of borate buffer. 8 μL of the magnetic bead suspension (containing 2 μg beads) was introduced into the microchannel and the magnetic beads were captured by the external magnet for imaging.

2.4. Results and discussion

The thin film hydration method was used to prepare the liposomes with QDs entrapped within. The method of reverse-phase evaporation (as described by Seibert et al.[22]) was also investigated for the same synthesis. However, it was not followed as it led to extensive aggregation of the QDs upon addition to the solution of lipids in organic solvents. For the synthesis of QD-loaded liposomes, hydrophilic QDs with amino-PEG functionality were employed. The QDs are capped by a layer of polymer. It is hypothesized that dispersion of the QDs in organic solvent led to disruption of the polymeric coating, leading to destabilization of the QDs and subsequent aggregation. Hence, the method of thin film hydration was selected since in this process, the organic solvent is evaporated prior to the incorporation of the QDs. This method was found to side-step any potential deleterious effects of organic solvents on the QDs.

After synthesis of the liposomes, they were subjected to extrusion to homogenize the preparation and obtain unilamellar vesicles. To avoid any clogging of

the polycarbonate membrane during the extrusion process, this step was performed at 45°C, which is above the gel to liquid phase transition temperature for the lipids used. Cholesterol was included in the liposome as it promotes denser packing of the phospholipid chains, thereby reducing the permeability of the liposomes. 0.5 mol percent biotin was used in the synthesis of liposomes to enable further modification using neutravidin-biotin bonds.

It was expected that the encapsulation of the QDs in the aqueous core of the liposome would not alter their optical properties compared to free QDs suspended in water or buffer. Figure 2.1 depicts the emission spectra of free QDs in buffer, QDs encapsulated in liposomes as well as buffer-loaded liposomes. It can be seen that the sharp emission peak of the free QDs were preserved subsequent to their encapsulation in the liposomes. The fluorescence intensity of the QD-liposomes was lower than that of the free QDs in buffer (for the same starting concentration of QDs). Jamal et al.[14] attributed the changes in optical properties of QDs upon encapsulation in liposomes to the interaction of the QDs and the lipid bilayer. However, unlike Jamal et al., no shifts in the emission maxima were observed in the present case, indicating that the size of the quantum dots underwent no changes through the encapsulation process by the film hydration method.

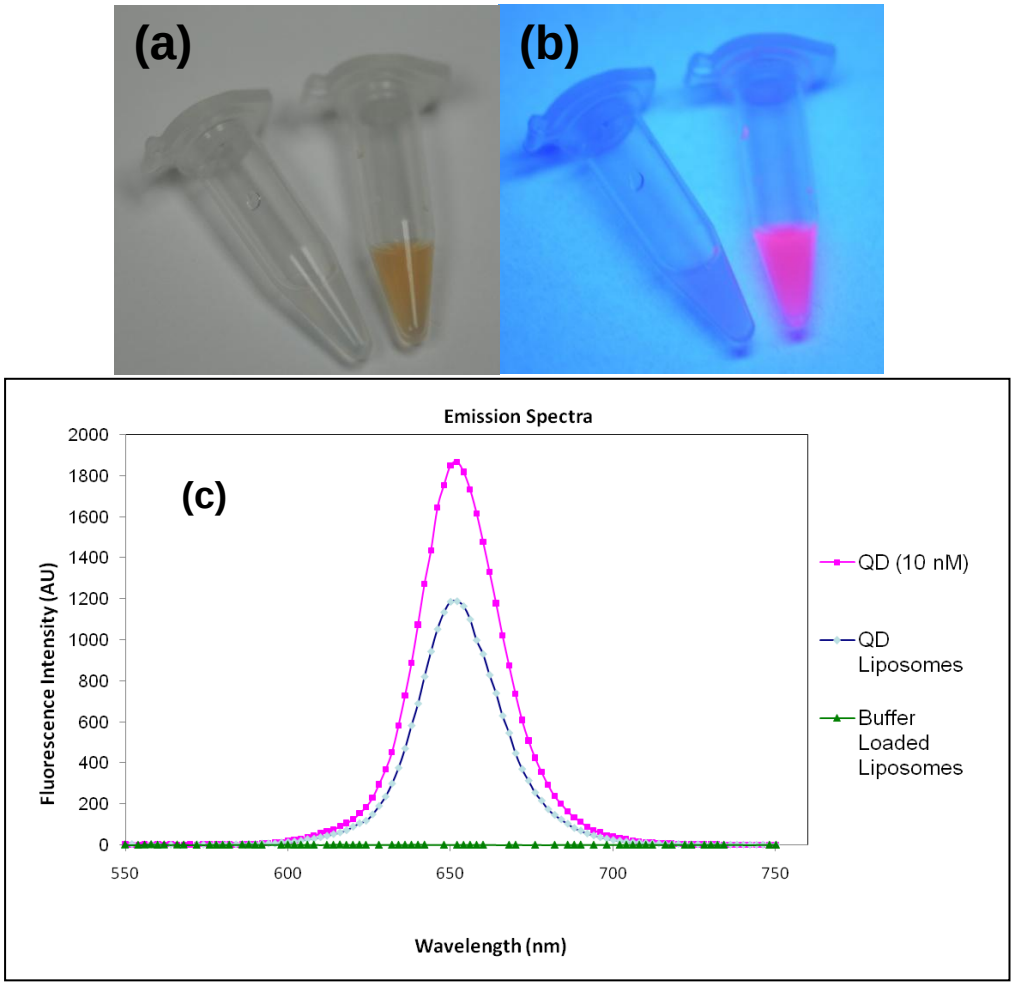

Figure 2.1 (a) Buffer-loaded liposomes (left) and QD-liposomes (right) as observed in ambient light **(b)** as observed under UV illumination **(c)** Comparison of the fluorescence emission spectra of free QDs in solution, QD-encapsulating liposomes and buffer loaded liposomes.

The hydrodynamic radii and size distribution of the QD-liposome preparation was determined by PCS. PCS is a technique that measures the size of particles by measuring their rate of diffusion through a fluid. The SDP mode of data analysis was chosen as it is more suited for samples that have complex distributions. This mode was considered suitable in the present case since post-synthesis, no step was carried out for the separation of unencapsulated quantum dots from the liposome preparation. SDP

analysis uses an algorithm based on a FORTRAN program called CONTIN. This algorithm mathematically separates the decay times of particles of various sizes from the composite ACF. The results (as shown in figure 2.2) indicate a fairly narrow distribution of liposome sizes. From the average of three measurements, the mean hydrodynamic diameter of the liposomal preparation was determined to be 201.8 ± 25.44nm.

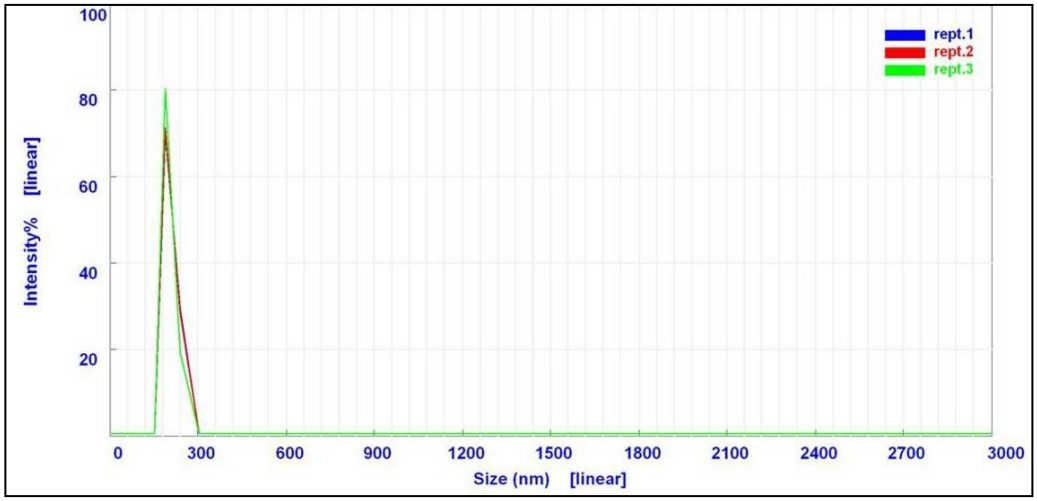

Figure 2.2 Scattering intensity-weighted size distribution of QD-liposomes as determined by photon corelation spectroscopy.The mean diameter was determined to be 201.8 ± 25.44nm.

To determine the number of QDs encapsulated per liposome, two methods were explored. The first method exploited the ability of Cu^{2+} ions to quench fluorescence of the QDs. It was demonstrated by Ghosh et al.[23] that the quenching of photoluminescence of CdTe QDs occurs by the photoinduced reduction of Cu^{2+} to Cu^{+}. The photo excited CdTe QDs were postulated to give up the electron to Cu^{2+} ions, thus reducing them to Cu^{+} ions. The general opinion is that lipid bilayers are effective barriers to the transport of ions in and out of cells and vesicles[24]. It was

hypothesized that on the addition of copper chloride, QDs encapsulated within the liposome would retain their fluorescence while those remaining unencapsulated would undergo quenching. The concentration of copper required to completely quench a given amount of QDs (equivalent to the starting concentration used for liposome synthesis) was determined by obtaining a titration curve for increasing amounts of copper added to a fixed concentration of QDs. From the titration curve (depicted in figure 2.3), it was concluded that 50 μM of copper (II) ions were required in order to completely quench the equivalent of 10 nm QD in a 100μL sample.

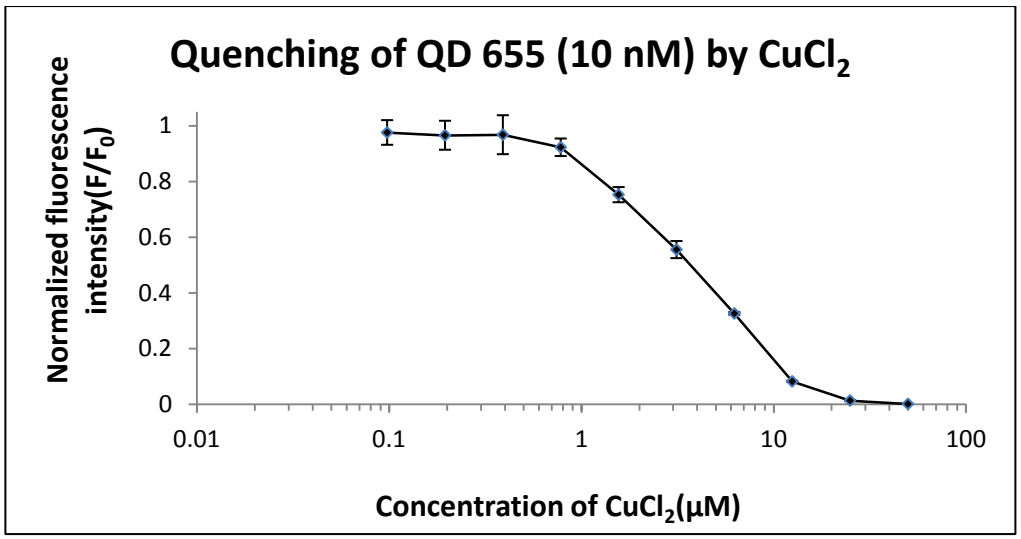

Figure 2.3 Quenching titration curve of QD 655 (10 nM,100 μL) treated with increasing concentrations of copper (II) chloride, ranging from 0.1 to 50 μM. Plotted points represent the average of three measurements while the error bars represent one standard deviation.

In the subsequent step, QD-liposomes were diluted 1: 20 with borate buffer in order to obtain a final QD concentration equivalent to 10 nM and the fluorescence intensities were observed in the absence and presence of Cu^{2+} (table 2.1) . The

corresponding QD concentrations were calculated by intrapolation of the fluorescence intensities from the calibration curve for QD 655 (figure 2.4). It was found that in the absence of Cu^{2+} ions, the QD-liposomes gave a fluorescence signal intensity equivalent to 105.09 nM of unencapsulated QD. This is just about half the concentration of QDs used for the original synthesis. The reduction in fluorescence signal of the QDs might be attributed to the loss of QDs during synthesis as well as decrease in photoluminescence of the individual QDs upon interaction with the lipid bilayer of the liposomes. The addition of Cu^{2+} to the QD-liposomes reduced the signal to negligible levels, equivalent to 2.60 nM of unencapsulated QD. This was an unexpected outcome. It is hypothesized that the addition of Cu^{2+} destabilized the lipid bilayer of the liposome either by interactions with the lipids or due to changes in osmotic pressure outside the liposome membrane.

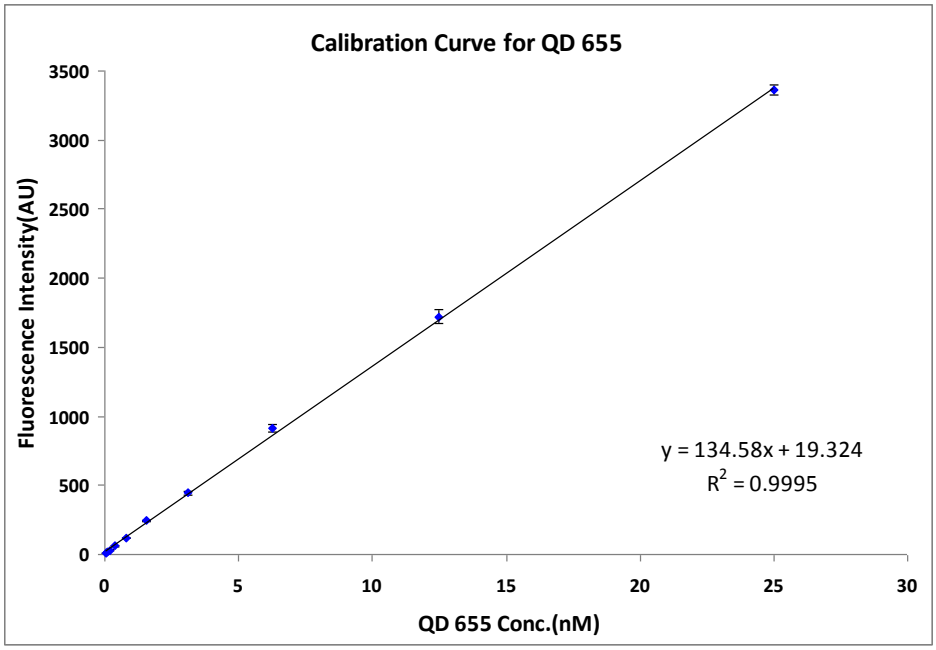

Figure 2.4 Calibration curve for QD 655(n=3) generated using a microplate reader (excitation: 405 nm; emission: 655 nm).

Table 2.1 Results for the fluorescence intensity of QD-liposomes (diluted 1:20) without and with the addition of copper for quenching. The respective QD concentrations were calculated by intrapolation of the fluorescence intensities from the calibration curve for QD 655 depicted in figure 2.4.

	QD-Liposomes (Not quenched)	QD-Liposomes + Cu (Quenched)
Signal ± SD (n=3)	726.50 ± 18.04	23.36 ± 1.31
QD conc. (nM)	105.09	2.60

Subsequently, a gentler alternative method was explored in order to determine the QD encapsulation within liposomes. The liposome preparation was centrifuged gently so that the liposomes settled down as a pellet while unencapsulated QDs remained in the supernatant. Centrifugation was followed by the removal of the supernatant and redispersing the pellet in more borate buffer. After two such centrifuge/wash cycles, the supernatant was pooled and its concentration was determined by intrapolation from the standard curve depicted in figure 2.4. This concentration was subtracted from the concentration of QDs used in liposome synthesis initially (200nM). It was determined that the QD concentration encapsulated in the liposomes was 198.65 nM, i.e. 99.33 % encapsulation was achieved.

Although the above number is derived from a "bulk" measurement, it serves as a good index for encapsulation efficiency. Accurate measurements can be made using techniques such fluorescence correlation spectroscopy (FCS). In dual-color, cross-correlation FCS, the fluorescence signals from two fluorophores are recorded simultaneously, and the fluctuations in the fluorescence signal of one fluorophore are correlated with those of the other fluorophore[19]. The number of QD encapsulated per

liposome can be calculated from the size of the liposomes (determined earlier by DLS) and the concentration of encapsulated QDs. Assuming the lipid bilayer to be 4 nm thick[25], it was calculated that on an average 0.5 QDs were encapsulated per liposome. For the purposes of signal amplification, however, greater encapsulation efficiencies need to be achieved. QD/liposome ratios of 1.5-2 were achieved using a starting QD concentration of 1000 nM for the liposome synthesis (data not shown). Chen et al. were able to get three QDs / liposome using a starting concentration of 0.8 µM of QDs[19]. The properties of the QD-liposomes have been summarized in table 2.2.

Table 2.2 Characteristics of QD-encapsulating liposomes

Mean Diameter (± S.D.) (nm)	201.8 ± 25.44
Volume of liposome (µL)	4.3×10^{-12}
Volume entrapped (µL)	3.8×10^{-12}
QD concentration(nM)	198.65
QD per liposome	0.5
Stability	Unstable

The potential utility of the QD-liposomes for labeling in magnetic bead-based assays in a microfluidic format was explored. QD-liposomes were conjugated to magnetic beads via streptavidin-biotin bonding and were introduced into a microfluidic chip fabricated out of PMMA. As seen from figure 2.5(a), the beads were immobilized in a packed bed ~ 1 mm in length, by using an external magnet. The liposomes retained their form after being immobilized in a packed bed, as seen by the fluorescence in figure 2.5(d). The fluorescent signal arises due to the presence of QD-

liposomes captured by the magnetic beads. The QDs used for the synthesis have an amine-terminated PEG coating and hence, are not expected to be retained by the streptavidin-coated magnetic beads. The magnetic beads labeled with liposomes (figure 2.5(d)) showed distinctly higher fluorescence than the control set (figure 2.5(b)). No non-specific absorption of the liposomes was observed on the walls of the PMMA microchip, indicating the compatibility of the liposomes with PMMA.

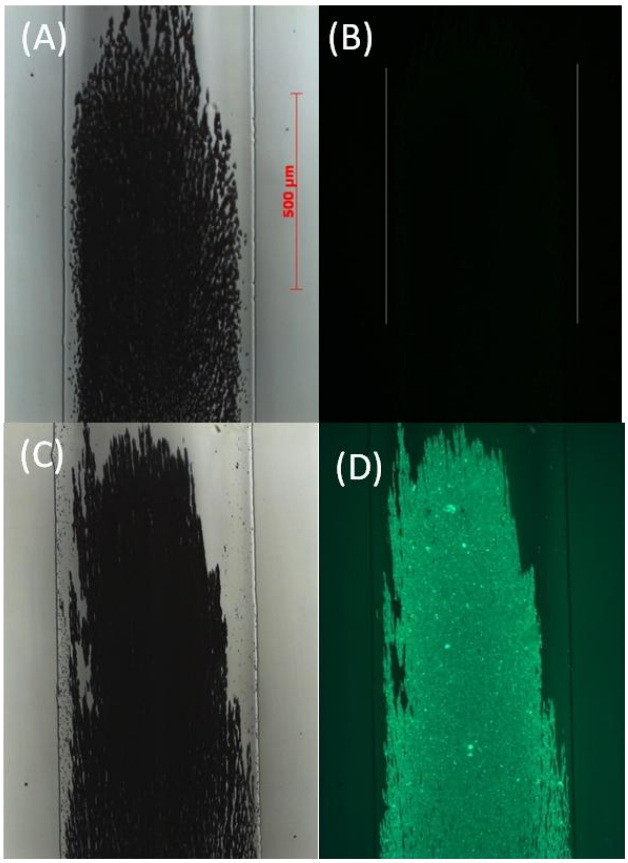

Figure 2.5 Fluorescence images of streptavidin-coated magnetic beads with **(b)** no label and **(d)** labeled with biotinylated QD 525-liposomes and immobilized in a microfluidic channel. **(a)** and **(c)** represent brightfield images of (b) and (c), respectively.

However, inspite of these promising results, further experimentation was hampered largely by the instability of the liposomes. The QD-liposomes undergo leakage and/or rupture after a few days of storage, as shown in figure 2.6. It is hypothesized that with time, the QDs within the liposome undergo oxidation, giving rise to Cd ions[26]. This changes the osmotic pressure differential between the interior and exterior of the liposome, leading to rupture. Addition of sucrose (0.1 M) to the liposome suspension did not prevent the rupture of liposomes. The possibility of the polymeric coating of the QDs interacting with the phospholipid bilayer cannot be ruled out either. This drawback severely limited the window of time in which the QD-liposomes could be used for assays. QDs with better passivation layers, such as silica cladding, might prove to be more suited for encapsulation within liposomes.

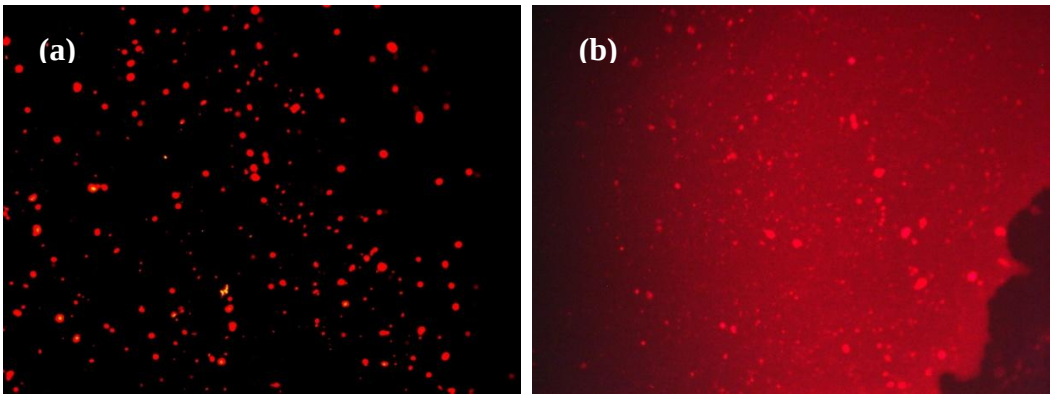

Figure 2.6 Fluorescence images of **(a)** freshly prepared QD 655-liposomes **(b)** QD 655-liposomes after a week, showing the release of QDs

2.5. Conclusions

The use of QDs as a marker in liposomes was investigated on account of the advantageous combination of signal amplification derived from liposomes and the

stronger fluorescent signal generated by QDs. Liposomes encapsulating QD 525 and QD 655 were synthesized and characterized for their spectral properties and size. The encapsulation efficiency of QDs within the liposomes was 99.33 %. These liposomes were successfully applied towards a magnetic-bead based assay in a microfluidic chip as proof-of-concept. Further development of the assay was, however, impeded by the unstable nature of the QD-liposome hybrid structure. QDs need to be modified with improved and resilient coatings in order to form stable hybrids with liposomes.

2.6. Acknowledgements

The authors would like to thank Dr. Chih-hung (Alex) Chang for the use of the N4 Plus and Dr. Myra Koesdjojo for her advice about microfluidic chip fabrication. We wish to thank Dr. Neal Sleszynski for his suggestions regarding QD quenching and David Mandrell for his help with fabricating a fixture for the microfluidic chip.

2.7. References

1. Bailey, R.E., Smith, A.M. & Nie, S. Quantum dots in biology and medicine. *Physica E* **25**, 1-12 (2004).
2. Chan, W.C.W. & Nie, S. Quantum dot bioconjugates for ultrasensitive nonisotopic detection. *Science* **281**, 2016 -2018 (1998).
3. Roberts, M.A. & Durst, R.A. Investigation of liposome-based immunomigration sensors for the detection of polychlorinated biphenyls. *Anal. Chem.* **67**, 482-491 (1995).
4. Hwang, S.Y. et al. Characteristics of a liposome immunoassay on a poly(methyl methacrylate) surface. *Anal. Bioanal. Chem.* **389**, 2251-2257 (2007).

5. Goral, V.N., Zaytseva, N.V. & Baeumner, A.J. Electrochemical microfluidic biosensor for the detection of nucleic acid sequences. *Lab. Chip* **6**, 414 (2006).

6. Zhan, W. & Bard, A.J. Electrogenerated Chemiluminescence. 83. Immunoassay of human C-reactive protein by using $Ru(bpy)_3^{2+}$ encapsulated liposomes as labels. *Anal. Chem.* **79**, 459-463 (2007).

7. Edwards, K.A. & Baeumner, A.J. Optimization of DNA-tagged liposomes for use in microtiter plate analyses. *Anal. Bioanal. Chem.* **386**, 1613-1623 (2006).

8. Ho, J. A. & Durst, R.A. Detection of fumonisin B1: comparison of flow-injection liposome immunoanalysis with high-performance liquid chromatography. *Anal. Biochem.* **312**, 7-13 (2003).

9. Rongen, H.A.H., Bult, A. & van Bennekom, W.P. Liposomes and immunoassays. *J. Immunol. Methods* **204**, 105-133 (1997).

10. Edwards, K.A. & Baeumner, A.J. Liposomes in analyses. *Talanta* **68**, 1421-1431 (2006).

11. Zaytseva, N.V., Goral, V.N., Montagna, R.A. & Baeumner, A.J. Development of a microfluidic biosensor module for pathogen detection. *Lab. Chip* **5**, 805 (2005).

12. Singh, A.K., Harrison, S.H. & Schoeniger, J.S. Gangliosides as receptors for biological toxins: development of sensitive fluoroimmunoassays using ganglioside-bearing liposomes. *Anal. Chem.* **72**, 6019-6024 (2000).

13. Dubertret, B. et al. In-vivo imaging of quantum dots encapsulated in phospholipid micelles. *Science* **298**, 1759 -1762 (2002).

14. Al-Jamal, W.T., Al-Jamal, K.T., Bomans, P.H., Frederik, P.M. & Kostarelos, K. Functionalized-quantum-dot–liposome hybrids as multimodal nanoparticles for cancer. *Small* **4**, 1406-1415 (2008).

15. Dudu, V., Ramcharan, M., Gilchrist, M.L., Holland, E.C. & Vazquez, M. Liposome delivery of quantum dots to the cytosol of live cells. *J. Nanosci. Nanotechnol*. **8**, 2293-2300 (2008).

16. Al-Jamal, W.T. et al. Tumor targeting of functionalized quantum dot-liposome hybrids by intravenous administration. *Mol. Pharm.* **6**, 520-530 (2009).

17. Yang, C. et al. Folate receptor-targeted quantum dot liposomes as fluorescence probes. *J. Drug Target* **17**, 502-511 (2009).

18. Kloepfer, J.A., Cohen, N. & Nadeau, J.L. FRET between CdSe quantum dots in lipid vesicles and water- and lipid-soluble dyes. *J. Phys. Chem. B* **108**, 17042-17049 (2004).

19. Chen, C.-S., Yao, J. & Durst, R.A. Liposome encapsulation of fluorescent nanoparticles: quantum dots and silica nanoparticles. *J. Nanopart. Res.* **8**, 1033-1038 (2006).

20. Ou, L.J., Liu, S.J., Chu, X., Shen, G.-L. & Yu, R.-Q. DNA encapsulating liposome based rolling circle amplification immunoassay as a versatile platform for ultrasensitive detection of protein. *Anal. Chem.* **81**, 9664-9673 (2009).

21. Koesdjojo, M.T., Koch, C.R. & Remcho, V.T. Technique for microfabrication of polymeric-based microchips from an SU-8 master with temperature-assisted vaporized organic solvent bonding. *Anal. Chem.* **81**, 1652-1659 (2009).

22. Siebert, S.T.A., Reeves, S.G. & Durst, R.A. Liposome immunomigration field assay device for Alachlor determination. *Anal. Chim. Acta* **282**, 297-305 (1993).

23. Ghosh, S., Priyam, A., Bhattacharya, S.C. & Saha, A. Mechanistic aspects of quantum dot based probing of Cu (II) ions: role of dendrimer in sensor efficiency. *J. Fluoresc.* **19**, 723-731 (2009).

24. Gerami, R. & Bruinsma, R.F. Continuum theory of lipid bilayer electrostatics. *Eur. Phys. J. E* **30**, 197-204 (2009).

25. Ho, J.-A.A. et al. Application of ganglioside-sensitized liposomes in a flow injection immunoanalytical system for the determination of cholera toxin. *Anal. Chem.* **79**, 246-250 (2007).

26. Derfus, A.M., Chan, W.C.W. & Bhatia, S.N. Probing the cytotoxicity of semiconductor quantum dots. *Nano Lett.* **4**, 11-18 (2004).

CHAPTER 3

HOMOGENEOUS ASSAY DEVELOPMENT BASED ON ENERGY TRANSFER BETWEEN QUANTUM DOTS AND GOLD NANOPARTICLES

3.1. Abstract

A simple and rapid method for the detection of proteins via energy transfer between quantum dots (QDs) and gold nanoparticles (AuNPs) is presented. The method requires only two oligonucleotides - an aptamer that binds the protein and a complementary strand. Thrombin was used as the model analyte in this study. The anti-thrombin aptamer was conjugated to 10 nm AuNPs while a complementary sequence was conjugated to the QDs with emission maxima of 585 nm. The hybridization of the complementary sequences placed the AuNPs and QDs in close proximity, such that quenching of the fluorescence of QDs occurred. The fluorescence of the QDs was enhanced as a function of thrombin concentration, enabling quantitative detection of thrombin. Experimental parameters such as buffer system and ratio of AuNPs to QDs were optimized. The assay simply required the mixing of the sample with the reagents and could be completed in ~ 40 minutes total. The limit of detection for thrombin by this method was 5 nM. This simple homogeneous assay is ideal for applications that require multiplexed detection.

3.2. Introduction

The goal of this study was to develop a simple and unique biosensing approach by harnessing the excellent optical properties of quantum dots (QDs) and gold nanoparticles (AuNPs) for fluorescence energy resonance transfer (FRET). The phenomenon of FRET can be used quantify biomolecule interactions on account of its dependence on the distance between the interacting moieties[1]. The occurrence of FRET between QDs and AuNPs and its application for detection is a promising approach. QDs, as fluorescent probes, have generated a lot of interest for bioimaging and detection applications on account of their unique optical properties[2,3]. Their broad excitation spectrum, narrow and tunable emission peaks and highly stable photoluminescence compared to organic fluors make them ideal for applications that require sensitive and multiplexed detection[4]. AuNPs have been recently investigated as components for immunoassays based on their ability to quench the fluorescence of organic dyes and QDs[5-7]. AuNPs have high extinction co-efficients and a broad absorption spectrum in visible light, which overlaps with the emission spectrum of energy donors such as organic dyes and quantum dots. The ease with which biomolecules containing reactive thiol groups can be conjugated to gold surfaces through gold-sulfur bonds makes AuNPs particularly attractive for bioanalytical applications.

FRET between organic dyes and AuNPs and dyes have been the subject of quite a few recent investigations[1,8]. However, owing to the limitations of organic dyes (photobleaching, self-quenching, etc.), QDs have emerged as an attractive alternative.

Oh et al. were the first to demonstrate an assay for avidin based on the modulation in FRET efficiency between streptavidin-conjugated QDs and biotinylated AuNPs[9]. Subsequently, the same principle has been applied for the detection of a range of molecules such as DNA, proteases, glyosylated proteins and 2,4,6-trinitrotoluene[5,10-13]. Recently, the potential for multiplexed detection of analytes using the QD-AuNP combination was established by Liu et al.[14]. In this study, the simultaneous detection and quantification of adenosine and cocaine was performed by means of colorimetry and fluorescence. However, the construct of the sensor was complicated by the requirement of large QD-AuNP aggregate formation to enable colorimetric detection. For each analyte detected, two different types of AuNPs, functionalized with different aptamer sequences, were called for. A total of two types of AuNPs, one type of QD and three kinds of aptamer/oligonucleotide sequences were involved for the analysis of each analyte. The role of the second AuNP in this study was mainly to facilitate the formation of large nanoparticle assemblies. The use of multiple oligonucleotide-conjugated AuNPs not only involves longer times for the synthesis of these conjugates but also, additional effort and costs for the design and synthesis of different aptamer/oligonculeotide sequences.

In this work, a simpler construct was demonstrated for the use of aptamer-linked nanostructures for FRET-based quenching studies. For every analyte, only one type of AuNP, one QD and two aptamer/oligonculeotide sequences are required. The use of fewer components also simplifies the method optimization, particularly for multiplexed applications. Thrombin was chosen as the model analyte since its

interaction with the anti-thrombin aptamer has been very well documented[15] and widely established[1,16-18]. For this investigation, aptamers were employed as the biospecific ligands since they exhibit high binding constants for a target molecule by "recognition" of a specific epitope on that molecule. Owing to their relative ease of isolation and modification, good stability, cost effectiveness and wide applicability, they are an excellent alternative to antibodies[19]. A homogeneous assay format was chosen for this study since, unlike heterogeneous assays, no cumbersome washing steps would be required to remove free and bound labels prior to detection. Elimination of multiple separation steps makes homogeneous assays much faster, simpler in design as well as straightforward to integrate into automated systems or point-of-care diagnostic devices.

In this study, the quenching of the fluorescence of QDs with emission maxima of 585 nm was accomplished by using AuNP 10 nm in diameter. However, the addition of thrombin was observed to cause an enhancement in the fluorescence of the QDs. The buffer and AuNP: QD ratio to be used for assays were optimized. This simple method was able to detect thrombin in the concentration range of 2.5-40 nM, with a limit of detection of 5 nM. However, the instability of the QDs was found to introduce large variabilities in the assay and needs to be addressed. The details of the proposed FRET-based sensing method are reported herein.

3.3. Materials and methods

3.3.1.Materials and reagents

AuNP (10 nm diameter), 3-mercapto-1-propanol (MCP), bovine serum albumin (BSA), were obtained from Sigma Aldrich (St. Louis, MO). Tris (2-carboxyethyl) phosphine hydrochloride (TCEP) was obtained from Tokyo Chemical Industry (Tokyo, Japan). Streptavidin modified quantum dots (Qdot® 585 and Qdot® 705) were purchased from Invitrogen (Eugene, OR). All the oligonucleotides used in this study (listed in table 3.2) were purchased from Integrated DNA Technologies, Inc. (Coralville, IA) and were purified by standard desalting. Human α-thrombin was purchased from Haematologic Technologies Inc. (Essex Junction, VT). Nanosep® devices from Pall Corporation (Ann Arbor, MI) with 3K and 30K MWCO membranes were used for centrifugal filtration of AuNPs. All other general reagents and solvents were procured from Sigma or VWR.

All chemicals were used as received, without further purification. Ultrapure water, with specific resistance of 18 MΩ cm, was obtained from a Barnstead™ E-Pure™ deionization system (Waltham, MA) and was used for rinses and the preparation of buffers throughout the experiments. The buffers employed in this study were: (a) Phosphate buffer (abbreviated to PB, pH 7, 10 mM) (b) Borate buffer (abbreviated to BB, pH 8.3, 50 mM) and (c) "Selection buffer" (abbreviated to SB, pH 7.5) comprised of 20 mM tris-acetate, 140 mM NaCl, 5 mM KCl, 1 mM $MgCl_2$, and 1 mM $CaCl_2$.Siliconized micro-centrifuge tubes or glass vials were used for carrying out all reactions. Microfluor™ flat bottom, 96-well black plates (medium binding) were

procured from Thermo Scientific (Pittsburgh, PA).Fluorescence measurements were performed on a Spectramax Gemini XS microplate reader from Molecular Devices (Sunnyvale, CA). For all experiments, an excitation wavelength of 350 nm and a cut-off of 495 nm was used.

Table 3.1 DNA sequences used in this study

Oligonucleotide	Sequence	Modification
A_T	5´-GGT-TGG-TGT-GGT-TGG-TTT-TTT-3´	3´-SH
C_T	5´-CCA-ACC-ACA-CCA-ACC-3´	3´-biotin

3.3.2. Conjugation of AuNP to aptamer

The thrombin-binding aptamer, $A_{T,}$ was conjugated to AuNP by modification of previously published protocol[1,20]. The thiol-modified aptamer (18 μL, 200 μM) was activated by treating it with 15 μL of 10 mM TCEP solution in a 50 mM acetate buffer (pH 5.2) for an hour at room temperature (RT). The activated aptamer was denatured by heating to 90º C for 3 minutes and allowed to cool down for 15 minutes at RT to allow renaturation of the aptamer. The aptamer was added to 3600 uL of 10 nm AuNP followed by the addition of PB to make the total volume 6 mL. The mixture was incubated at RT overnight followed by the addition of NaCl to a final concentration of 0.1M. The solution was allowed to age at RT for two days. The excess DNA was removed by centrifugal filtration through a 30 K MWCO membrane and the precipitate was washed thrice with PB to which NaCl was added to a final concentration of 0.1M (0.1 M PBS). The AuNPs were redispersed in 2 mL of 0.1M PBS and treated with MCP (to a final concentration of 3 μM) for 2 hours at RT. The

AuNPs were separated by centrifugal filtration, rinsed thrice with SB and resuspended in 1 mL of the same. The final concentration of the modified AuNPs was determined from the maximum absorbance of the SPR band and the extinction co-efficient of similar AuNPs as reported in literature[21].

3.3.3.Conjugation of QD to complement

The biotinylated DNA sequence, C_T, was denatured by heating to 90º C for 3 minutes and allowed to cool down to RT before use. Streptavidin conjugated QD (1 μM), 40 μL was mixed with 20 equivalents of C_T (4 μL, 200 μM) at 4 ºC for at least 2 hours. The QDs were centrifuged to remove unbound DNA and rinsed with BB. The supernatant was removed and reconstituted in 80 μL of BB to produce a 500 nM QD solution. This concentrated solution was stored at 4 ºC and aliquots were diluted to 50 nM with BB immediately before use in quenching experiments.

3.3.4. Buffer selection for AuNP-QD quenching

The biotinylated DNA sequence, C_T, was conjugated to streptavidin-QDs 705 by the procedure described above. The QD 705-C_T conjugates were reconstituted in BB to produce a 50 nM QD solution. 245 μL each of BB, SB and PB were dispensed in triplicate into the wells of a 96-well plate. 5 μL of the 50nM QD 705-C_T conjugate was dispensed in each well, resulting in a final concentration of 1 nM QDs in each well. The plates were transferred to the plate reader and shaken for 10 seconds before

reading the fluorescence signal at 705 nm at various time intervals over a period of two hours. For each data point, the average and standard deviation of triplicate measurements were reported.

3.3.5. Quenching of fluorescence of QDs by AuNPs

For the quenching experiments, AuNP-A_T conjugates were added in different molar ratios to a fixed amount of the QD 585-C_T conjugate and the emission spectra of the QDs were monitored. The final concentration of QDs in each well was maintained at 1 nM while the total sample volume was 250 µL. The buffer system employed was a 1:1 mix of BB and SB, determined to be optimal from prior experiments. AuNP: QD 585 ratios of 1, 2, 5, and 10 were investigated. AuNP-A_T conjugates were mixed with the QD 585-C_T conjugates in microcentrifuge tubes and allowed to incubate for 15 or 30 minutes at 4 ºC to allow the DNA strands to hybridize. The solutions were transferred to 96 well-plates before recording the fluorescence emission spectra. For control studies, the unmodified AuNP and streptavidin QDs were used in a similar manner, the only exception being that the fluorescence intensity was read right after mixing to minimize non-specific interactions between the AuNPs and QDs.

For the detection of thrombin, 10 µL of concentrated thrombin solutions were added to the wells, together with AuNP-A_T and QD 585-C_T conjugates and incubated for 30 minutes at 4ºC before reading. The buffer system (1:1 mixture of SB and BB) was modified by adding BSA to a final concentration of 0.01 % (w/v).

3.4. Results and discussion

3.4.1. Principle of the homogeneous assay

The principle of the sensing method for the proposed homogeneous assay is depicted in figure 3.1. The thiolated thrombin binding aptamer (A_T) was conjugated to the 10 nm AuNPs through gold-sulfur bonds while MCP was used to block any non-specific binding to the AuNP surface. The aptamer functionalized AuNPs are referred to as AuNP-A_T henceforth. The DNA sequence complementary to A_T, C_T, was obtained with a biotin moiety at the 3´ end, which facilitated their conjugation to the streptavidin-modified 585 QDs (referred to as QD 585-C_T). When the two sequences (A_T and C_T) bind to each other, the corresponding AuNP and QD are drawn closer, forming a duplex (henceforth, referred to as AuNP-QD). The proximity of the QD to the AuNP enables energy transfer from former to the latter, leading to quenching of the fluorescence of the QD. Addition of thrombin causes dissociation of this duplex and release of the QD-labeled sequence, C_T, with subsequent recovery of the QD fluorescence. Hence, the fluorescence signal detected will increase with an increase in the amount of thrombin present in the sample.

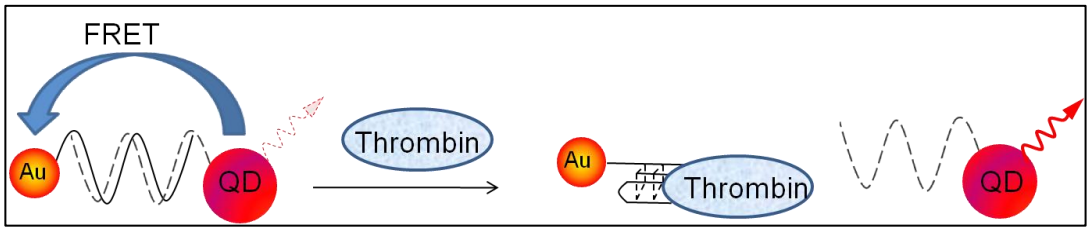

Figure 3.1 Schematic representation of the homogeneous assay based on energy transfer from QDs to AuNPs

For FRET to occur, the absorption of the AuNPs and the emission of the QDs have to overlap, which is true for the AuNPs and QDs chosen for this study. Figure 3.2(a) represents the absorption spectrum of the 10 nm AuNP-A_T (solid line) and fluorescence spectrum of QD-C_T (dotted line). QD 585 was chosen for this study for two reasons (a) they have a higher extinction co-efficient compared to QDs that emit at smaller wavelengths (e.g. ~ 6 times higher than QD 525 at excitation of 405 nm) (b) commonly used polymers show lower autofluorescence at higher wavelengths, which would be favorable for possible integration with polymeric microfluidic devices.

The proposed sensor concept was tested by measuring the recovery of the fluorescence signal of QD 585 quenched with AuNP in the presence of thrombin. As shown in figure 3.2(b), the addition of AuNP-A_T in 1:1 molar ratio to 1nM QD-C_T (with 15 minute incubation at 4°C) leads to quenching of the fluorescence intensity of the QD (dotted line) to about half of the original value (solid line). In the presence of 160 nM thrombin and under similar conditions, the fluorescence signal of the QDs was 67 % higher (dashed line) than in the absence of thrombin. This proves that thrombin can preferentially displace the sequence C_T and bind to the aptamer A_T and that the ensuing signal recovery of QDs is sufficient to enable the sensing of thrombin.

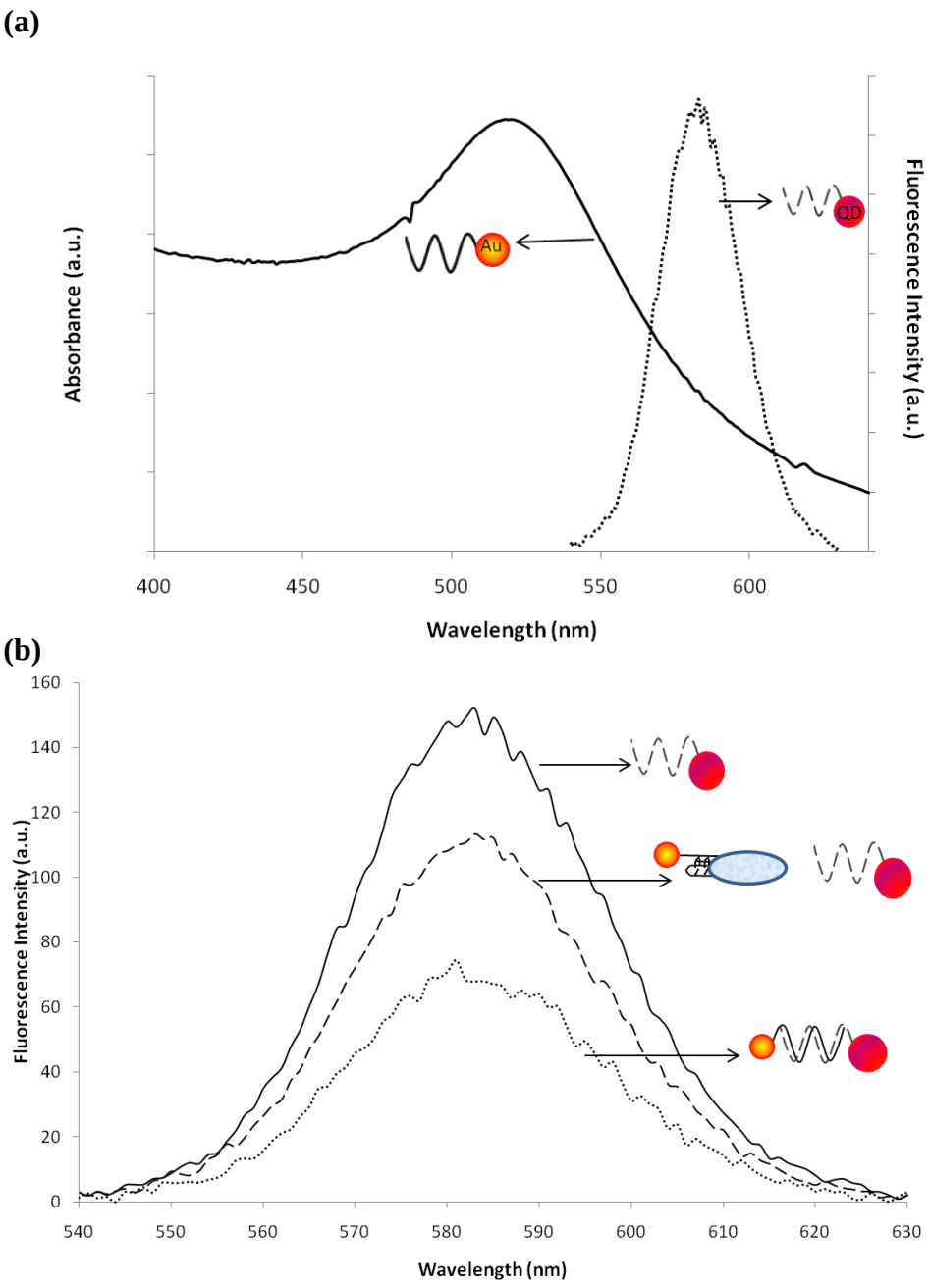

Figure 3.2 (a) Absorbance spectrum of 10 nm AuNP-A_T (solid line) and fluorescence spectrum of QD 585-C_T (dotted line). **(b)** Fluorescence spectra of QD 585-C_T (solid line), QD-Au (1:1) without thrombin (dotted line) and QD-Au with 160 nM thrombin (dashed line).

3.4.2. Buffer selection for AuNP-QD quenching

The signal from QDs has been shown to be highly dependent on the nature of the buffer used for immunoassays[22]. The exact mechanism for this instability is not known but the general opinion is that the chemical composition of the buffer affects the surface charge of the QDs, thereby inducing colloidal instability. This leads to aggregation of the QDs and a reduction in the effective surface area available for photon absorption and emission, causing a loss in fluorescence signal[22]. Zhu et al. have studied the stability of QDs with different surface chemistries (amine-terminated, streptavidin-coated and antibody-conjugated). However, previous studies have not specifically addressed the stability of ssDNA- conjugated QDs in different buffer systems. The ssDNA molecule is highly negatively charged and hence, the colloidal stability of its conjugates is expected to be different from protein conjugated QDs.

In order to determine the most compatible buffer for this particular study (involving aptamer-complement and aptamer-thrombin interactions), three relevant buffers were investigated. PB was selected as it is used for the preparation and storage of AuNP-aptamer conjugates while BB was included on account of the maximal stability demonstrated by QDs in this system[22]. SB was investigated as it is the medium in which the thrombin-binding aptamer was selected by the process of SELEX (Systematic Evolution of Ligands by Exponential Enrichment)[23].

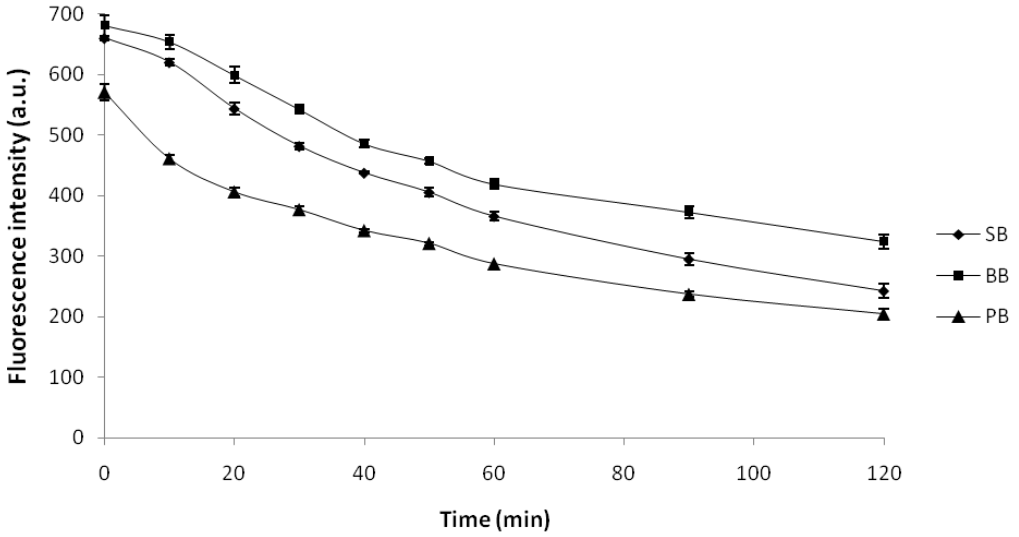

Figure 3.3 Effect of different buffers on fluorescence signal of QDs. The error bars represent the standard deviation in triplicate measurements. The lines joining the data points are meant to be a guide for the eye only. (SB: Selection buffer; BB: Borate buffer; PB: Phosphate buffer)

Figure 3.3 shows the fluorescence signals obtained from the C_T-QD 585 conjugate, measured over a period of two hours. Overall, the maximum fluorescence signal is obtained from the conjugates suspended in BB. The signal is reduced in both SB and PB, with the latter showing a much greater dimuntion of fluorescence. The fluorescence signal from QDs in all three buffers was observed to decrease with time to about 50 % of the original signal. It is hypothesized that the QD-conjugates are stabilized by electrostatic repulsion due to surface charges and aggregate in the presence of low concentrations of divalent anions (hydrogen phosphate ions) or relatively higher concentrations of monovalent anions (chloride ions). Aggregation reduces the effective QD surface area available for photon excitation and emission, leading to attenuation of the fluorescence signal. However, such an instability is not

observed in presence of borate buffer, possibly due to the existence boric acid in uncharged form at pH 8.3 (pKa of boric acid= 9.2). However, other means of instability such as the degradation of QDs by oxidation cannot be ruled out[24] . SB, though not optimal for fluorescence stability, needed to be included as it contains the relevant monovalent/divalent cations which maintain the G-quartet structure needed for α-thrombin binding by the aptamer. Hence, a 1:1 ratio of BB and SB was selected as the buffer of choice for further experiments.

3.4.3. Effect of AuNPs on the fluorescence of QDs

In order to develop a sensitive FRET-based quenching assay, it is important to determine the molar ratio of AuNP to QD 585 at which maximal quenching of the QDs occurs together with minimal contribution from non-specific elements. In order to do this, AuNP-A_T conjugates were added in different molar ratios to a fixed amount of the QD 585-C_T conjugate and the emission spectra of the QDs were monitored. Figure 3.4(a) shows the change in fluorescence intensity of QD 585-C_T conjugates with the addition of increasing quantities of AuNP-A_T. The fluorescence intensity of QD 585 was observed to decrease progressively with an increase in the ratio of added AuNP. A AuNP: QD ratio of 1 caused almost 50 % reduction quenching of the fluorescence signal, while maximal quenching was observed at a ratio of 10, with the signal being decreased to less than 15% of the original intensity after 30 minutes of incubation. Molar ratios of AuNP: QD 585 greater than 10 were not investigated since each QD is expected to have 5-10 molecules of streptavidin (as per the product leaflet

provided), and thus, will be able to interact with a maximum of 10 AuNPs through hybridization of complementary ssDNA immobilized on their respective surfaces.

(a)

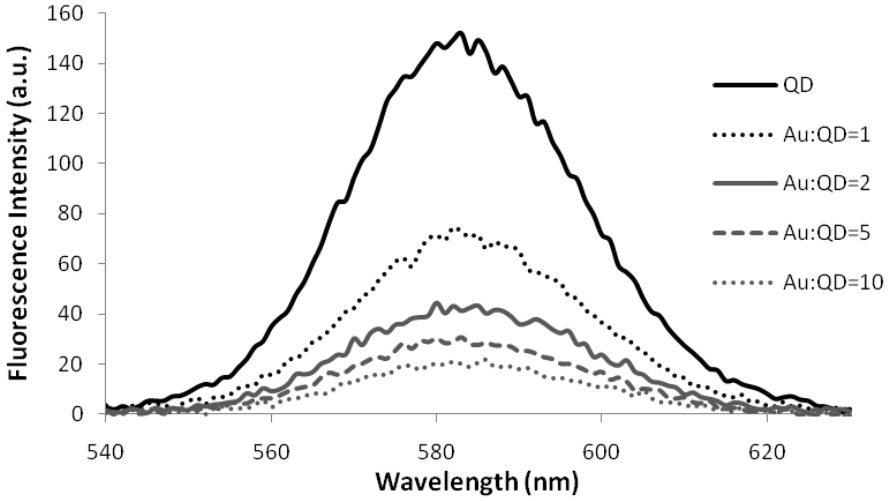

(b)

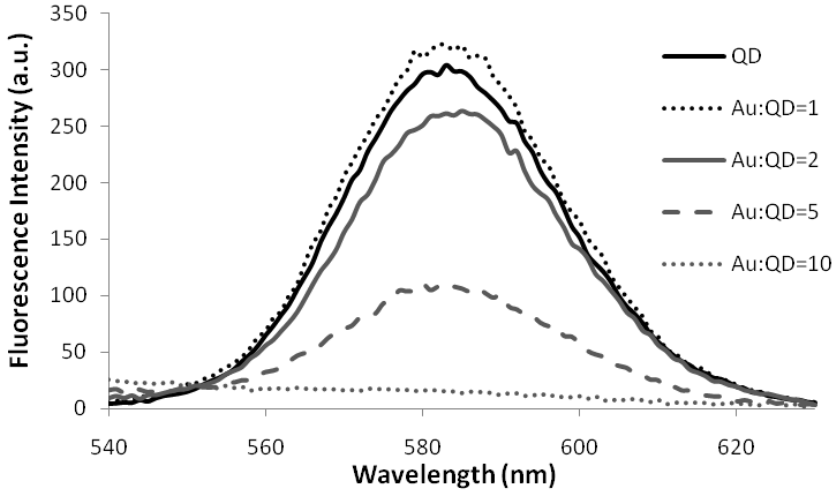

Figure 3.4 Evolution of the fluorescence intensity of (a) QD 585-C_T conjugates (due to aptamer-complement interactions) as a function of the molar ratio between AuNP-A_T and QD 585-C_T. (b) QD 585 (due to non-specific interactions) as a function of the molar ratio between AuNP and QD 585. The legends represent the molar ratio of AuNP: QD 585.

In order to investigate the possibility of inner-filter effects, scattering or quenching due to non-specific interactions between the AuNP and QDs, non-ssDNA conjugated AuNP and QDs were used. It should be noted that the surface of AuNP-A_T was previously blocked with MCP to reduce non-specific interactions and hence, determination of quenching, if any, due to inner-filter effects or scattering due to AuNPs was the primary objective. In order to investigate these optical interferences, AuNPs blocked with a layer of MCP should be used to reduce non-specific interactions of proteins with the AuNP surface. However, in practice, it was not possible to obtain a stable suspension of MCP-functionalized AuNPs. Even brief treatments with extremely dilute solutions of MCP (~100 nM) rendered the AuNPs prone to aggregation, probably due to the removal of the stabilizing layer of citrate ions. Hence, citrate-stabilized AuNPs were used without any modification and the fluorescence intensity was measured immediately after mixing to minimize contribution from non-specific interactions between the AuNPs and QDs.

As depicted in figure 3.4(b), significant quenching of QD fluorescence was observed with increasing proportion of AuNP: QD. A AuNP: QD ratio of 1 exhibited no quenching (within limits of experimental error) while a ratio of 10 showed complete obliteration of the signal. There could be two possible reasons for this observation (a) significant self-absorbance/inner-filter and scattering effects associated with higher concentrations of AuNPs (b) higher concentration of AuNPs enable greater non-specific absorption of streptavidin-QDs to their surface, leading to quenching. For comparison, the percentage residual fluorescence intensities at each

AuNP: QD ratio for quenching by both specific (involving ssDNA hybridization) and non-specific means were plotted as shown in figure 3.5. The residual fluorescence intensity, F_R, at various AuNP: QD ratios were calculated as below:

$$F_R = F / F_0 \qquad [1]$$

where F and F_0 are the fluorescence intensities at 585 nm for samples with and without AuNP, respectively. For a highly sensitive assay, maximal quenching is desirable, together with minimal non-specific effects. From figure 5, it can be seen that both Au:QD ratios of 1 and 2 demonstrate none or minimal non-specific quenching, coupled with 50% and 70 % quenching of fluorescence due to aptamer-complement interactions. A AuNP: QD ratio of 1 was selected for further experiments due to the smaller requirement of AuNPs.

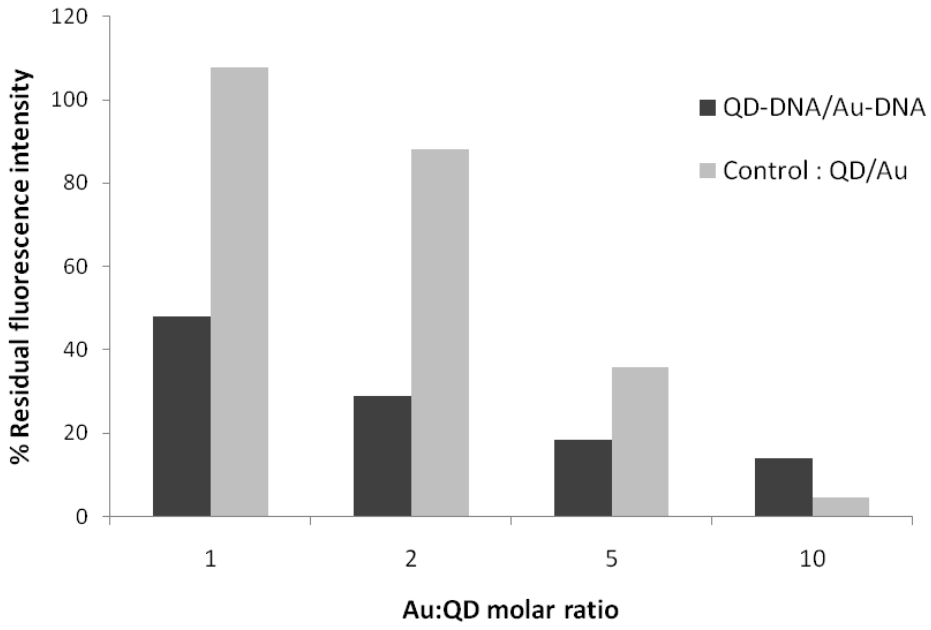

Figure 3.5 Percentage residual fluorescence intensities at various AuNP: QD ratios for quenching by specific QD and Au coupling (dark grey) and non-specific means (light grey).

3.4.4. Detection of Thrombin

For the detection of thrombin, the buffer system from previous experiments was modified by the addition of trace amount of BSA (final concentration of 0.01 % w/v). This was done in order to stabilize the fluorescence signals from the AuNP-QD duplex after incubation since, as can be seen from figure 3.2(b), the fluorescence signal of the QDs is quite noisy even after 15 minutes of incubation. Addition of 0.01% BSA stabilized the fluorescence of the QDs, enabling a longer incubation time of 30 minutes without significant interference with the hybridization of A_T and C_T. Also, prior to use, thrombin samples (commercially supplied as a solution in 50 % glycerol) were subjected to extensive centrifugal filtration to remove all traces of glycerol and resuspended in ultrapure water. This purification step was necessitated by the fact that the presence of trace quantities of glycerol hampered the fluorescence recovery of the QDs upon thrombin addition (data not shown). Glycerol changes the refractive index of the medium causing a red-shift of the SPR band of the AuNPs, which in turn, leads to a greater overlap with the emission spectrum of QD 585[25].

(a)

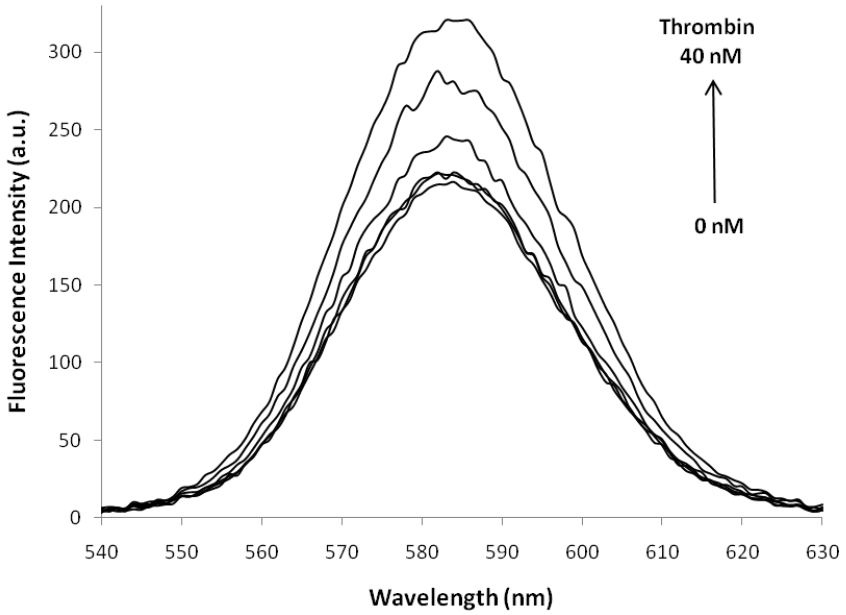

(b)

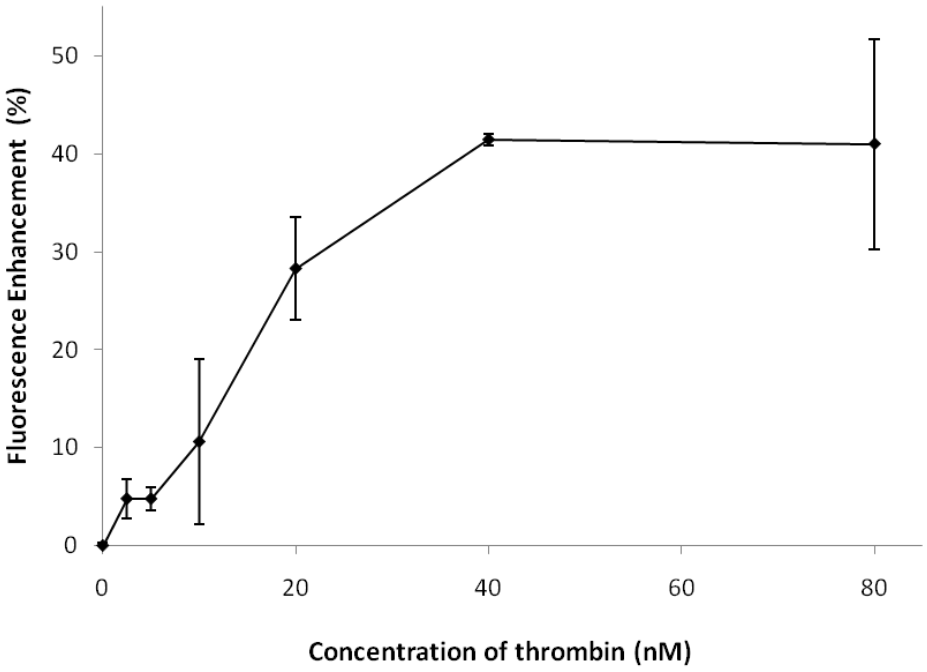

Figure 3.6 (a) Evolution of the fluorescence spectra of AuNP-QD 585 (1:1 molar ratio) in the presence of increasing concentrations of thrombin. Thrombin concentrations from bottom to top are 0, 2.5, 5, 10, 20 and 40 nM, respectively. **(b)**Fluorescence enhancement as a function of thrombin concentration. The error bars represent the standard deviation in triplicate measurements.

The evolution of the fluorescence spectra of AuNP-QD 585 in the presence of increasing concentrations of thrombin is shown in figure 3.6(a). The fluorescence signals, overall, were much higher after the addition of BSA (compare to figure 3.2(b)) and were seen to increase with an increase in the concentration of thrombin from 0 to 40 nM. Higher concentrations of thrombin did not induce any further increase in fluorescence signals. The fluorescence enhancement, F_E, caused by the addition of thrombin was calculated as a percentage as follows:

$$F_E = \{(F_{Thrombin} - F_{Control}) / F_{Control}\} \times 100 \qquad [2]$$

where $F_{Thrombin}$ and $F_{Control}$ are the fluorescence intensities at 585 nm in the presence and absence of thrombin, respectively. The data from triplicate experiments were plotted as shown in figure 3.6(b). Fluorescence enhancement of 5-40 % was produced in response to the presence of 2.5 to 40 nM of thrombin (the dynamic range). The linear range of the assay, using 1 nM of QDs, spans the same range with an R^2 value of 0.9654. The limit of detection (LOD) was calculated to be 5nM (LOD= average signal of the blank + 3 times standard deviation of the signal of 2.5 nM thrombin). It is also noteworthy that the sensor was able to specifically detect 5 nM of thrombin, within 30 minutes, in the presence of 0.01 % BSA (equivalent to 1.5 µM of BSA, a 300 fold molar excess).

Inspite of these promising preliminary results, the variability of signals arising from instability of QDs posed a serious challenge to further development. The variability in the data can be observed from the large relative standard deviations associated with some data points. This can be attributed to the fact that only 1 nM of

QDs were being used for each sample coupled with the extreme instability of QDs, particularly when they undergo dilution. This instability probably offsets some of the fluorescence enhancement due to addition of thrombin, decreasing the sensitivity of the assay. The addition of BSA helped reduce the extent of this signal loss but was not sufficient to eliminate all QD instability. It is anticipated that using a larger concentration of QDs will increase both the sensitivity and the linear range of the assay. Additionally, other methods or additives for stabilizing QDs in aqueous environments need to be investigated. An added requirement is that the stabilizing layer cannot be too bulky or else it might hinder FRET between the QDs and the quencher.

3.5. Conclusions

The goal of this study was to demonstrate the feasibility of using aptamer-linked nanostructures in FRET-based quenching for the detection of proteins. Thrombin was used as the model analyte in this study. The anti-thrombin aptamer was conjugated to 10 nm AuNPs while a complementary sequence was conjugated to the QDs with emission maxima of 585 nm. Quenching of the fluorescence of QDs occurred when the aptamer and the complementary sequences were allowed to hybridize. The addition of thrombin caused an enhancement in the fluorescence of the QDs which was proportional to the concentration of thrombin. The stability of QDs in different buffers was studied and a buffer system containing borate buffer and selection buffer in 1:1 ratio was determined to be optimal. A 1:1 ratio of AuNP: QD

was used for the assays as it provided maximal quenching with negligible optical interference from AuNPs. This simple method was able to detect thrombin in the concentration range of 2.5-40 nM, with a limit of detection of 5 nM. However, the instability of the QDs was found to introduce large variabilities in the assay and needs to be addressed prior to further development.

3.6. References

1. Wang, W., Chen, C., Qian, M. & Zhao, X.S. Aptamer biosensor for protein detection using gold nanoparticles. *Anal. Biochem.* **373**, 213-219 (2008).

2. Han, M., Gao, X., Su, J.Z. & Nie, S. Quantum-dot-tagged microbeads for multiplexed optical coding of biomolecules. *Nat. Biotechnol.* **19**, 631-635 (2001).

3. Sapsford, K.E., Pons, T., Medintz, I.L. & Mattoussi, H. Biosensing with Luminescent Semiconductor Quantum Dots. *Sensors* **6**, 925-953 (2006).

4. Bailey, R.E., Smith, A.M. & Nie, S. Quantum dots in biology and medicine. *Physica E* **25**, 1-12 (2004).

5. Dyadyusha, L. et al. Quenching of CdSe quantum dot emission, a new approach for biosensing. *Chem. Commun.* 3201-3203 (2005).

6. Ao, L., Gao, F., Pan, B., He, R. & Cui, D. Fluoroimmunoassay for antigen based on fluorescence quenching signal of gold nanoparticles. *Anal. Chem.* **78**, 1104-1106 (2006).

7. Mayilo, S. et al. Competitive homogeneous digoxigenin immunoassay based on fluorescence quenching by gold nanoparticles. *Anal. Chim. Acta* **646**, 119-122 (2009).

8. Lichlyter, D.J., Grant, S.A. & Soykan, O. Development of a novel FRET immunosensor technique. *Biosens. Bioelectron.* **19**, 219-226 (2003).

9. Oh, E. et al. Inhibition assay of biomolecules based on fluorescence resonance energy transfer (FRET) between quantum dots and gold nanoparticles. *J. Am. Chem. Soc.* **127**, 3270-3271 (2005).

10. Chang, E. et al. Protease-activated quantum dot probes. *Biochem. Bioph. Res. Co.* **334**, 1317-1321 (2005).

11. Oh, E. et al. Nanoparticle-based energy transfer for rapid and simple detection of protein glycosylation. *Angew. Chem.* **118**, 8127-8131 (2006).

12. Kim, Y.-P. et al. Energy transfer-based multiplexed assay of proteases by using gold nanoparticle and quantum dot conjugates on a surface. *Anal. Chem.* **80**, 4634-4641 (2008).

13. Xia, Y., Song, L. & Zhu, C. Turn-on and near-infrared fluorescent sensing for 2,4,6-trinitrotoluene based on hybrid (gold nanorod)−(quantum dots) assembly. *Anal. Chem.* **83**, 1401-1407 (2011).

14. Liu, J., Lee, J.H. & Lu, Y. Quantum dot encoding of aptamer-linked nanostructures for one-pot simultaneous detection of multiple analytes. *Anal. Chem.* **79**, 4120-4125 (2007).

15. Paborsky, L.R., McCurdy, S.N., Griffin, L.C., Toole, J.J. & Leung, L.L. The single-stranded DNA aptamer-binding site of human thrombin. *J. Biol. Chem.* **268**, 20808-20811 (1993).

16. Centi, S., Tombelli, S., Minunni, M. & Mascini, M. Aptamer-based detection of plasma proteins by an electrochemical assay coupled to magnetic beads. *Anal. Chem.* **79**, 1466-1473 (2007).

17. Sheila A. Grant, Darcy J. Lichlyter, Susan Lever, Fabio Gallazzi & Orhan Soykan A novel sensing technique to detect thrombin. *Sens. Lett.* **2**, 164-170 (2004).

18. Kang, Y. et al. Electrochemical detection of thrombin by sandwich approach using antibody and aptamer. *Bioelectrochemistry* **73**, 76-81 (2008).

19. Numnuam, A. et al. Aptamer-based potentiometric measurements of proteins using ion-selective microelectrodes. *Anal. Chem.* **80**, 707-712 (2008).

20. Liu, J. & Lu, Y. Preparation of aptamer-linked gold nanoparticle purple aggregates for colorimetric sensing of analytes. *Nat. Protoc.* **1**, 246-252 (2006).

21. Liu, X., Atwater, M., Wang, J. & Huo, Q. Extinction coefficient of gold nanoparticles with different sizes and different capping ligands. *Colloid. Surface. B* **58**, 3-7 (2007).

22. Zhu, X., Duan, D., Madsen, S. & Publicover, N.G. Compatibility of quantum dots with immunobuffers, and its effect on signal/background of quantum dot-based immunoassay. *Anal. Bioanal. Chem.* **396**, 1345-1353 (2009).

23. Bock, L.C., Griffin, L.C., Latham, J.A., Vermaas, E.H. & Toole, J.J. Selection of single-stranded DNA molecules that bind and inhibit human thrombin. *Nature* **355**, 564-566 (1992).

24. Derfus, A.M., Chan, W.C.W. & Bhatia, S.N. Probing the cytotoxicity of semiconductor quantum dots. *Nano Lett.* **4**, 11-18 (2004).

25. Chen, H., Kou, X., Yang, Z., Ni, W. & Wang, J. Shape- and size-dependent refractive index sensitivity of gold nanoparticles. *Langmuir* **24**, 5233-5237 (2008).

CHAPTER 4

A MICROFLUIDIC SENSOR BASED ON FERROMAGNETIC RESONANCE INDUCED IN MAGNETIC BEAD LABELS

Esha Chatterjee, Tim Marr, Pallavi Dhagat, and Vincent T. Remcho

Sensors and Actuators B: Chemical

1183 Westline Industrial Drive, St. Louis, MO 63146

Volume 156 (2011), Issue 2, 651-656.

4.1. Abstract

This report details preliminary studies towards the development of a microfluidic sensor that exploits ferromagnetic resonance, excited in magnetic bead labels, for signal transduction. The device consists of a microwave circuit in which a slotline and a coplanar waveguide are integrated with a biochemically activated sensor area. The magnetic beads are immobilized in the sensor area by bio-specific reactions. A microwave signal applied to the slotline is coupled to the coplanar waveguide only in the presence of magnetic beads at the functionalized sensor area. Ferromagnetic resonance in the beads further enhances the coupling. This inductive detection technique lends itself to miniaturization, is inexpensive to fabricate and can be adapted for the detection of a wide range of molecules for which bio-specific ligands are available.

Experimentally, the variation of the output signal as a function of the location of magnetic beads was studied for the proposed technique. Subsequently, a prototype device was constructed by biotinylation of the sensor area and integration with a microfluidic chip fabricated in polydimethyl siloxane (PDMS). Preliminary experiments were conducted on this prototype using streptavidin-functionalized magnetic beads as labels. It was shown that the magnetic beads, immobilized at the sensor area by streptavidin-biotin linkage, produced a distinct ferromagnetic resonance response easily discernable from the background signal.

Keywords: Microfluidics, Sensors, Ferromagnetic resonance, Magnetic beads

4.2. Introduction

An important step towards the development of a portable, standalone, point-of-use diagnostic device involves integration of a highly sensitive transduction system with the sensing module. Typically, immunoassay-based techniques employ a label attached to a biochemical probe for detection. Labels may be molecules such as radioisotopes, fluorescent dyes or enzymes, or may be particulate in nature, such as quantum dots and nanoparticles. Label-free methods of detection, such as surface plasmon resonance (SPR) and quartz crystal microgravimetry (QCM) are gaining popularity as they bypass the traditional labeling steps to provide a rapid and highly specific means of identifying and quantifying analytes. While these label-free techniques offer advantages in terms of reduced assay time, which is essential in the field of rapid-onset-illness diagnostics, they cannot at present match the detection limits of traditional labeled assays such as ELISA or radioimmunoassay (RIA) [1]. SPR can only detect molecules in close proximity of the sensing surface, which is not suitable for typical microfluidic devices since they have channel heights much greater than 200 nm [2]. Also, instrumentation based on QCM and SPR are not as amenable to miniaturization and batch fabrication [3]. Conventional techniques for detection of labeled molecules are highly sensitive but suffer from certain drawbacks. Radioactive labels have a limited shelf life and stringent waste disposal requirements. Optical detection requires the use of instrumentation that is bulky and difficult to miniaturize [4]. Thus, there is a need for investigation into alternative methods of transduction that are highly sensitive, conducive to miniaturization and suitable for mass production.

This report presents a novel high-sensitivity inductive detection technique for potential immunosensing applications using magnetic beads as labels: a microwave circuit, designed for operation at frequencies from 2 GHz to 4 GHz, was used to excite ferromagnetic resonance (FMR) in beads immobilized at the sensor area and detect the resulting signal. The biotin-avidin pair was employed to demonstrate the potential of this technique for bio-specific detection. High sensitivity was achieved both by operating at high frequency and matching the microwave excitation to the ferromagnetic resonance frequency in the beads. To our knowledge, this is the first report that demonstrates inductive detection of FMR excited in magnetic bead labels for biosensing applications. In contrast to commonly proposed magnetoimpedance [5-11] or Hall-effect [12-13] sensors, the microwave circuit requires no specialty thin films or complex processing. The circuit was implemented in a single metal layer and fabricated using standard, inexpensive, integrated circuit (IC) processes. This report establishes the feasibility of using FMR-based detection of magnetic labels towards an inexpensive, mass-producible, hand-held sensor for biomolecules. In the following sections, the principle of operation, fabrication techniques, experimental setup and results are elaborated.

4.3. Description of Sensor Operation

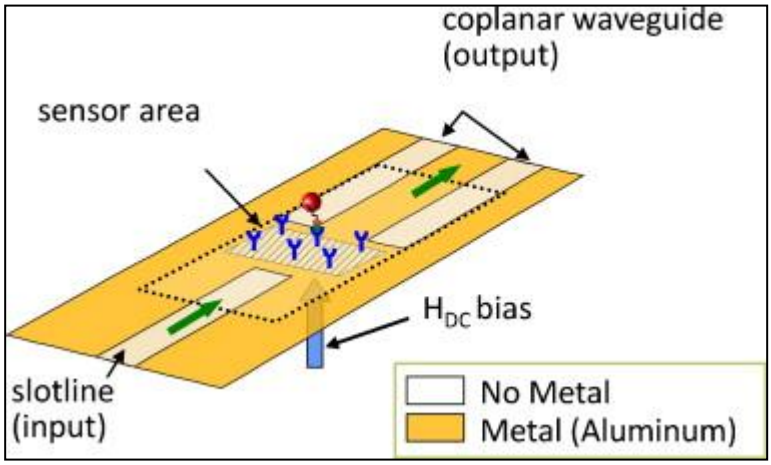

Figure 4.1 Schematic of the microwave circuit (Not drawn to scale). The dotted line around the sensor area represents the spatial orientation of the actual area functionalized with biotin.

As shown in Fig.4.1, the microwave circuit consists of a slotline and a coplanar waveguide (CPW). The junction between the slotline and coplanar waveguide is the active sensor area, which may be functionalized with analyte-specific ligands such as antibodies or aptamers. In this study, the avidin-biotin pair was employed to demonstrate biospecific interactions due to unique properties such as (i) the exceptionally strong interaction between biotin and avidin ($K_a = 10^{15}\ M^{-1}$) (ii) availability of multiple sites on avidin for binding biotin, so that it can act as a cross-linker between two biotinylated moieties (iii) easy commercial availability of a wide variety of biotinylated antibodies and aptamers, which allows incorporation of these bio-specific ligands in the device in future. The waveguides were patterned in thin-film aluminum, thermally evaporated on a glass substrate. The active sensor area was defined using a facile method of photo-activated patterning of biotin.

When the slotline is excited by a microwave signal, *ac* magnetic fields are generated at the junction. These fields are orthogonal to the electromagnetic wave modes allowed in the coplanar waveguide. Consequently, no signal couples from the slotline into the coplanar waveguide. When magnetically labeled moieties are immobilized at the junction, the field distribution is perturbed resulting in the input signal being inductively coupled to the output at the coplanar waveguide. The output signal is proportional to the frequency of microwave excitation and is further enhanced by stimulating ferromagnetic resonance in the beads. The design of the microwave waveguides has previously been reported in [14] and is based on equations found in [15-16]. The condition for FMR is described as follows [17]:

$$\omega_{FMR}=\gamma\mu_0 H_{DC} \qquad \text{(Eq. 1)}$$

where ω_{FMR} is the FMR frequency; γ, the gyromagnetic ratio (~175 GHz/Tesla); μ_0, the permeability of free space and H_{DC}, a *dc* magnetic field bias. The bias field must be adequate to saturate the magnetic beads to ensure that their magnetization precesses in phase at resonance.

4.4. Materials and methods

4.4.1. Materials and reagents

Superparamagnetic beads, 1 μm in diameter, were obtained from MagSense Life Sciences (West Lafayette, IN, USA). Streptavidin coated magnetic beads (nanomag-D, 250 nm) were purchased from Micromod (Rostock-Warnemuende,

Germany). Bovine serum albumin (BSA), (3-aminopropyl) triethoxysilane (APTS) and dimethyl sulfoxide, anhydrous (DMSO) were obtained from Sigma Aldrich (St. Louis, MO, USA). A photoactivable form of biotin with tetrafluorophenyl azide moiety, EZ-Link TFPA-PEG_3-Biotin, and fluorescein labeled Neutravidin were purchased from Pierce Biotechnology, Inc. (Rockford, IL, USA). SU-8 3050, a negative tone, epoxy based Photoresist was purchased from Microchem (Newton, MA, USA). Sylgard® 184 (Silicone elastomer kit) comprised of polydimethyl siloxane (PDMS) prepolymer and curing agent was obtained from Dow Corning Corp. (Midland, MI, USA). Corning 1737 (Corning, NY, USA) one inch square glass slides were used as the substrate for the detection circuit.

All general reagents and solvents were procured from Sigma Aldrich or VWR (West Chester, PA, USA). The phosphate buffer solution (PBS) consisted of 10 mM phosphate-buffered saline and 149 mM NaCl (pH 7.4). The blocking buffer used was a 1% (w/v) solution of BSA in PBS (pH 7.4). All chemicals were used as received, without further purification. Ultrapure water, with specific resistance of 18 MΩ-cm, was obtained from a Barnstead™ E-Pure™ deionization system (Waltham, MA) and was used for rinses and the preparation of buffers throughout the experiments. An Axiotron Inspection Microscope (Carl Zeiss MicroImaging, Germany) with an attached camera (Model TCA-3.0C from Tucsen Imaging Technology, Fujian, China) was used for acquiring the images shown in Fig. 4.7.

4.4.2. Microwave circuit fabrication

The microwave circuit was fabricated using photolithography and wet chemical etching. A 500 nm film of aluminum was deposited onto a one inch square glass slide by thermal evaporation. The waveguides were then patterned using a 1:1 chrome mask and Karl Suss MJB3 (Garching, Germany) contact aligner to expose positive photoresist (Shipley 1818, Microchem) spin coated onto the slide. The exposed aluminum was etched in a standard aluminum etchant (16:2:2:1 solution of H_3PO_4, H_20, HNO_3, CH_3COOH) to form the waveguides. The remaining photoresist was removed with acetone. Finally, a 500 nm layer of silicon dioxide was sputtered onto the sensor surface for insulation and subsequent functionalization with biotin (as detailed in section 4.4.5.1.).

The waveguides were designed to allow propagation of frequencies in the 2-4 GHz range. As determined by Eq. 1, these frequencies correspond to the *dc* bias field required to saturate the magnetic beads. The microwave circuit was modeled for Corning 1737 glass substrate. Details of the modeling parameters used and the results obtained were published in an earlier report [14]. Briefly, both the slotline and CPW were designed to have a 50 Ω characteristic impedance to match available instrumentation (section 4.4.3.and depicted in Fig.4.2). The slot line is 78 μm wide and the CPW has a 78 μm center conductor separated from the ground plane on both sides by 28 μm gaps. The distance from the end of the slotline to the CPW is 50 μm providing an active sensor area of approximately 50 μm by 78 μm (Fig. 4.5a). In order to allow the slotline to be driven from a coaxial cable, a ¼-wave stub, CPW-to-slotline

transformer was also patterned on the glass slide. External electrical connections were made to the waveguides by wire bonding to a printed circuit board having coaxial cable connectors.

4.4.3. Electronic Instrumentation

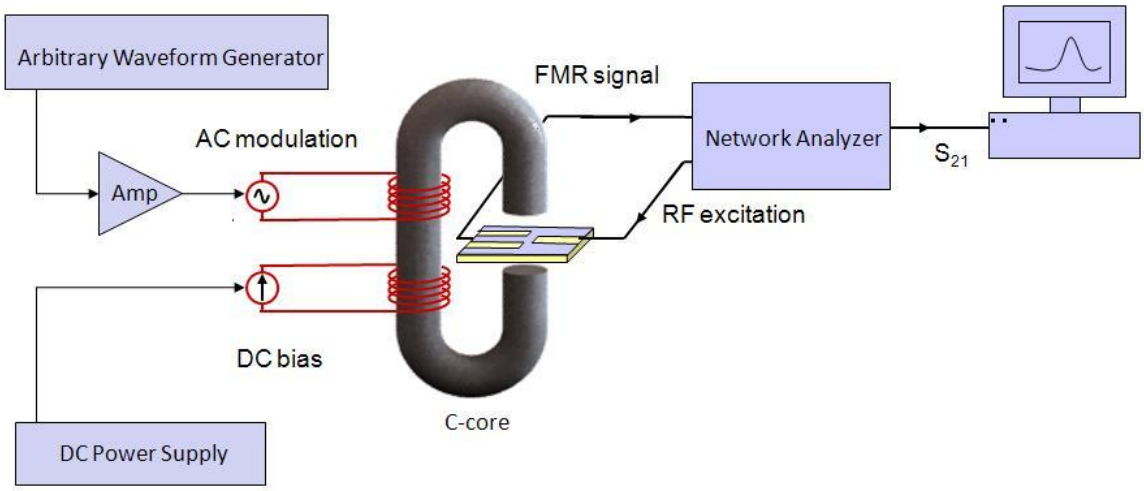

Figure 4.2. Instrumentation setup for detecting FMR signal coupled from the slotline to the CPW.

The laboratory instrumentation used to measure the magnetic bead response of the sensor is shown in Fig. 4.2. A network analyzer (ENA5071C, Agilent Technologies, Santa Clara, CA) was used to excite the slotline with a microwave signal and monitor the signal coupled to the CPW. The excitation frequency, chosen to be 2.7 GHz in these experiments, lies within the designed range of operating frequencies for the microwave circuit. The network analyzer measures the transmission parameter, S_{21} - i.e. the ratio of microwave power received at the CPW to

the power input at the slotline. The detected S_{21} signal depends on the number and location of magnetic beads present at the junction area and peaks when the excitation frequency matches the ferromagnetic resonance frequency set by the *dc* bias field (Eq. 1).

The bias field was applied using a C-shaped iron core wound with two independent wire coils. The first winding is used to generate a *dc* field using a programmable power supply (Model 2400, Keithley Instruments, Cleveland, OH). The microwave circuit was placed within the gap of the C-core so that the magnetic fields were perpendicular to the plane of the device. The second winding on the C-core was used to modulate the *dc* field at 160 Hz to allow lock-in detection of the signal. Since the FMR response is a strongly non-linear function of the bias field, the modulation results in a second harmonic (320 Hz) variation in the amplitude of the microwave signal coupled to the CPW. Detection of this second harmonic component uniquely identifies the FMR effect of the magnetic beads and distinguishes the signal from stray, field-independent coupling as well as possible feed-through of the modulation signal. The current in the modulation coil, supplied by an arbitrary waveform generator (N8242A, Agilent Technologies, Santa Clara, CA) and audio amplifier, provided an *ac* field amplitude of 42 mT.

The S_{21} signal, at 2.7 GHz, was measured as the *dc* bias field was varied from 0 to 0.2 T. The second harmonic (320 Hz) modulation in the 2.7 GHz carrier was then extracted from the S_{21} data using custom software implemented in MATLAB and plotted as a function of the *dc* bias field (Fig. 4.6c).

4.4.4. Characterization of variation in sensitivity

The spatial variation in sensitivity was characterized by measuring the output signal from a fixed number of beads placed at varying locations on the sensor area. Approximately 40 MagSense beads, glued to the end of a fine-tipped glass probe, were rastered across the active sensor area using an x-y stage. The signal obtained at each location was then mapped as shown in Fig. 4.4.

4.4.5. Sensor area functionalization and characterization

4.4.5.1. Photo-activated patterning of biotin on sensor area

The active sensor area (the area between the slotline and CPW where detection will occur) is approximately 50 μm by 78 μm. However, a much larger area (about 500 μm by 1000 μm) was deliberately chosen for biotin patterning. This was done in order to facilitate easy alignment of the sensor area with the pattern for UV exposure, within the limitations imposed by our exposure system. The waveguide substrate was passivated with silicon dioxide prior to biotin patterning both for electrical isolation and to provide a compatible layer for functionalization.

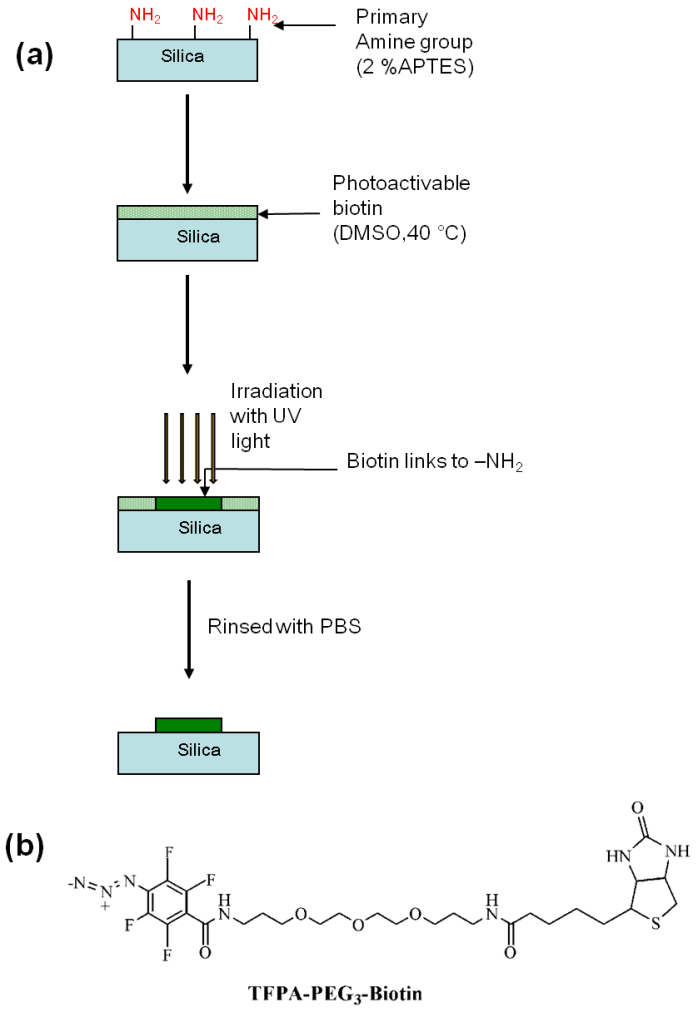

Figure 4.3 (a) Reaction scheme for the functionalization of the sensor area with photoactivable biotin **(b)** Structure of photobiotin used (TFPA-PEG_3-Biotin: Tetrafluorophenyl azide-poly (ethylene glycol) $_3$-biotin).

The reaction scheme for the functionalization of the sensor area is depicted in figure 4.3. The silica-coated device was rinsed with deionized water followed by isopropanol. The sensor area between the slotline and co-planar waveguides was treated with 50 µL of 2% (v/v) aqueous solution of APTS for 1 hour. The device was rinsed with deionized water and dried overnight in an oven at 100°C. 20 µL of a 10 mg/mL solution of EZ-Link TFPA-PEG_3-Biotin in DMSO was deposited on the

sensor area and allowed to dry at 40°C for about 2 hours. A maskless exposure system, SF-100 (Intelligent Micro Patterning, LLC, St. Petersburg, FL), was used to align and pattern a 500 µm by 1000 µm area encompassing the sensor using UV light. An exposure time of 30 minutes was used. Immediately after UV exposure, the slide was rinsed with PBS to wash away any unconjugated biotin. The sensor area was incubated with 100 µL of the blocking buffer for 15 minutes followed by rinsing with a copious amount of PBS.

4.4.5.2. Verification of biotin patterning by fluorescence microscopy

For verification of the biotin patterning by fluorescence microscopy, the sensor area was treated with 200 µL of a 2 mg/mL solution of Neutravidin-fluorescein in PBS for 30 minutes. The devices were rinsed with PBS prior to imaging by an inverted fluorescence microscope, Olympus IX-71 (Olympus, Center Valley, PA) equipped with a PIXIS-512 cooled CCD camera (Princeton Instruments, Trenton, NJ). The camera was controlled by WinSpec32 software (Princeton Instruments, Trenton, NJ). A 300 Watt xenon arc lamp was employed as the light source. The setup used for imaging was: a 40x/0.17 objective (UplanSApo, Olympus, Center Valley, PA), a 450/50 nm excitation filter and a 515 nm long pass emission filter.

4.4.6. Fabrication of microfluidic chip

The microfluidic chips used in this study were fabricated by replica molding of PDMS from a SU-8 master. The SU-8 master, containing negative-relief of the microchannel, was fabricated employing standard photolithographic techniques as described in an earlier study [18]. To obtain a PDMS replica, a 10:1 (w/w) mixture of the prepolymer and curing agent was mixed thoroughly and allowed to degas under vacuum. The SU-8 master was placed in a mold and the degassed prepolymer-curing agent mixture was poured on it. The assembly was then placed overnight in an oven at 65 °C to cure the polymer. Subsequently, the assembly was removed from the oven and allowed to cool to room temperature, prior to gently peeling off the PDMS replica from the SU-8 master. The chip thus obtained was a single, straight flow-through channel ~ 100 µm wide, ~ 100 µm deep and ~ 2 cm in length. Inlet and outlet holes were punched into the PDMS chip using a belt-puncher.

4.4.7. Demonstration of detection technique

The detection technique was demonstrated by measuring the output signal obtained from beads immobilized at the sensor area due to biotin-avidin binding. The microchannel fabricated earlier in PDMS was carefully aligned, under an optical microsope, to the biotin-patterned sensor area. In all subsequent steps, fluid was introduced into the microchip using a syringe and drawn out using tubing connected to house-vacuum. Prior to experiments, the PDMS chip was conditioned with a solution

of 1% BSA (w/v) in PBS for 30 minutes to minimize non-specific binding of magnetic labels. The chip was thoroughly rinsed by flowing copious amounts of PBS. Subsequently, 10 μL of a 1mg/mL suspension of nanomag-D streptavidin-coated magnetic beads was introduced into the chip. A magnetic field gradient, to attract the beads to the junction area, was created by applying a dc current (160 mA) at the terminals of the CPW. After 15 minutes, the current was switched off and the unbound beads removed by rinsing with PBS. The chip with the immobilized beads was placed in the gap of the C-core and the FMR signal measured. For a control, the experiment was also repeated on a second device without biotin patterning.

4.5. Results and discussion

4.5.1. Characterization of spatial variation in sensitivity

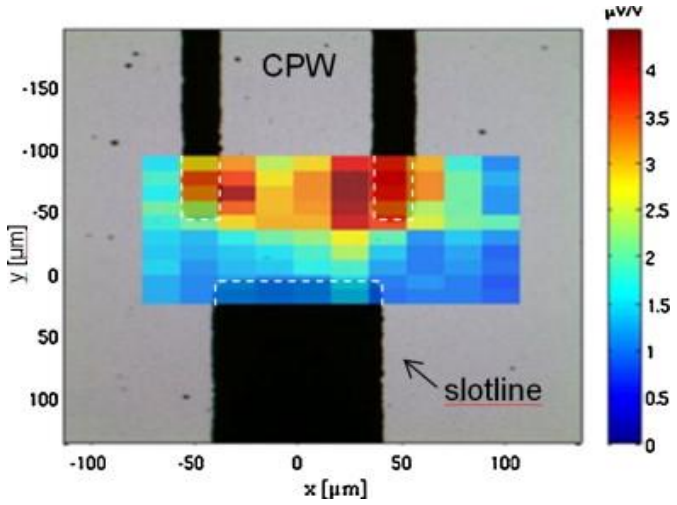

Figure 4.4 Characterization of spatial uniformity. Highest sensitivity, shown in dark red, occurs around the tips of the CPW.

MagSense beads affixed to a glass probe were scanned over the active sensor area. The output signal varied with the location of the beads, as illustrated by the color map in Fig. 4.4. The highest sensitivity, shown in dark red, was observed around the inner tips of the CPW. The spatial variation in sensitivity arises due to non-uniformity in the microwave magnetic field within the active sensor area. The distribution of the field depends on the geometry and layout of the waveguides, and was discussed in [14]. Intuitively, a larger output signal can be expected if the beads are immobilized closer to the pickup waveguide (CPW). These measurements enable placement of the fluidic channel and the bio-chemically activated area to coincide with regions of highest detection sensitivity.

Additionally, it should be noted that the data in Fig. 4.4 represent the signal obtained from approximately 40 beads. The variation of the output signal has also been studied with respect to variation in the number of magnetic beads (ranging from 60 to 900) at the sensor area (data not shown). A lower output signal was observed with fewer beads or with beads placed further away from the coplanar waveguide (the pickup waveguide). Further, at the lowest number of beads measured (approximately 60 beads), the observed signal to noise ratio was approximately ten. These measurements characterize the sensitivity of FMR detection and will enable optimization of the microwave waveguide design for single bead detection in subsequent studies. As reported in [14], single bead sensitivity may be achieved with optimization of the junction geometry, in particular, the spacing between the slotline (source) and CPW (pickup).

4.5.2. Sensor area functionalization and characterization

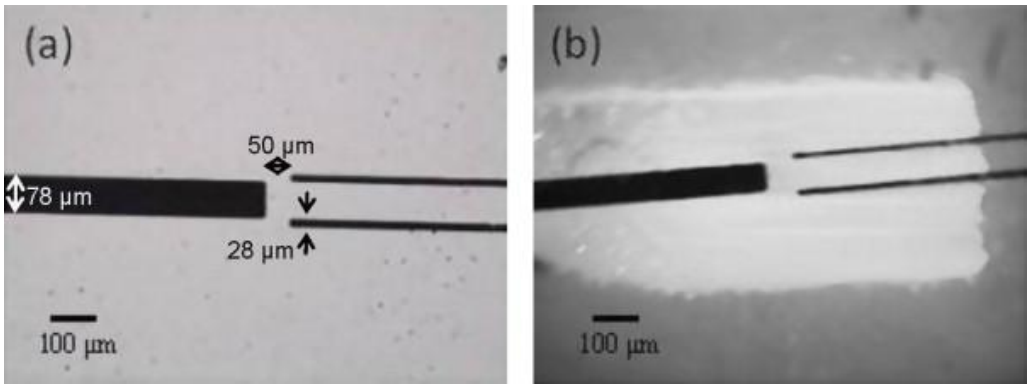

Figure 4.5 (a) Optical micrograph of the sensor area between the slotline and CPW. The linear distance between the slotline and CPW= 50 µm. **(b)** Fluorescence micrograph depicting the biotin patterned sensor area labelled with fluorescein-neutravidin.

The method of photo-activated patterning was chosen to biotinylate the sensor area as it enabled better spatial control of the area to be functionalized compared to other methods such as microcontact printing. As discussed in Section 4.4.5.1. , the silica-coated sensor area was functionalized with EZ-Link TFPA-PEG_3-Biotin, a photoactivable biotin containing the tetrafluorophenyl azide group. Upon UV irradiation, TFPA forms a highly reactive perfluoroaryl nitrene group that covalently bonds with the primary amino groups on the silica surface, previously introduced by treatment with 2% (v/v) APTS solution. The region where biotin is conjugated to the amine groups defines the active sensor area.

The photo-patterning protocol was verified by then treating the biotinylated area with fluorescein-neutravidin and imaging under a fluorescence microsocpe. As

can be seen from figure 4.5 (b), the technique produces homogeneous biotin coverage at the sensor area.

4.5.3. Demonstration of detection technique

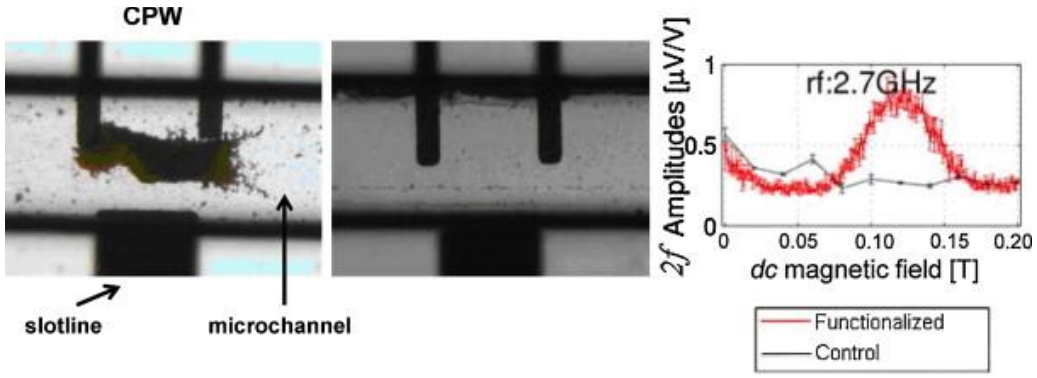

Figure 4.6 Optical micrograph of sensor area overlaid with PDMS microchannel. **(a)** sensor area with patterned biotin shows retained streptavidin coated magnetic beads due to binding **(b)** control device without biotin does not retain any streptavidin coated magnetic beads. **(c)** Signal obtained for immobilized magnetic beads in (a).

Streptavidin-coated beads were flowed in the microchannel over the biotinylated junction. Simultaneously, a *dc* current was applied to the CPW. The resulting magnetic field gradient attracted the beads to the tips around the CPW – coincidentally, also the region of highest sensitivity. The efficiency of biomolecular reactions in immunosensing techniques is typically limited by the diffusion rate of the molecular species. Applying a magnetic field gradient draws the beads from solution and enhances the likelihood of streptavidin-biotin interactions and thereby improves the binding efficiency. Fig. 4.6 (a) shows the immobilized beads remaining on the

junction after thorough rinsing with PBS. For comparison, the control device without biotin is also shown (Fig. 4.6(b)). As expected, no beads were retained after rinsing. The signal measured from the immobilized beads was plotted in Fig. 4.6(c) and is easily discerned from the control. These data demonstrate the proof-of-concept of inductive detection of magnetic labels using a sensor implemented with standard semiconductor processing techniques. Further experiments are underway to adapt the sensor for detection using antibodies and aptamers and to fully establish the analytical figures of merit for this sensor.

4.6. Conclusion

To summarize, a new microfluidic immunosensing technology using FMR-enhanced, inductive detection of magnetic bead labels has been demonstrated. The key advantage of this approach lies in the use of materials and processes compatible with and standard in integrated circuit manufacture. The sensor can thus be readily integrated with electronic circuitry for a low-cost, immunosensing platform amenable to a wide range of biosensing applications.

The variation of the output signal as a function of the location of magnetic beads on the sensor area was studied to determine regions of highest detection sensitivity. Proof-of-concept experiments were conducted using biotin-avidin binding. An integrated PDMS microfluidic channel was used to introduce streptavidin-functionalized magnetic beads. The resulting binding of the beads produced a distinct sensor output compared to a control. The use of magnetic fields to enhance the

interaction of the beads with the biochemically functionalized surface was also demonstrated. The beads were attracted to the most sensitive regions of the sensor. This enhancement of the interaction rate between the analyte and sensor will be essential for the detection of very low concentrations of analyte. Experiments are currently under way to determine the ultimate chemical sensitivity of this approach.

4.7. Acknowledgements

This work has been supported by the Army Research Laboratories (ARL) under grant no. W911NF-07-2-0083. The authors would like to acknowledge Simon Ghionea for his help with the experimental work.

4.8. References

1. Herrmann, M., Veres, T. & Tabrizian, M. Enzymatically-generated fluorescent detection in micro-channels with internal magnetic mixing for the development of parallel microfluidic ELISA. *Lab. Chip* **6**, 555-560 (2006).

2. Martin, S. M. & Eesley, G. L. Optical fiber refractometer. *Rev. Sci. Instrum.* **58**, 2047-2048 (1987).

3. Burg, T. P. et al. Vacuum-packaged suspended microchannel resonant mass sensor for biomolecular detection. *J. Microelectromech. Syst.* **15**, 1466-1476 (2006).

4. Dong, H., Li, C., Zhang, Y., Cao, X. & Gan, Y.Screen-printed microfluidic device for electrochemical immunoassay. *Lab. Chip* **7**, 1752-1758 (2007).

5. Graham, D., Ferreira, H., Bernardo, J., Freitas, P. & Cabral,J. Single magnetic microsphere placement and detection on-chip using current line designs with integrated spin valve sensors: Biotechnological applications, *J. Appl. Phys.* **91**, 7786-7788 (2002).

6. Baselt, D. et al. A biosensor based on magneto resistance technology. *Biosens. Bioelectron.* **13**, 731-739 (1998).

7. Li, G. et al. Detection of single micron-sized magnetic bead and magnetic nanoparticles using spin valve sensors for biological applications. *J. Appl. Phys.* **93**, 7557-7559 (2003).

8. Shen, W., Liu, X., Mazumdar, D. & Xiao G. In situ detection of single micron-sized magnetic beads using magnetic tunnel junction sensors. *Appl. Phys. Lett.* **86**, 253901-253903 (2005).

9. Edelstein, R. et al. The BARC biosensor applied to the detection of biological warfare agents. *Biosens. Bioelectron.* **14**, 805-813 (2000).

10. Rife, J. et al. Design and performance of GMR sensors for the detection of magnetic microbeads in biosensors. *Sens. Actuators A* **107**, 209-218(2003).

11. Miller, M., Prinz, G., Cheng, S. & Bounnak, S. Detection of a micronsized magnetic sphere using a ring-shaped anisotropic magnetoresistance-based sensor: A model for a magnetoresistance-based biosensor. *Appl. Phys. Lett.* **81**, 2211-2213 (2002).

12. Besse, P., Boero, G., Demierre, M., Pott, V. & Popovic, R. Detection of a single magnetic microbead using a miniaturized silicon Hall sensor. *Appl. Phys. Lett.* **80**, 4199–4201 (2002).

13. Sandhu, A., Sanbonsugi, H., Shibasaki, I., Abe, M. & Handa, H. High sensitivity InSb ultra-thin film micro-hall sensors for bioscreening applications. *Jpn. J. Appl. Phys. Lett.* **43**, L868–L870 (2004).

14. Ghionea, S., Dhagat, P. & Jander, A. Ferromagnetic resonance detection for magnetic microbead sensors. *IEEE Sens. J.* **8**, 896-902 (2008).

15. Wolff, I. *Coplanar Microwave Integrated Circuits* (Wiley-Interscience, 2006).

16. Garg, R. & Gupta, K. Expressions for wavelength and impedance of a slotline. *IEEE T. Microw. Theory* **24**, 532 (1976).

17. Kittel, C. On the Theory of Ferromagnetic Resonance Absorption. *Phys. Rev*. **73**, 155-161 (1948).

18. Koesdjojo, M. T., Koch, C. R. & Remcho, V. T. Technique for microfabrication of polymeric-based microchips from an SU-8 master with temperature-assisted vaporized organic solvent bonding. Anal. Chem. **81**, 1652–1659 (2009).

CHAPTER 5

MICROSCALE PHOTOPATTERNING OF CHITOSAN SURFACES FOR BIOMOLECULE IMMOBILIZATION

5.1. Abstract

The selective assembly and development of patterned arrays of biomolecules has important applications in a variety of fields, including biosensor development and studies of cell biology. Chitosan is a biocompatible and biodegradable polymer which has been widely investigated for various bio-medical and bio-analytical applications. This report describes a simple and widely applicable method for the photopatterning of chitosan films with biotin. This method is capable of forming spatially defined biotin features (on the order of tens of microns) and can be completed in under an hour. The issue of non-specific binding of proteins can be overcome effectively with a blocking step with Tween 20. The biotin moiety allows the subsequent immobilization of other biotinylated biochemical ligands, such as antibodies, using neutravidin as a cross-linker. This straightforward method for the selective patterning of chitosan is expected to be widely useful in the field of bioanalysis.

5.2. Introduction

This article describes a simple and widely applicable method for the photopatterning of chitosan films with biotin. This method is capable of forming spatially defined biotin features on the order of tens of microns, together with a

significant reduction of non-specific protein binding in the adjoining areas. Photopatterning with biotin as a first step towards the selective immobilization of proteins precludes the possibility of exposure of the proteins to damaging UV radiation. The use of Tween 20, a biocompatible and commonly used detergent in biochemistry, to reduce non-specific binding eliminates the need for complex chemical modification of chitosan. The entire patterning process, inclusive of the blocking step, can be completed in under an hour. The biotin moiety allows the subsequent immobilization of other biotinylated biochemical ligands, such as antibodies, using neutravidin as a cross-linker. This straightforward method for the selective patterning of the biocompatible polymer chitosan is expected to be widely useful in the field of bioanalysis.

The ability to selectively immobilize biomolecules on surfaces has important applications in a wide variety of fields such as biosensor development, tissue engineering, biotechnology and fundamental studies of cell biology. A growing interest in the patterning of biomolecules has led to the development of techniques such as microcontact printing, photolithographic methods, ink-jet printing, dip-pen nanolithography and photochemical techniques[1, 2]. Photochemical patterning methods use UV light to activate chemically labile species, which subsequently bind to the functional groups of interest[1]. Such methods are particularly convenient as they allow biomolecules to be patterned in a defined location within enclosed structures such as microfluidic networks[3] and with resolution on the order of tens of microns[4-6].

Photochemical methods allow the selection of solvents etc. for optimal protein activity[1] and also, enable multiple proteins to be patterned on the same surface[6, 7].

The use of photoactive forms of biotin for selective patterning of surfaces is a promising approach on account of the highly specific interaction of biotin with avidin. The avidin-biotin pair has been widely employed due to its unique properties such as (i) the exceptionally strong bond between biotin and avidin($K_a = 10^{15} M^{-1}$) (ii) availability of multiple binding sites on avidin for binding biotin, so that it can act as a cross-linker between two biotinylated moieties (iii) easy commercial availability of a wide variety of biotinylated antibodies and aptamers. Photoactive derivatives of biotin have been used to pattern biomolecules on a variety of substrates such as silica, gold, nitrocellulose, glassy carbon, quartz, acrylic, polystyrene, acetonitrilebutadiene-styrene, polycarbonate, and poly (dimethylsiloxane)[4, 5, 8-10]. Due to these advantages, a photoactive form of biotin was used for the selective patterning of chitosan films.

Chitosan is a biocompatible and biodegradable polymer derived from the exoskeletons of arthropods. It has been used in a wide variety of fields including photography, biotechnology and pharmaceuticals[11]. Biomedical applications of chitosan include its use for drug-delivery systems, implants, wound-dressings and tissue-engineering[12-14]. Chitosan displays certain unique properties that make it attractive for use in bio-analytical systems. Chitosan is a linear β-1,4-linked amino polysaccharide and is obtained by the partial deacetylation of chitin[15]. It can transition from soluble to insoluble form with a change in pH from 6 to 6.5. Chitosan is film-forming, i.e. it forms a stable hydrogel network in the insoluble form. The pH-

responsive and film-forming abilities of chitosan allow it to be electrodeposited with high spatial and temporal control. Various molecules of interest can also be co-deposited with chitosan due to the stable nature of its hydrogel network[16]. Another unique feature of chitosan is the presence of the primary amine groups at the C-2 position of the glucosamine residues (figure 5.1)[15]. These amine groups can be readily functionalized via standard coupling chemistries, enabling bio-modification of the chitosan films.

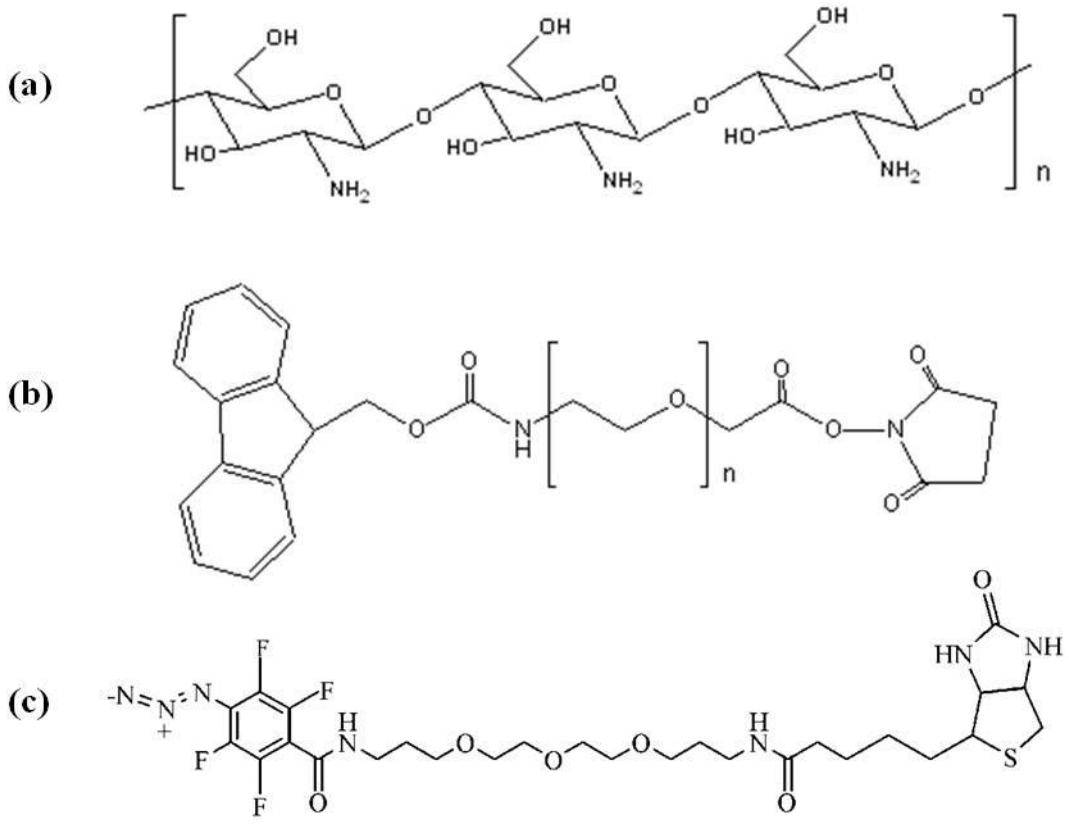

Figure 5.1 Chemical structures of **(a)** Chitosan **(b)** Fmoc-PEG2000-NHS ester **(c)** EZ-Link TFPA-PEG_3-Biotin.

Most of the studies involving the use of chitosan as a component of bio-analytical devices have been conducted by the groups of Payne and Ghodssi at the University of Maryland[15-19]. These studies are based on the spatially selective electrodeposition of chitosan, which is subsequently modified for protein assembly. However, this method of protein assembly requires prior fabrication of electrodes on the substrate, which adds significant complexity to the patterning protocol. The same group presented the technique of thermolithography in 2004[20]. This method involves the use of a layer of gelatin over a chitosan substrate as a sacrificial, heat-sensitive thermoresist. This method involves multiple steps while sub-millimeter resolution is accomplished for patterned areas. Another approach demonstrated by Karp et al. in 2006 involves the synthesis of a photocrosslinkable form of chitosan for the creation of cellular micropatterns[21].

The present study presents a simple and fast alternative method for the patterning of chitosan. Chitosan films were patterned using a photoactive form of biotin, depicted in figure 5.1(c), that reacts with the abundant primary amine groups available on the chitosan surface upon UV illumination. This method produced feature sizes that were about 60 μm wide and spaced 20 μm apart. Different methods of reducing the background were investigated and a blocking step with Tween 20 was found to be most suitable for this purpose. Contact angle measurements of chitosan surfaces treated with Tween 20 revealed a significant increase in hydrophilicity compared to untreated surfaces. Details of this method of selective patterning are described herein.

5.3. Materials and methods

5.3.1. Materials and reagents

Chitosan (low molecular weight, 75-85% deacetylated), bovine serum albumin (BSA), Tween 20 and anhydrous dimethyl sulfoxide (DMSO) were obtained from Sigma Aldrich (St. Louis, MO, USA). A photoactivable form of biotin with tetrafluorophenyl azide moiety, EZ-Link TFPA-PEG_3-Biotin, and fluorescein labeled neutravidin were purchased from Pierce Biotechnology, Inc. (Rockford, IL, USA).Fmoc-PEG2000-NHS ester was purchased from JenKem Technology USA (Allen, TX). All general reagents and solvents were procured from Sigma Aldrich or VWR (West Chester, PA, USA). All chemicals were used as received, without further purification. Ultrapure water, with specific resistance of 18 MΩ-cm, was obtained from a Barnstead™ E-Pure™ deionization system (Waltham, MA) and was used for rinses and the preparation of buffers throughout the experiments.

The UV-light source used for patterning was X-Cite 120 ®, equipped with a 120-W metal halide short arc lamp (EXFO Life sciences and industrial division, Mississauga, ON, Canada). Imaging was performed on a Zeiss Axio Imager M1m fluorescence microscope (Thornwood, NY, USA), equipped with a GFP filter cube. The GFP filter has an excitation filter with bandpass of 450-490 nm, a 495 nm beamsplitter and emission filter with bandpass of 500-550 nm. Analysis of the fluorescence intensity of images was done using AxioVision 4.8 software (Carl Zeiss, Inc., Thornwood, NY, USA).

5.3.2. Patterning of chitosan films

The strategy employed for the site-specific immobilization of biotin is depicted in figure 5.2. Chitosan (0.2 g) was dissolved in a mixture of 1 mL deionized water and 5 mL glacial acetic acid to obtain a 3.3 % w/v solution. To obtain a film of chitosan, 15 µL of this solution was placed on a 18 mm×18 mm glass coverslip and smeared to form a film using a second coverslip. Chitosan films thus formed were allowed to dry at least overnight at ambient temperature before use. Prior to photopatterning, 10 µL of a 2 mg/mL solution of photobiotin in deionized water was deposited on each coverslip, spread with a coverslip and allowed to dry heating in a 100°C oven for about 2 minutes. Using a 300 mesh TEM grid as a photomask, the coverslips were irradiated with UV light from a 120 W halogen source through 5X objective of the microscope for 5 minutes. Immediately after patterning, the surfaces were rinsed extensively with deionized water and incubated with 20 µL of blocking solution (5 % BSA and 2 % Tween 20) for 30 minutes. The surfaces were rinsed and treated with a 0.5 mg/mL solution of neutravidin-fluorescein in 10mM phosphate buffer (pH 7) (containing 2.5 % w/v of BSA) for 30 minutes. The surfaces were finally rinsed with deionized water, dried with compressed air and imaged to observe the fluorescence intensity of the patterned areas.

To study the effect of PEG-derivatization of the chitosan surface on non-specific binding of proteins, 100 µL of the chitosan solution was modified by adding 40 mg of Fmoc-PEG2000-NHS in 200 µL water. The mixture was allowed to react at room temperature overnight. The PEG-derivatized chitosan was spread on a coverslip

and allowed to dry overnight. Before photopatterning, the amine group on the PEG arm was deprotected by treating with 20% v/v solution of piperidine in dimethylformamide for 30 minutes at room temperature.

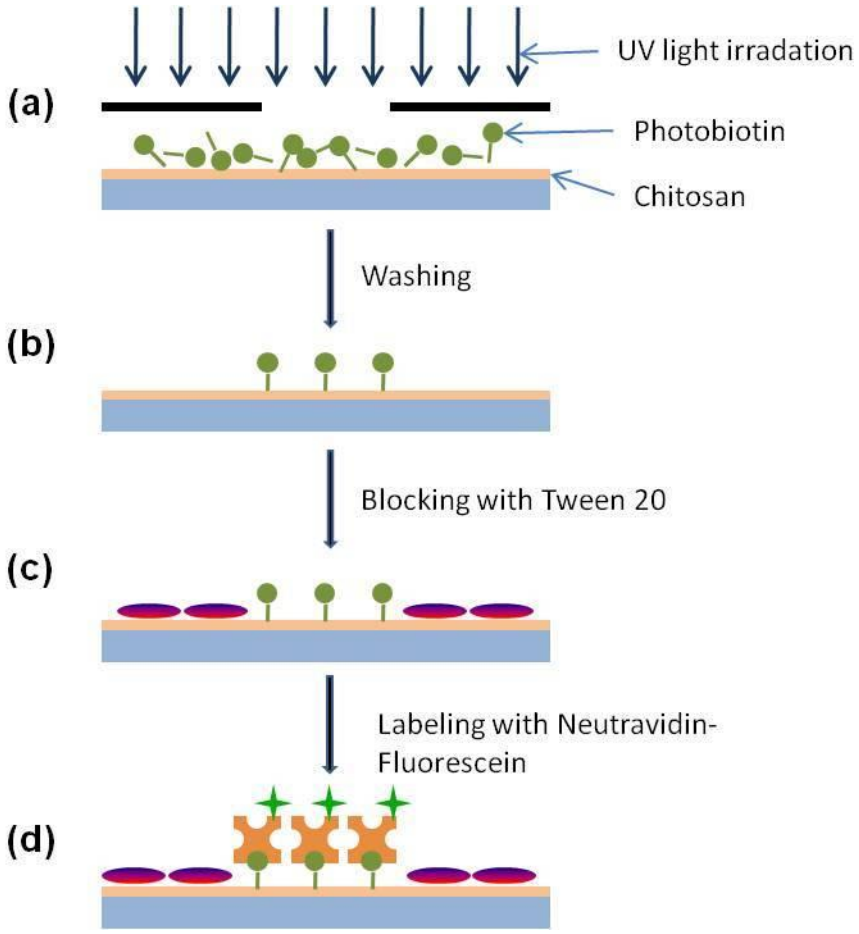

Figure 5.2 Schematic depiction of the photopatterning process **(a)** Photobiotin is deposited on a film of chitosan, dried and exposed to UV light through a photomask **(b)** Photobiotin not conjugated to the chitosan surface is washed away **(c)** Areas not modified by biotin are blocked using 2% Tween 20 **(d)** Binding of fluorescein-labeled neutravidin to patterned areas of biotin.

5.3.3. Contact angle measurements

Contact angle measurements were carried out by pipetting 3 μL of deionized water onto the chitosan films. The water drops were imaged after 10 seconds using a Dino-Lite Professional (AM413T) digital microscope (Naarden, The Netherlands) and the contact angles were measured using the three-point angle function of the Dinocapture software. Contact angles were measured in triplicate and the average contact angle for each substrate was reported.

5.4. Results and discussion

The goal of this study was to establish photochemical patterning as a quick and simple method for the micron-scale patterning of chitosan films. A photoactivable biotin containing the tetrafluorophenyl azide group (EZ-Link TFPA-PEG_3-Biotin) was used for this purpose. Upon UV irradiation, TFPA forms a highly reactive perfluoroaryl nitrene group that covalently bonds with the primary amino groups present on the chitosan film. In preliminary studies, it was observed that the irradiation of photobiotin solutions deposited on chitosan films failed to form any defined patterns. This can be attributed to the rapid reaction of the nitrene group with water[7, 9]. However, dried films of photobiotin gave rise to highly defined patterns which could be observed under a microscope, as shown in figure 5.3(a). The patterning was done

using a 300-mesh TEM-grid as the photomask. The resulting features were 60 μm wide squares that were spaced 20 μm apart from each other.

Chitosan membranes thus patterned with biotin, when reacted with neutravidin-fluorescein, were observed to exhibit a great degree of non-specific binding of proteins. As shown in the fluorescence micrograph in figure 5.3(b), the areas that were not exposed to UV-light (i.e. were under the TEM-grid mesh) appear to be brighter than the exposed areas. This unexpected outcome is due to the fact that the photobiotin used incorporates a PEG linker (figure 5.1 (b)). Upon conjugation to the chitosan surface, the PEG moiety prevents non-specific binding in the patterned areas. The unmodified chitosan surface exhibits relatively greater non-specific binding of neutravidin-fluorescein and consequently, appears brighter.

In order to overcome the issue of non-specific binding, chitosan was modified by derivatization with PEG. An amine-reactive ester, Fmoc-PEG2000-NHS, was chosen so that the PEG moiety could be attached to chitosan via its abundant primary amine groups. After PEG-derivatization of the chitosan surface, the Fmoc blocking group was cleaved by treatment with 20% piperidine in dimethylformamide to reveal primary amine groups and photopatterning of the chitosan surface was conducted. The ratio (by weight) of Fmoc-PEG2000-NHS ester used for modification of chitosan was roughly 12:1 to ensure that all the available primary amine groups on chitosan were conjugated to the PEG moiety. Chitosan thus modified with PEG did not show any marked reduction in non-specific binding of proteins, as can be seen from figure 5.3(c). An inversion of the photomask pattern, similar to unmodified chitosan films,

was also observed. It is hypothesized that the conjugation reaction of the Fmoc-PEG2000-NHS ester to chitosan was incomplete due to the existence of the primary amine groups on chitosan in protonated form in the acetic acid solution. The PEG-modification of neutralized chitosan films might be able to overcome this limitation. However, this is anticipated to make the process of selective protein deposition much more time consuming.

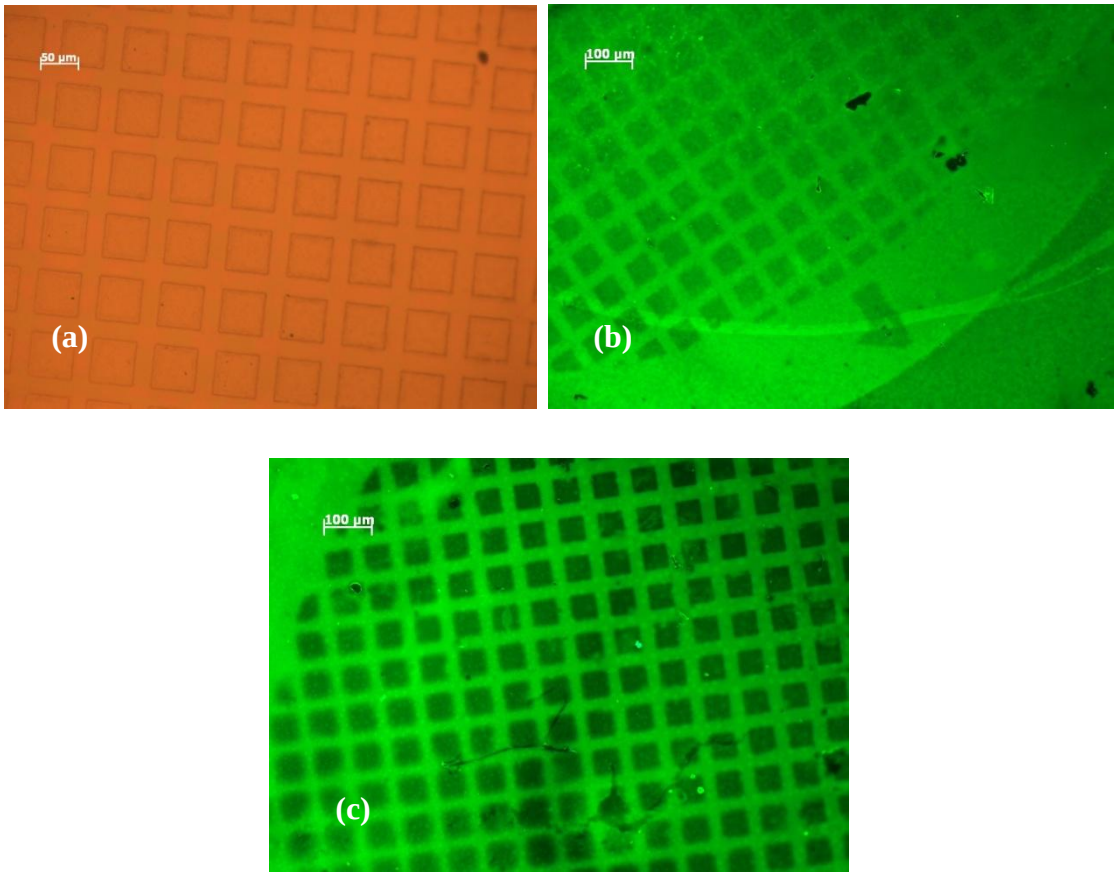

Figure 5.3 (a) A brightfield photomicrograph (20 × magnification) of the chitosan film after patterning with photobiotin. Fluorescence images of photopatterened chitosan film (labeled with neutravidin-fluorescein) (5 × magnification) **(b)** with no blocking step **(c)** chitosan modified with Fmoc-PEG2000-NHS.

As a faster alternative for the reduction of non-specific binding, a 30 minute blocking step was introduced after the photopatterning. Commonly used blocking agents, BSA and Tween 20, were investigated for this purpose. The results of incorporating a blocking step are shown in figure 5.4 (a) and (b) while (c) and (d) represent the fluorescence intensity line-plots for the features shown in (a) and (b), respectively. The line-plots were obtained by measuring the fluorescence intensity at every pixel across a horizontal line drawn through the center of the first four features (from the left) of the second row in images (a) and (b). As shown in figure 5.4 (a), blocking with a 5 % solution of BSA prior to neutravidin –fluorescein labeling reduced non-specific binding of proteins to chitosan such that the features patterned by UV are observed distinctly. This indicates that the specific binding of neutravidin-fluorescein with the immobilized biotin was greater than its non-specific binding to the chitosan surface pre-treated with BSA. A line-plot across these features reveals a relatively low signal-to-noise ratio of about 1.5. On the other hand, use of a 2% solution of Tween 20 for blocking results in a much lower background as can be seen from figure 5.4 (b). The signal-to-noise ratio in this case was determined to be about 6.5, a significant improvement over the BSA-treated samples.

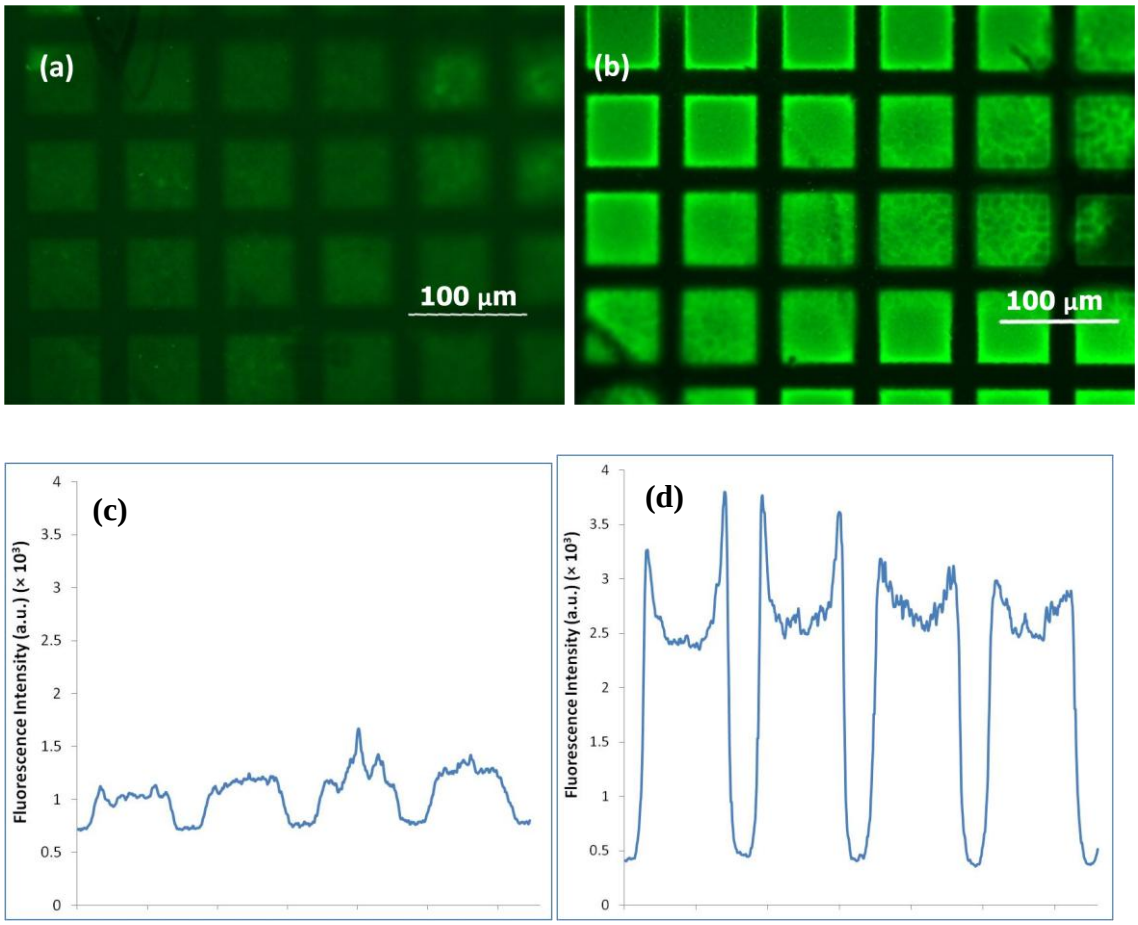

Figure 5.4 Fluorescence images of photopatterened chitosan film (labeled with neutravidin-fluorescein) depicting the effect of blocking with **(a)** 5% BSA **(b)** 2% Tween 20. Images **(c)** and **(d)** represent line-plots of the fluorescence intensity across the first four features from the left of the second row in images (a) and (b).

The difference in the blocking efficacy of BSA and Tween 20 may be attributed to the mode of their interaction with the chitosan surface. Proteins are believed to adsorb strongly to hydrophobic surfaces due to the presence of hydrophobic domains. Hence, hydrophilic surfaces have been commonly associated with reduced non-specific protein binding[22]. Tween 20 is amphiphilic in nature, with a hydrophilic part that is much bulkier than the hydrophobic part of the molecule. It is

hypothesized that the hydrophobic part of Tween 20 adheres to the chitosan surface while the hydrophilic part remains exposed to air. This leads to a marked increase in the hydrophilicity of the chitosan surfaces treated with Tween-20 (relative to untreated or BSA-treated chitosan surfaces), as seen from the contact angle measurements shown in figure 5.5 (c). This increased hydrophilicity results in reduced non-specific adsorption of proteins. BSA, on the other hand, is adsorbed onto the chitosan surface but the surface still remains markedly hydrophobic, as can be seen from figure 5.5 (b). This hydrophobic surface leads to the adsorption of proteins to some extent. An added benefit of the increased hydrophilicity of Tween 20-treated chitosan surfaces is that it enables even spreading and wetting of the surface with aqueous solutions. This is encouraging for applications in which the patterned area is enclosed (such as within a microfluidic channel) since fluid flow can be accomplished simply by capillary forces or under very low pressures.

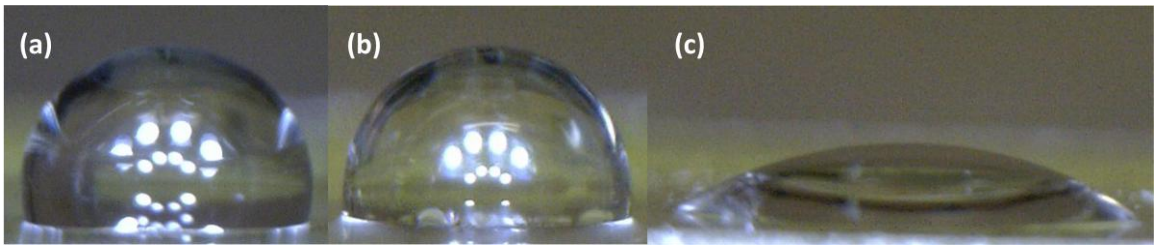

Figure 5.5 Contact angles of a 3µL drop of deionized water on surfaces comprised of **(a)** untreated chitosan (96.58 ± 1.40) **(b)** chitosan treated with 5 % BSA (83.03 ± 2.61) **(c)** chitosan treated with 2 % Tween 20 (29.63 ± 3.68).

5.5. Conclusions

A simple and straightforward method for the selective patterning of chitosan surfaces with photobiotin was demonstrated. The entire patterning process, inclusive of the blocking step, can be completed in about 40 minutes and no complex fabrication steps are involved. This method is capable of forming spatially defined biotin features on the order of tens of microns, together with a significant reduction of non-specific protein binding in the adjoining areas. The resulting surface shows a significant increase in hydrophilicity. The biotin moiety can allow for the subsequent immobilization of other biotinylated biochemical ligands, such as antibodies, using neutravidin as a cross-linker. This simple method of patterning is expected to enable numerous applications of chitosan in the fields of bioanalysis and cellular studies, to name a few.

5.6. Acknowledgements

The authors would like to acknowledge Beth Dunfield for her suggestions about chitosan and help with the experimental work.

5.7. References

1. Blawas, A.S. & Reichert, W.M. Protein patterning. *Biomaterials* **19**, 595-609 (1998).

2. Mendes, P.M., Yeung, C.L. & Preece, J.A. Bio-nanopatterning of surfaces. *Nanoscale Res. Lett.* **2**, 373-384 (2007).

3. Lewandowski, A.T. et al. Protein assembly onto patterned microfabricated devices through enzymatic activation of fusion pro-tag. *Biotechnol. Bioeng.* **99**, 499-507 (2008).

4. Pritchard, D.J., Morgan, H. & Cooper, J.M. Patterning and regeneration of surfaces with antibodies. *Anal. Chem.* **67**, 3605-3607 (1995).

5. Brooks, S.A. et al. Segregation of micrometer-dimension biosensor elements on a variety of substrate surfaces. *Anal. Chem.* **72**, 3253-3259 (2000).

6. Doh, J. & Irvine, D.J. Photogenerated polyelectrolyte bilayers from an aqueous-processible photoresist for multicomponent protein patterning. *J. Am. Chem. Soc.* **126**, 9170-9171 (2004).

7. Ahn, J., Shin, Y.-B., Chang, W. S. & Kim, M. G. Sequential patterning of two fluorescent streptavidins assisted by photoactivatable biotin on an aminodextran-coated surface. *Colloid. Surface. B* **87**, 67-72 (2011).

8. Pritchard, D.J., Morgan, H. & Cooper, J.M. Micron-scale patterning of biological molecules. *Angew. Chem. Int. Edit.* **34**, 91-93 (1995).

9. Hengsakul, M. & Cass, A.E.G. Protein Patterning with a photoactivatable derivative of biotin. *Bioconjugate Chem.* **7**, 249-254 (1996).

10. Choi, H.J., Kim, N.H., Chung, B.H. & Seong, G.H. Micropatterning of biomolecules on glass surfaces modified with various functional groups using photoactivatable biotin. *Anal. Biochem.* **347**, 60-66 (2005).

11. Ravi Kumar, M.N.V. A review of chitin and chitosan applications. *React. Funct. Polym.* **46**, 1-27 (2000).

12. Madihally, S.V. & Matthew, H.W.T. Porous chitosan scaffolds for tissue engineering. *Biomaterials* **20**, 1133-1142 (1999).

13. Francis Suh, J. K. & Matthew, H.W.T. Application of chitosan-based polysaccharide biomaterials in cartilage tissue engineering: a review. *Biomaterials* **21**, 2589-2598 (2000).

14. Di Martino, A., Sittinger, M. & Risbud, M.V. Chitosan: A versatile biopolymer for orthopaedic tissue-engineering. *Biomaterials* **26**, 5983-5990 (2005).

15. Yi, H. et al. Biofabrication with chitosan. *Biomacromolecules* **6**, 2881-2894 (2005).

16. Koev, S.T. et al. Mechano-transduction of DNA hybridization and dopamine oxidation through electrodeposited chitosan network. *Lab. Chip* **7**, 103-111 (2007).

17. Dykstra, P. et al. An optical MEMS sensor utilizing a chitosan film for catechol detection. *Sensor. Actuat. B-Chem.* **138**, 64-70 (2009).

18. Ghodssi, R. et al. Integration of diverse biological materials in micro/nano devices. *Advanced Materials and Technologies for Micro/Nano-Devices, Sensors and Actuators* 275-285 (Springer, 2010).

19. Liu, Y. et al. Chitosan to electroaddress biological components in lab-on-a-chip devices. *Carbohyd. Polym.* **84**, 704-708 (2011).

20. Fernandes, R. et al. Thermo-biolithography: a technique for patterning nucleic acids and proteins. *Langmuir* **20**, 906-913 (2004).

21. Karp, J.M. et al. A photolithographic method to create cellular micropatterns. *Biomaterials* **27**, 4755-4764 (2006).

22. Sorribas, H., Padeste, C. & Tiefenauer, L. Photolithographic generation of protein micropatterns for neuron culture applications. *Biomaterials* **23**, 893-900 (2002).

CHAPTER 6

SUMMARY AND CONCLUSIONS

Rapid advances in the field of nanotechnology have resulted in the development and characterization of a host of nanomaterials including metallic nanoparticles, nanorods, semi-conductor nanocrystals and carbon nanotubes. These nanomaterials, on account of their dimensions, demonstrate unique electronic, optical, magnetic and catalytic properties that are not exhibited by their bulk counterparts. Hence, nanomaterials are being exploited in a variety of different fields ranging from diagnostics to cleaner energy applications. In particular, these materials have shown great promise for biosensing, especially for applications with miniaturized analytical platforms and limited sample volumes. Continued interest in the development of portable biosensors necessitates the investigation and development of sensitive methods for the detection of trace analytes. In this context, nanomaterials can overcome a number of limitations of traditional labeling reagents as well as enable the exploration of novel functionalities.

The all-encompassing goal of this dissertation is to explore the use of semi-conductor nanocrystals and magnetic particles for the development of sensitive detection techniques for biomolecules. Semi-conductor nanocrystals overcome a number of drawbacks of traditional fluorophores. Hence, they are attractive candidates for the development of sensitive optical detection techniques for small sample

volumes which are characteristic of microfluidic devices. In the realm of biosensing, magnetic nanoparticles have been widely used for separations and contrast-agents for imaging. With the emergence of the field of magnetoelectronics, bio-functionalized micrometer or nanometer-sized magnetic beads were used as labels and detected by magnetic field sensors. Such alternative strategies of detection merit investigation as they can be easily miniaturized and scaled up for mass production.

In this context, semi-conductor nanocrystals or quantum dots were investigated as alternative fluorescent labels. The use of quantum dots encapsulated in liposomes was investigated on account of the advantageous combination of signal amplification derived from liposomes and the stronger fluorescent signal generated by the quantum dots. Liposomes encapsulating quantum dots were synthesized and characterized for their spectral properties and size. The encapsulation efficiency of quantum dots within the liposomes was almost 100 %. These liposomes were successfully applied towards a magnetic-bead based assay in a microfluidic chip as proof-of-concept. Further development of the assay was, however, impeded by the long-term instability of the quantum dot-liposome hybrid structure. For further development, quantum dots need to be modified with improved and resilient coatings in order to form stable hybrids with liposomes.

To overcome the long-term instability presented by quantum dots, a homogeneous assay was explored that exploited the ability of gold nanoparticles to quench the optical signals obtained from quantum dots. The goal of this study was to demonstrate the feasibility of using aptamer-linked nanostructures in FRET-based

quenching for the detection of proteins. Thrombin was used as the model analyte in this study. The anti-thrombin aptamer was conjugated to 10 nm gold nanoparticles while a complementary sequence was conjugated to quantum. Quenching of the fluorescence of quantum dots occurred when the aptamer and the complementary sequences were allowed to hybridize. The addition of thrombin caused an enhancement in the fluorescence which was proportional to the concentration of thrombin. This simple method could be completed in under an hour and was able to detect thrombin in the concentration range of 2.5-40 nM, with a limit of detection of 5 nM. However, the instability of the quantum dots was found to introduce large variabilities in the assay and needs to be addressed prior to further development.

Another alternative sensing technique investigated the use of ferromagnetic resonance-enhanced, inductive detection of magnetic bead labels. The key advantage of this approach lies in the use of materials and processes compatible with and standard in integrated circuit manufacture. The sensor can be readily integrated with electronic circuitry for a low-cost, sensing platform suited for a wide range of biosensing applications. A prototype device was constructed by biotinylation of the sensor area and integration with a microfluidic chip fabricated in polydimethyl siloxane (PDMS). Preliminary experiments were conducted on this prototype using streptavidin-functionalized magnetic beads as labels. It was shown that the magnetic beads, immobilized at the sensor area by streptavidin-biotin linkage, produced a distinct ferromagnetic resonance response easily discernable from the background signal. Future plans for the development of this technique involve optimization of bio-

patterning techniques for the sensor area, integration of antibodies or aptamers as the bio-recognition element and the investigation into the use of hard polymers for fabrication of the microfluidic channel.

A key step in the development of an integrated biosensing system is the integration of biomolecules on the sensors surface. This step is complicated by the fragile nature of biomolecules and the requirement for extensive surface modification of the sensing surfaces. Incorporation of a biocompatible polymer such as chitosan into the sensing surface can overcome these complexities. The biocompatible polymer chitosan was investigated for selective photochemical patterning. The patterning process was straightforward and fast. This method is capable of forming spatially defined biotin features on the order of tens of microns, together with a significant reduction of non-specific protein binding and increase in hydrophilicity of the chitosan surface. The biotin moiety can be used for the incorporation of other biotinylated biochemical ligands, such as antibodies, using neutravidin as a cross-linker. Further studies involving the immobilization of antibodies on chitosan are required. This simple method of patterning is expected to facilitate the integration of biomolecules onto sensor surfaces.

In conclusion, the use of nanomaterials, such as semi-conductor nanocrystals and magnetic beads, shows definite promise towards the improvement of existing detection methods as well as the development of alternate methods that can be miniaturized and mass produced. However, the limited stability of these nanomaterials, particularly in media simulating physiological conditions, is an

impediment to widespread application. A better understanding of the surface chemistry together with the development of effective coating methods is required. For biosensing applications, stability in the presence of high salt concentrations and minimal non-specific adsorption are particularly desirable. Addressing these limitations will strengthen and expand the scope of bioanalytical technologies enabled by nanomaterials.

BIBLIOGRAPHY

1. Ahn, J., Shin, Y.-B., Chang, W. S. & Kim, M. G. Sequential patterning of two fluorescent streptavidins assisted by photoactivatable biotin on an aminodextran-coated surface. *Colloid. Surface. B* **87**, 67-72 (2011).

2. Al-Jamal, W.T. et al. Tumor targeting of functionalized quantum dot-liposome hybrids by intravenous administration. *Mol. Pharm.* **6**, 520-530 (2009).

3. Al-Jamal, W.T., Al-Jamal, K.T., Bomans, P.H., Frederik, P.M. & Kostarelos, K. Functionalized-quantum-dot–liposome hybrids as multimodal nanoparticles for cancer. *Small* **4**, 1406-1415 (2008).

4. Ao, L., Gao, F., Pan, B., He, R. & Cui, D. Fluoroimmunoassay for antigen based on fluorescence quenching signal of gold nanoparticles. *Anal. Chem.* **78**, 1104-1106 (2006).

5. Bailey, R.E., Smith, A.M. & Nie, S. Quantum dots in biology and medicine. *Physica E* **25**, 1-12 (2004).

6. Baptista, P. et al. Gold nanoparticles for the development of clinical diagnosis methods. *Anal. Bioanal. Chem.* **391**, 943-950 (2007).

7. Baselt, D. et al. A biosensor based on magneto resistance technology. *Biosens. Bioelectron.* **13**, 731-739 (1998).

8. Besse, P., Boero, G., Demierre, M., Pott, V. & Popovic, R. Detection of a single magnetic microbead using a miniaturized silicon Hall sensor. *Appl. Phys. Lett.* **80**, 4199–4201 (2002).

9. Blawas, A.S. & Reichert, W.M. Protein patterning. *Biomaterials* **19**, 595-609 (1998).

10. Bock, L.C., Griffin, L.C., Latham, J.A., Vermaas, E.H. & Toole, J.J. Selection of single-stranded DNA molecules that bind and inhibit human thrombin. *Nature* **355**, 564-566 (1992).

11. Boisselier, E. & Astruc, D. Gold nanoparticles in nanomedicine: preparations, imaging, diagnostics, therapies and toxicity. *Chem. Soc. Rev.* **38**, 1759 (2009).

12. Brooks, S.A. et al. Segregation of micrometer-dimension biosensor elements on a variety of substrate surfaces. *Anal. Chem.* **72**, 3253-3259 (2000).

13. Bruchez, M., Moronne, M., Gin, P., Weiss, S. & Alivisatos, A.P. Semiconductor nanocrystals as fluorescent biological labels. *Science* **281**, 2013 -2016 (1998).

14. Burg, T. P. et al. Vacuum-packaged suspended microchannel resonant mass sensor for biomolecular detection. *J. Microelectromech. Syst.* **15**, 1466-1476 (2006).

15. Centi, S., Tombelli, S., Minunni, M. & Mascini, M. Aptamer-based detection of plasma proteins by an electrochemical assay coupled to magnetic beads. *Anal. Chem.* **79**, 1466-1473 (2007).

16. Chan, W.C.W. & Nie, S. Quantum dot bioconjugates for ultrasensitive nonisotopic detection. *Science* **281**, 2016 -2018 (1998).

17. Chang, E. et al. Protease-activated quantum dot probes. *Biochem. Bioph. Res. Co.* **334**, 1317-1321 (2005).

18. Chemla, Y.R. et al. Ultrasensitive magnetic biosensor for homogeneous immunoassay. *P. Natl. Acad. Sci. USA* **97**, 14268 -14272 (2000).

19. Chen, C.-S., Yao, J. & Durst, R.A. Liposome encapsulation of fluorescent nanoparticles: quantum dots and silica nanoparticles. *J. Nanopart. Res.* **8**, 1033-1038 (2006).

20. Chen, H., Kou, X., Yang, Z., Ni, W. & Wang, J. Shape- and size-dependent refractive index sensitivity of gold nanoparticles. *Langmuir* **24**, 5233-5237 (2008).

21. Choi, H.J., Kim, N.H., Chung, B.H. & Seong, G.H. Micropatterning of biomolecules on glass surfaces modified with various functional groups using photoactivatable biotin. *Anal. Biochem.* **347**, 60-66 (2005).

22. Chonn, A. & Cullis, P.R. Recent advances in liposomal drug-delivery systems. *Curr. Opin. Biotech.* **6**, 698-708 (1995).

23. Co, C.C., Wang, Y. C. & Ho, C. C. Biocompatible micropatterning of two different cell types. *J. Am. Chem. Soc.* **127**, 1598-1599 (2011).

24. Copland, J.A. et al. Bioconjugated gold nanoparticles as a molecular based contrast agent: implications for imaging of deep tumors using optoacoustic tomography. *Mol. Imaging Biol.* **6**, 341-349 (2004).

25. Cui, R., Huang, H., Yin, Z., Gao, D. & Zhu, J.-J. Horseradish peroxidase-functionalized gold nanoparticle label for amplified immunoanalysis based on

gold nanoparticles/carbon nanotubes hybrids modified biosensor. *Biosens. Bioelectron.* **23**, 1666-1673 (2008).

26. Dams, R., Lambert, W.E., Comhaire, F. & De Leenheer, A.P. Production and characterization of sulforhodamine B containing large unilamellar vesicles labeled with atrazine. *Anal. Chim. Acta* **399**, 185-191 (1999).

27. Daniel, M.-C. & Astruc, D. Gold nanoparticles: assembly, supramolecular chemistry, quantum-size-related properties, and applications toward biology, catalysis, and nanotechnology. *Chem. Rev.* **104**, 293-346 (2004).

28. Demers, L.M. et al. A fluorescence-based method for determining the surface coverage and hybridization efficiency of thiol-capped oligonucleotides bound to gold thin films and nanoparticles. *Anal. Chem.* **72**, 5535-5541 (2000).

29. Derfus, A.M., Chan, W.C.W. & Bhatia, S.N. Probing the cytotoxicity of semiconductor quantum dots. *Nano Lett.* **4**, 11-18 (2004).

30. Di Martino, A., Sittinger, M. & Risbud, M.V. Chitosan: A versatile biopolymer for orthopaedic tissue-engineering. *Biomaterials* **26**, 5983-5990 (2005).

31. Doh, J. & Irvine, D.J. Photogenerated polyelectrolyte bilayers from an aqueous-processible photoresist for multicomponent protein patterning. *J. Am. Chem. Soc.* **126**, 9170-9171 (2004).

32. Dong, H., Li, C., Zhang, Y., Cao, X. & Gan, Y.Screen-printed microfluidic device for electrochemical immunoassay. *Lab. Chip* **7**, 1752-1758 (2007).

33. Dubertret, B. et al. In vivo imaging of quantum dots encapsulated in phospholipid micelles. *Science* **298**, 1759 -1762 (2002).

34. Dudu, V., Ramcharan, M., Gilchrist, M.L., Holland, E.C. & Vazquez, M. Liposome delivery of quantum dots to the cytosol of live cells. *J. Nanosci. Nanotechnol*. **8**, 2293-2300 (2008).

35. Dyadyusha, L. et al. Quenching of CdSe quantum dot emission, a new approach for biosensing. *Chem. Commun.* 3201-3203 (2005).

36. Dykstra, P. et al. An optical MEMS sensor utilizing a chitosan film for catechol detection. *Sensor. Actuat. B-Chem.* **138**, 64-70 (2009).

37. Eck, W. et al. PEGylated gold nanoparticles conjugated to monoclonal F19 antibodies as targeted labeling agents for human pancreatic carcinoma tissue. *ACS Nano* **2**, 2263-2272 (2008).

38. Edelstein, R. et al. The BARC biosensor applied to the detection of biological warfare agents. *Biosens. Bioelectron.* **14**, 805-813 (2000).

39. Edwards, K.A. & Baeumner, A.J. Liposomes in analyses. *Talanta* **68**, 1421-1431 (2006).

40. Edwards, K.A. & Baeumner, A.J. Optimization of DNA-tagged liposomes for use in microtiter plate analyses. *Anal. Bioanal. Chem.* **386**, 1613-1623 (2006).

41. Egbaria, K. & Weiner, N. Liposomes as a topical drug delivery system. *Adv. Drug Deliver. Rev.* **5**, 287-300 (1990).

42. Elghanian, R., Storhoff, J.J., Mucic, R.C., Letsinger, R.L. & Mirkin, C.A. Selective colorimetric detection of polynucleotides based on the distance-dependent optical properties of gold nanoparticles. *Science* **277**, 1078 -1081 (1997).

43. Elsayed, I., Huang, X. & Elsayed, M. Selective laser photo-thermal therapy of epithelial carcinoma using anti-EGFR antibody conjugated gold nanoparticles. *Cancer Lett.* **239**, 129-135 (2006).

44. El-Sayed, I.H., Huang, X. & El-Sayed, M.A. Surface plasmon resonance scattering and absorption of anti-EGFR antibody conjugated gold nanoparticles in cancer diagnostics: applications in oral cancer. *Nano Lett.* **5**, 829-834 (2005).

45. Eustis, S. & El-Sayed, M.A. Why gold nanoparticles are more precious than pretty gold: Noble metal surface plasmon resonance and its enhancement of the radiative and nonradiative properties of nanocrystals of different shapes. *Chem. Soc. Rev.* **35**, 209 (2006).

46. Fernandes, R. et al. Thermo-biolithography: a technique for patterning nucleic acids and proteins. *Langmuir* **20**, 906-913 (2004).

47. Ferreira, H.A., Freitas, P.P. & Graham, D.L. Magnetoresistive-based biosensors and biochips. *Trends Biotechnol.* **22**, 455-462 (2004).

48. Fountaine, T.J., Wincovitch, S.M., Geho, D.H., Garfield, S.H. & Pittaluga, S. Multispectral imaging of clinically relevant cellular targets in tonsil and lymphoid tissue using semiconductor quantum dots. *Mod. Pathol.* **19**, 1181-1191 (2006).

49. Francis Suh, J. K. & Matthew, H.W.T. Application of chitosan-based polysaccharide biomaterials in cartilage tissue engineering: a review. *Biomaterials* **21**, 2589-2598 (2000).

50. Frens, G. Controlled nucleation for the regulation of the particle size in monodisperse gold suspensions. *Nature Phys. Sci.* **241**, 20-22 (1973).

51. Garg, R. & Gupta, K. Expressions for wavelength and impedance of a slotline. *IEEE T. Microw. Theory* **24**, 532 (1976).

52. Gearheart, L.A., Ploehn, H.J. & Murphy, C.J. Oligonucleotide adsorption to gold nanoparticles: a surface-enhanced raman spectroscopy study of intrinsically bent DNA. *J. Phys. Chem. B* **105**, 12609-12615 (2001).

53. Gerami, R. & Bruinsma, R.F. Continuum theory of lipid bilayer electrostatics. *Eur. Phys. J. E* **30**, 197-204 (2009).

54. Ghionea, S., Dhagat, P. & Jander, A. Ferromagnetic resonance detection for magnetic microbead sensors. *IEEE Sens. J.* **8**, 896-902 (2008).

55. Ghodssi, R. et al. Integration of diverse biological materials in micro/nano devices. *Advanced Materials and Technologies for Micro/Nano-Devices, Sensors and Actuators* 275-285 (Springer, 2010).

56. Ghosh, S., Priyam, A., Bhattacharya, S.C. & Saha, A. Mechanistic aspects of quantum dot based probing of Cu (II) ions: role of dendrimer in sensor efficiency. *J. Fluoresc.* **19**, 723-731 (2009).

57. Gómez-Hens, A. & Manuel Fernández-Romero, J. The role of liposomes in analytical processes. *TrAC-Trend. Anal. Chem.* **24**, 9-19 (2005).

58. Goral, V.N., Zaytseva, N.V. & Baeumner, A.J. Electrochemical microfluidic biosensor for the detection of nucleic acid sequences. *Lab. Chip* **6**, 414 (2006).

59. Graham, D., Ferreira, H., Bernardo, J., Freitas, P. & Cabral,J. Single magnetic microsphere placement and detection on-chip using current line designs with integrated spin valve sensors: Biotechnological applications, *J. Appl. Phys.* **91**, 7786-7788 (2002).

60. Gupta, A.K. & Gupta, M. Synthesis and surface engineering of iron oxide nanoparticles for biomedical applications. *Biomaterials* **26**, 3995-4021 (2005).

61. Hammond, J.W & Liu, C.C. Silicon-based microfabricated tin oxide gas sensor incorporating use of Hall effect measurement. *Sensor. Actuat. B-Chem.* **81**, 25-31 (2001).

62. Han, M., Gao, X., Su, J.Z. & Nie, S. Quantum-dot-tagged microbeads for multiplexed optical coding of biomolecules. *Nat. Biotechnol.* **19**, 631-635 (2001).

63. Hao, R. et al. Synthesis, functionalization, and biomedical applications of multifunctional magnetic nanoparticles. *Adv. Mater.* **22**, 2729-2742 (2010).

64. Haun, J.B., Yoon, T.-J., Lee, H. and Weissleder, R. Magnetic nanoparticle biosensors. *WIREs Nanomed. Nanobiotechnol.* **2**, 291-304 (2010).

65. Hengsakul, M. & Cass, A.E.G. Protein Patterning with a photoactivatable derivative of biotin. *Bioconjugate Chem.* **7**, 249-254 (1996).

66. Herrmann, M., Veres, T. & Tabrizian, M. Enzymatically-generated fluorescent detection in micro-channels with internal magnetic mixing for the development of parallel microfluidic ELISA. *Lab. Chip* **6**, 555-560 (2006).

67. Ho, J. A. & Durst, R.A. Detection of fumonisin B1: comparison of flow-injection liposome immunoanalysis with high-performance liquid chromatography. *Anal. Biochem.* **312**, 7-13 (2003).

68. Ho, J.-A.A. et al. Application of ganglioside-sensitized liposomes in a flow injection immunoanalytical system for the determination of cholera toxin. *Anal. Chem.* **79**, 246-250 (2007).

69. Holden, M.A., Jung, S.-Y. & Cremer, P.S. Patterning enzymes inside microfluidic channels via photoattachment chemistry. *Anal. Chem.* **76**, 1838-1843 (2004).

70. Huang, C.-C., Huang, Y.-F., Cao, Z., Tan, W. & Chang, H.-T. Aptamer-modified gold nanoparticles for colorimetric determination of platelet-derived growth factors and their receptors. *Anal. Chem.* **77**, 5735-5741 (2005).

71. Hwang, S.Y. et al. Characteristics of a liposome immunoassay on a poly(methyl methacrylate) surface. *Anal. Bioanal. Chem.* **389**, 2251-2257 (2007).

72. Ito, A., Shinkai, M., Honda, H. & Kobayashi, T. Medical application of functionalized magnetic nanoparticles. *J. Biosci. Bioeng.* **100**, 1-11 (2005).

73. Kang, Y. et al. Electrochemical detection of thrombin by sandwich approach using antibody and aptamer. *Bioelectrochemistry* **73**, 76-81 (2008).

74. Karp, J.M. et al. A photolithographic method to create cellular micropatterns. *Biomaterials* **27**, 4755-4764 (2006).

75. Kim, Y.-P. et al. Energy transfer-based multiplexed assay of proteases by using gold nanoparticle and quantum dot conjugates on a surface. *Anal. Chem.* **80**, 4634-4641 (2008).

76. Kimling, J. et al. Turkevich method for gold nanoparticle synthesis revisited. *J. Phys. Chem. B* **110**, 15700-15707 (2006).

77. Kittel, C. On the Theory of Ferromagnetic Resonance Absorption. *Phys. Rev*. **73**, 155-161 (1948).

78. Kloepfer, J.A., Cohen, N. & Nadeau, J.L. FRET between CdSe quantum dots in lipid vesicles and water- and lipid-soluble dyes. *J. Phys. Chem. B* **108**, 17042-17049 (2004).

79. Kobayashi, Y., Horie, M., Konno, M., Rodríguez-González, B. & Liz-Marzán, L.M. Preparation and properties of silica-coated cobalt nanoparticles. *J. Phys. Chem. B* **107**, 7420-7425 (2003).

80. Koesdjojo, M. T., Koch, C. R. & Remcho, V. T. Technique for microfabrication of polymeric-based microchips from an SU-8 master with temperature-assisted vaporized organic solvent bonding. Anal. Chem. **81**, 1652–1659 (2009).

81. Koev, S.T. et al. Chitosan: an integrative biomaterial for lab-on-a-chip devices. *Lab. Chip* **10**, 3026-3042 (2010).

82. Koev, S.T. et al. Mechano-transduction of DNA hybridization and dopamine oxidation through electrodeposited chitosan network. *Lab. Chip* **7**, 103 (2007).

83. Lasic, D.D. & Barenholz, Y. *Handbook of Nonmedical Applications of Liposomes: From gene delivery and diagnostics to ecology*. (CRC Press: 1996).

84. Lee, M., Durst, R.A. & Wong, R.B. Comparison of liposome amplification and fluorophor detection in flow-injection immunoanalyses. *Anal. Chim. Acta* **354**, 23-28 (1997).

85. Lewandowski, A.T. et al. Protein assembly onto patterned microfabricated devices through enzymatic activation of fusion pro-tag. *Biotechnol. Bioeng.* **99**, 499-507 (2008).

86. Li, G. et al. Detection of single micron-sized magnetic bead and magnetic nanoparticles using spin valve sensors for biological applications. *J. Appl. Phys.* **93**, 7557-7559 (2003).

87. Li, X., Qian, J., Jiang, L. & He, S. Fluorescence quenching of quantum dots by gold nanorods and its application to DNA detection. *Appl. Phys. Lett.* **94**, 063111 (2009).

88. Lichlyter, D.J., Grant, S.A. & Soykan, O. Development of a novel FRET immunosensor technique. *Biosens. Bioelectron.* **19**, 219-226 (2003).

89. Liu, J. & Lu, Y. Preparation of aptamer-linked gold nanoparticle purple aggregates for colorimetric sensing of analytes. *Nat. Protoc.* **1**, 246-252 (2006).

90. Liu, J., Lee, J.H. & Lu, Y. Quantum dot encoding of aptamer-linked nanostructures for one-pot simultaneous detection of multiple analytes. *Anal. Chem.* **79**, 4120-4125 (2007).

91. Liu, X., Atwater, M., Wang, J. & Huo, Q. Extinction coefficient of gold nanoparticles with different sizes and different capping ligands. *Colloid. Surface. B* **58**, 3-7 (2007).

92. Liu, Y. et al. Chitosan to electroaddress biological components in lab-on-a-chip devices. *Carbohyd. Polym.* **84**, 704-708 (2011).

93. Lohse, S.E., Dahl, J.A. & Hutchison, J.E. Direct synthesis of large water-soluble functionalized gold nanoparticles using Bunte salts as ligand precursors. *Langmuir* **26**, 7504-7511 (2010).

94. Lu, A., Salabas, E.L. & Schüth, F. Magnetic nanoparticles: synthesis, protection, functionalization, and application. *Angew. Chem.Int. Edit.* **46**, 1222-1244 (2007).

95. Luccardini, C., Tribet, C., Vial, F., Marchi-Artzner, V. & Dahan, M. Size, charge, and interactions with giant lipid vesicles of quantum dots coated with an amphiphilic macromolecule. *Langmuir* **22**, 2304-2310 (2006).

96. Madihally, S.V. & Matthew, H.W.T. Porous chitosan scaffolds for tissue engineering. *Biomaterials* **20**, 1133-1142 (1999).

97. Mangeney, C. et al. Synthesis and properties of water-soluble gold colloids covalently derivatized with neutral polymer monolayers. *J. Am. Chem. Soc.* **124**, 5811-5821 (2002).

98. Martin, S. M. & Eesley, G. L. Optical fiber refractometer. *Rev. Sci. Instrum.* **58**, 2047-2048 (1987).

99. Mayilo, S. et al. Competitive homogeneous digoxigenin immunoassay based on fluorescence quenching by gold nanoparticles. *Anal. Chim. Acta* **646**, 119-122 (2009).

100. Mello, L.D. & Kubota, L.T. Review of the use of biosensors as analytical tools in the food and drink industries. *Food Chem.* **77**, 237-256 (2002).

101. Mendes, P.M., Yeung, C.L. & Preece, J.A. Bio-nanopatterning of surfaces. *Nanoscale Res. Lett.* **2**, 373-384 (2007).

102. Mie, G. Beiträge zur optik trüber medien, speziell kolloidaler metallösungen. *Annalen der Physik* **330**, 377-445 (1908).

103. Miller, M., Prinz, G., Cheng, S. & Bounnak, S. Detection of a micronsized magnetic sphere using a ring-shaped anisotropic magnetoresistance-based sensor: A model for a magnetoresistance-based biosensor. *Appl. Phys. Lett.* **81**, 2211-2213 (2002).

104. Moussaoui, N., Cansell, M. & Denizot, A. Marinosomes®, marine lipid-based liposomes: physical characterization and potential application in cosmetics. *Int. J. Pharm.* **242**, 361-365 (2002).

105. Murphy, C.J. et al. Chemical sensing and imaging with metallic nanorods. *Chem. Commun.* 544-557 (2008).

106. Nakamura, H. & Karube, I. Current research activity in biosensors. *Anal. Bioanal. Chem.* **377**, 446-468 (2003).

107. Nawarathna, D. et al. SQUID-based biosensor for probing ion transporters in cell suspensions and tissue. *IEEE T. Appl. Supercon.* **17**, 812-815 (2007).

108. Numnuam, A. et al. Aptamer-based potentiometric measurements of proteins using ion-selective microelectrodes. *Anal. Chem.* **80**, 707-712 (2008).

109. Oh, E. et al. Inhibition assay of biomolecules based on fluorescence resonance energy transfer (FRET) between quantum dots and gold nanoparticles. *J. Am. Chem. Soc.* **127**, 3270-3271 (2005).

110. Oh, E. et al. Nanoparticle based energy transfer for rapid and simple detection of protein glycosylation. *Angew. Chem.* **118**, 8127-8131 (2006).

111. Oh, E., Susumu, K., Goswami, R. & Mattoussi, H. One-phase synthesis of water-soluble gold nanoparticles with control over size and surface functionalities. *Langmuir* **26**, 7604-7613 (2010).

112. Ojeda, R., de Paz, J.L., Barrientos, A.G., Martín-Lomas, M. & Penadés, S. Preparation of multifunctional glyconanoparticles as a platform for potential carbohydrate-based anticancer vaccines. *Carbohyd. Res.* **342**, 448-459 (2007).

113. Ou, L.-J., Liu, S.-J., Chu, X., Shen, G.-L. & Yu, R.-Q. DNA encapsulating liposome based rolling circle amplification immunoassay as a versatile platform for ultrasensitive detection of protein. *Anal. Chem.* **81**, 9664-9673 (2009).

114. Paborsky, L.R., McCurdy, S.N., Griffin, L.C., Toole, J.J. & Leung, L.L. The single-stranded DNA aptamer-binding site of human thrombin. *J. Biol. Chem.* **268**, 20808-20811 (1993).

115. Pingarrón, J.M., Yáñez-Sedeño, P. & González-Cortés, A. Gold nanoparticle-based electrochemical biosensors. *Electrochim. Acta* **53**, 5848-5866 (2008).

116. Pritchard, D.J., Morgan, H. & Cooper, J.M. Micron-scale patterning of biological molecules. *Angew. Chem. Int. Edit.* **34**, 91-93 (1995).

117. Pritchard, D.J., Morgan, H. & Cooper, J.M. Patterning and regeneration of surfaces with antibodies. *Anal. Chem.* **67**, 3605-3607 (1995).

118. Ravi Kumar, M.N.V. A review of chitin and chitosan applications. *React. Funct. Polym.* **46**, 1-27 (2000).

119. Rife, J. et al. Design and performance of GMR sensors for the detection of magnetic microbeads in biosensors. *Sens. Actuators A* **107**, 209-218(2003).

120. Rinaudo, M. Chitin and chitosan: properties and applications. *Prog. Polym. Sci.* **31**, 603-632 (2006).

121. Roberts, M.A. & Durst, R.A. Investigation of liposome-based immunomigration sensors for the detection of polychlorinated biphenyls. *Anal. Chem.* **67**, 482-491 (1995).

122. Rongen, H.A.H., Bult, A. & van Bennekom, W.P. Liposomes and immunoassays. *J. Immunol. Methods* **204**, 105-133 (1997).

123. Salgueirino-Maceira, V. & Correa-Duarte, M.A. Cobalt and silica based core-shell structured nanospheres. *J. Mater. Chem.* **16**, 3593 (2006).

124. Salgueiriño-Maceira, V. et al. Synthesis and characterization of large colloidal cobalt particles. *Langmuir* **22**, 1455-1458 (2006).

125. Sandhu, A. et al. High efficiency Hall effect micro-biosensor platform for detection of magnetically labeled biomolecules. *Biosens. Bioelectron.* **22**, 2115-2120 (2007).

126. Sandhu, A., Sanbonsugi, H., Shibasaki, I., Abe, M. & Handa, H. High sensitivity InSb ultra-thin film micro-hall sensors for bioscreening applications. *Jpn. J. Appl. Phys. Lett.* **43**, L868–L870 (2004).

127. Sapsford, K.E., Pons, T., Medintz, I.L. & Mattoussi, H. Biosensing with luminescent semiconductor quantum dots. *Sensors* **6**, 925-953 (2006).

128. Schmid, G. & Corain, B. Nanoparticulated gold: syntheses, structures, electronics, and reactivities. *Eur. J. Inorg. Chem.* **2003**, 3081-3098 (2003).

129. Seydack, M. Nanoparticle labels in immunosensing using optical detection methods. *Biosens. Bioelectron.* **20**, 2454-2469 (2005).

130. Sheila A. Grant, Darcy J. Lichlyter, Susan Lever, Fabio Gallazzi & Orhan Soykan A novel sensing technique to detect thrombin. *Sens. Lett.* **2**, 164-170 (2004).

131. Shen, W., Liu, X., Mazumdar, D. & Xiao G. In situ detection of single micron-sized magnetic beads using magnetic tunnel junction sensors. *Appl. Phys. Lett.* **86**, 253901-253903 (2005).

132. Shi, L., De Paoli, V., Rosenzweig, N. & Rosenzweig, Z. Synthesis and application of quantum dots FRET-based protease sensors. *J. Am. Chem. Soc.* **128**, 10378-10379 (2006).

133. Shi, X. et al. Chitosan biotinylation and electrodeposition for selective protein assembly. *Macromol. Biosci.* **8**, 451-457 (2008).

134. Siebert, S.T.A., Reeves, S.G. & Durst, R.A. Liposome immunomigration field assay device for Alachlor determination. *Anal. Chim. Acta* **282**, 297-305 (1993).

135. Singh, A.K., Harrison, S.H. & Schoeniger, J.S. Gangliosides as receptors for biological toxins: development of sensitive fluoroimmunoassays using ganglioside-bearing liposomes. *Anal. Chem.* **72**, 6019-6024 (2000).

136. Sokolov, K. et al. Real-time vital optical imaging of precancer using anti-epidermal growth factor receptor antibodies conjugated to gold nanoparticles. *Cancer Res.* **63**, 1999 -2004 (2003).

137. Sorribas, H., Padeste, C. & Tiefenauer, L. Photolithographic generation of protein micropatterns for neuron culture applications. *Biomaterials* **23**, 893-900 (2002).

138. Spindler, X., Hofstetter, O., McDonagh, A.M., Roux, C. & Lennard, C. Enhancement of latent fingermarks on non-porous surfaces using anti-L-amino acid antibodies conjugated to gold nanoparticles. *Chem. Commun.* **47**, 5602-5604 (2011).

139. Struss, A., Pasini, P., Ensor, C.M., Raut, N. & Daunert, S. Paper strip whole cell biosensors: A portable test for the semiquantitative detection of bacterial quorum signaling molecules. *Anal. Chem.* **82**, 4457-4463 (2010).

140. Sun, B. et al. Microminiaturized immunoassays using quantum dots as fluorescent label by laser confocal scanning fluorescence detection. *J. Immunol. Methods* **249**, 85-89 (2001).

141. Tanaka, R. et al. A novel enhancement assay for immunochromatographic test strips using gold nanoparticles. *Anal. Bioanal. Chem.* **385**, 1414-1420 (2006).

142. Tang, B. et al. A new nanobiosensor for glucose with high sensitivity and selectivity in serum based on fluorescence resonance energy transfer (FRET) between CdTe quantum qots and Au nanoparticles. *Chem.-Eur. J.* **14**, 3637-3644 (2008).

143. Tartaj, P., Morales, M. P., Veintemillas-Verdaguer, S., Gonz lez-Carreno, T. & Serna, C.J. The preparation of magnetic nanoparticles for applications in biomedicine. *J. Phys. D: Appl. Phys.* **36**, R182-R197 (2003).

144. Thanh, N.T.K. & Rosenzweig, Z. Development of an aggregation-based immunoassay for anti-protein A using gold nanoparticles. *Anal. Chem.* **74**, 1624-1628 (2002).

145. Thürer, R. et al. Potentiometric immunoassay with quantum dot labels. *Anal. Chem.* **79**, 5107-5110 (2007).

146. Turkevich, J., Stevenson, P.C. & Hillier, J. A study of the nucleation and growth processes in the synthesis of colloidal gold. *Discuss. Faraday Soc.* **11**, 55-75 (1951).

147. Vadgama, P. & Crump, P.W. Biosensors: recent trends. A review. *Analyst* **117**, 1657-1670 (1992).

148. Wang, J. Electrochemical biosensors: Towards point-of-care cancer diagnostics. *Biosens. Bioelectron.* **21**, 1887-1892 (2006).

149. Wang, J., Liu, G. & Merkoçi, A. Electrochemical coding technology for simultaneous detection of multiple DNA targets. *J. Am. Chem. Soc.* **125**, 3214-3215 (2003).

150. Wang, S.X. & Guanxiong Li Advances in giant magnetoresistance biosensors with magnetic nanoparticle tags: review and outlook. *IEEE T. Magn.* **44**, 1687-1702 (2008).

151. Wang, W., Chen, C., Qian, M. & Zhao, X.S. Aptamer biosensor for protein detection using gold nanoparticles. *Anal. Biochem.* **373**, 213-219 (2008).

152. Wang, X., Ramström, O. & Yan, M. A photochemically initiated chemistry for coupling underivatized carbohydrates to gold nanoparticles. *J. Mater. Chem.* **19**, 8944 (2009).

153. Wangoo, N., Bhasin, K.K., Boro, R. & Suri, C.R. Facile synthesis and functionalization of water-soluble gold nanoparticles for a bioprobe. *Anal. Chim. Acta* **610**, 142-148 (2008).

154. Whitesides, G.M. The "right" size in nanobiotechnology. *Nat. Biotech.* **21**, 1161-1165 (2003).

155. Wittung, P. et al. Phospholipid membrane permeability of peptide nucleic acid. *FEBS Lett.* **365**, 27-29 (1995).

156. Wolff, I. *Coplanar Microwave Integrated Circuits* (Wiley-Interscience, 2006).

157. Wu, L. Q, Ghodssi, R., Elabd, Y.A. & Payne, G.F. Biomimetic pattern transfer. *Adv. Funct. Mater.* **15**, 189-195 (2005).

158. Xia, Y., Song, L. & Zhu, C. Turn-on and near-infrared fluorescent sensing for 2,4,6-trinitrotoluene based on hybrid (gold nanorod)−(quantum dots) assembly. *Anal. Chem.* **83**, 1401-1407 (2011).

159. Xie, H.-Y. et al. Luminescent CdSe-ZnS quantum dots as selective Cu^{2+} probe. *Spectrochim. Acta A* **60**, 2527-2530 (2004).

160. Yang, C. et al. Folate receptor-targeted quantum dot liposomes as fluorescence probes. *J. Drug Target* **17**, 502-511 (2009).

161. Yi, H. et al. Biofabrication with chitosan. *Biomacromolecules* **6**, 2881-2894 (2005).

162. Zaytseva, N.V., Goral, V.N., Montagna, R.A. & Baeumner, A.J. Development of a microfluidic biosensor module for pathogen detection. *Lab. Chip* **5**, 805 (2005).

163. Zhan, W. & Bard, A.J. Electrogenerated Chemiluminescence. 83. Immunoassay of human C-reactive protein by using $Ru(bpy)_3^{2+}$ encapsulated liposomes as labels. *Anal. Chem.* **79**, 459-463 (2007).

164. Zhong, W. Nanomaterials in fluorescence-based biosensing. *Anal. Bioanal. Chem.* **394**, 47-59 (2009).

165. Zhu, X., Duan, D., Madsen, S. & Publicover, N.G. Compatibility of quantum dots with immunobuffers, and its effect on signal/background of quantum dot-based immunoassay. *Anal. Bioanal. Chem.* **396**, 1345-1353 (2009).